# Algebraic and computational aspects of quantum control and applications.

## Thesis

# Algebraic and Computational Aspects of Quantum Control and Applications

Submitted for the degree of Doctor of Philosophy

Ivan Christopher Hugh Pullen BEd (Cantab), BA, MSc (Open)

The Department of Mathematics

The Open University

March 4, 2006

DATE OF SUBMISSION 30 SEPTEMBER 2005

DATE OF AWARD 07 FEBRUARY 2006

## Abstract

We investigate the problem of control of quantum systems. Various notions of controllability of quantum systems are discussed and Lie algebraic techniques are employed to derive necessary and sufficient conditions for the resulting degrees of controllability. The results are employed to study the degree of controllability for various model systems.

The problem of optimal control is formulated as a problem of maximisation of the expectation value of an observable of the system subject to dynamical constraints and costs. A class of iterative algorithms is discussed, and shown to converge to a solution of the Euler-Lagrange equations, which is a necessary condition for optimality of a solution. A numerical realisation of the algorithm is presented and potential implementation of the resulting control fields in the laboratory is discussed.

The algorithm is applied to find optimal control fields for a variety of applications including selective and simultaneous excitation of individual quantum dots in a globally addressed ensemble, creation of superposition states, and selective excitation of certain vibrational modes of a simple molecule such as Hydrogen Fluoride. In each case we systematically explore the parameter space of the algorithm to select solutions with desirable physical features from the multitude of possible choices.

As there are many possible optimal control fields which give similar yields the question of whether some are more robust than others is investigated. A number of optimal fields are analysed quantitatively in terms of robustness with regard to temporal and spectral noise affecting the fields, uncertainty in the model parameters and the effect of experimental limitations such as restrictions on the bandwidth of the fields. It is shown that whilst the solutions tend to be sensitive to uncertainty in the energy levels chosen for the model, they appear to be surprisingly tolerant to even severe bandwidth limitations.

## Acknowledgements

My thanks go to my supervisors, Prof Allan Solomon of The Open University, and Dr Sonia Schirmer of the University of Cambridge, firstly for accepting me as a part-time research student, and secondly for their inspiration, encouragement, patience, and help in overcoming the difficulties I have encountered in the course of this work.

I would also like to express my gratitude to the Centre for Quantum Computing (CQC) at the University of Cambridge and Churchill College for hosting me as a visitor during the summers of 2004 and 2005, which provided me with the opportunity to meet and interact with many world-class researchers in the field of quantum science and technology. In particular, I have gained from discussions with Andrey Bychkov and Daniel Oi, both from CQC, as well as from valuable technical assistance provided by the latter.

Finally, I am also greatly indebted to my wife and daughters for their tolerance, understanding and total support throughout.

# Contents

# List of Figures

# List of Tables

# Chapter 1

# Introduction

One manifestation of man's enquiring nature is the search for the means to control the physical environment. There have been many notable scientific successes that have led to technological progress. Examples include, the invention of levers and pulleys which permitted the control and positioning of large masses required to build cathedrals, and the control of the energy released in chemical reactions, which is the basis of engines such as the internal combustion and jet engines. In various ways increases in the ability to control have had an impact on society and have resulted in lasting changes.

One of the focuses of attention now is the control of systems in which quantal effects are significant and for which, therefore, a quantum mechanical treatment is required. Examples include anything from large molecules to elementary particles. Lasers are one means by which these systems can be controlled but there are others such as electronic gates. The ability to control quantum systems is motivated by the prospect of progress in the fields of chemistry or quantum computing, for example, and also the potential to attain a greater understanding of the behaviour of quantum systems. The aim of this thesis is to consider the current state of knowledge in this area; to determine solutions to control problems; to investigate the quality of these solutions and to find further applications of the methods and techniques employed.

Controlling quantum systems has been a long standing dream of physicists and chemists [1, 2]. In the early days there seemed little likelihood of progress but following the development of lasers in the 1960's a possible means became apparent. The first problems considered were in Chemistry and involved attempting to break and create

selected bonds in molecules in order to build highly specific complex molecular structures. Early experiments were based on ideas derived from physical intuition. They treated the quantum system as closed i.e. they concentrated on excitation and considered the evolution processes as independent. From these experiments it was learnt that the energy, although initially concentrated on one molecular bond, was dissipated throughout the system and the environment through interactions. Researchers realised that the required control fields are subject to constraints and that finding an optimal pulse is a complicated problem involving balancing the requirement to satisfy dynamical laws with experimental constraints on such things as frequency and intensity and allowing for interaction with the environment. However it is often the case that interaction with the control is much stronger than that with the environment and takes place in an appreciably shorter time. It became recognised [3] that the wave nature of quantum dynamical processes needed to be taken into account and hence a theoretical approach as well as a practical is required.

The structure of the thesis is as follows.

In Chapter 2 the model of the quantum system is introduced. For the reason given above non-dissipative systems are considered, where the evolution of the system is Hamiltonian. There are various degrees of controllability for Hamiltonian systems and these are defined. The relationship between the degree of controllability of a system is described both in terms of the Lie algebra generated by the Hamiltonian of the system and the transition graph of the system. The degree of controllability for systems with just nearest neighbour interactions and a range of symmetrical relations between energy levels and dipole moments is found by identifying the Lie algebra generated by the Hamiltonian. The chapter ends with a result concerning multi-particle or composite systems and a discussion of its application to quantum dots.

Chapter 3 is concerned with the theoretical aspects of optimal quantum control. After mentioning some of the key methods the chapter moves on to set up the problem of optimal control and to state the elements that make up a solution. An iterative algorithm to find solutions, which I have developed, is introduced and shown to converge to an optimal solution. A scheme for implementing the algorithm numerically and a discussion of how such a solution may be realised in the laboratory rounds off the chapter.

In Chapter 4 we look at the effect of applying numerical realisations of the optimal control algorithm to various situations. Predictions are made from a theoretical point of view and then verified by the algorithm. Examples considered include a generic 3-level system, models of ensembles of quantum dots and a model of the Hydrogen Fluoride molecule.

For differing choices of algorithm parameters there are many possible solutions, which in terms of yield, are very similar. In Chapter 5 we investigate the sensitivity of solutions to noise and uncertainty in the model parameters. This is termed robustness. It is of particular interest to note the relatively acute sensitivity of all solutions to uncertainty in the values of the energy levels used for the model. The chapter goes on to look at the effect of limiting the bandwidth of solutions. In contrast to the sensitivity to energy level uncertainty it is noteworthy how robust solutions are, even in the event of severe limiting of their bandwidth.

Chapter 6 contains concluding remarks and is followed by the Appendix.

Many of the proofs of theorems presented in this thesis are included in the Appendix to aid the flow for the reader. These are however original work except where otherwise cited.

# Chapter 2

# Controllability of Quantum Systems

Notions of controllability of a quantum system include actions such as the ability to transform a system from a given initial state to a desired final state or to optimise the expectation value of a selected observable. There are a number of different approaches that have been taken to controllability. Some of the models studied have assumed the system to have infinitely many energy levels [4, 5, 6], but perhaps most have focussed on the case where the system of interested can be considered to have a finite number of energy levels [7, 8, 9]. Another important distinction is between closed or open quantum systems. The first refers to a model where the system is not subject to dissipative effects whereas the second refers to a system that is. A further classification that is made is to whether the type of control is closed-loop or open-loop control [10]. Closed-loop control relies on feedback from some form of measurement, while open-loop control relies only on a presumed knowledge of the initial state and the dynamical laws that govern the evolution of the system when control fields are applied. One of the advantages of the latter for quantum systems is that the inevitable *back action* from the measurement is avoided because the system is not monitored.

## 2.1 The Mathematical Model

The state space of a quantum system is a Hilbert space. For the purpose of this thesis we will consider a subspace of a Hilbert space, $\mathcal{H}$, which is of finite dimension, $N$. An element of $\mathcal{H}$, written $|\Psi_n\rangle$, specifies or describes the state of the system and it is called a wave function or a state vector. It is a unit vector in the form of an $N$-tuple of complex numbers $x_j^{(n)} + iy_j^{(n)}$ where

$$\langle\Psi_n|\Psi_n\rangle = \sum_{j=1}^{N}[x_j^{(n)}]^2 + [y_j^{(n)}]^2 \quad = 1$$

The set of $N$ state vectors $|\Psi_n\rangle$ where $1 \leq n \leq N$ can be chosen in such a way as to form an orthonormal set, that is they have the property

$$\langle\Psi_n|\Psi_m\rangle = \delta_{mn}$$

where $\delta_{mn}$ is the Kronecker delta, and for all $m, n \in \{j : 1 \leq j \leq N\}$.

A state can also be described by a density operator, $\hat{\rho}$, given by

$$\hat{\rho} = \sum_{n=1}^{N} w_n|\Psi_n\rangle\langle\Psi_n| \quad \text{where} \sum_{n=1}^{N} w_n = 1 \tag{2.1}$$

and where all the $w_n$'s are non-negative. The $w_n$'s are the eigenvalues of the density operator $\hat{\rho}$ and the state vectors, $|\Psi_n\rangle$, are an orthonormalised set of eigenvectors or eigenstates of $\hat{\rho}$. From 2.1 it follows that $\mathrm{Tr}(\hat{\rho}) = 1$. Density operators and hence possible states of the system can be classified either as Pure States or Mixed States. These are defined as follows

**Definition 1** Pure States.

*These are defined as density operators where the set of eigenvalues consists of two distinct eigenvalues, one of which occurs with multiplicity* 1 *and is* 1 *and the other, which is* 0*, occurs with multiplicity* $N - 1$*. Such a density matrix has rank* 1 *and* $[\mathrm{Tr}(\hat{\rho})]^2 = 1$.

**Definition 2** Mixed States.

*These are defined as density operators where the set of eigenvalues consists of* either *at least two distinct eigenvalues, at least one of which occurs with multiplicity* $N_1$ *where* $2 \leq N_1 \leq N - 2$ or $N$ *distinct eigenvalues*

Two special cases of mixed states are also identified as they have particular properties in terms of controllability. These are defined as follows.

**Definition 3** Pseudo-Pure States *or* Pure-state-like ensembles.
*These are defined as density operators where the set of eigenvalues consists of two distinct eigenvalues, one of which occurs with multiplicity* 1 *and the other with multiplicity* $N-1$.

**Definition 4** Completely Random States.
*These are defined as density operators where the set of eigenvalues consists of a single eigenvalue* $\frac{1}{N}$ *with multiplicity* $N$.

The next definition is of a Generic Mixed State, which can be thought of the opposite of a Completely Random State in terms of it eigenvalues.

**Definition 5** Generic Mixed States.
*These are defined as density operators where the set of eigenvalues consists of* $N$ *distinct eigenvalues i.e. each eigenvalue has multiplicity* 1.

In general the density operator $\hat{\rho}$ satisfies the quantum Liouville equation.

$$i\hbar\frac{d}{dt}\hat{\rho}(t) = \left[\hat{H}[\mathbf{f}(t)], \hat{\rho}\right] + i\hbar\mathcal{L}_D[\hat{\rho}(t)] \tag{2.2}$$

In this equation $\hat{H}[\mathbf{f}(t)]$ is the Hamiltonian and this will be assumed to be control-linear i.e. of the form

$$\hat{H}[\mathbf{f}(t)] = \hat{H}_0 + \sum_{m=1}^{M} f_m(t)\hat{H}_m \tag{2.3}$$

where $\hat{H}_0$ is the internal Hamiltonian and where

$$\mathbf{f}(t) = (f_1(t), f_2(t), \ldots f_M(t)) \tag{2.4}$$

represents the control fields. Each control field is continuous and has a continuous first derivative. $f_m(t)$ with $1 \leq m \leq M$ is the control field associated with the control Hamiltonian $\hat{H}_m$. Each control Hamiltonian is an $N \times N$ matrix whose real, off-diagonal elements representing transition dipole moments. It is customary to use the complete orthonormal set of eigenvectors $|n\rangle$ and the eigenvalues, $E_n$, of $\hat{H}_0$, or energy levels of the system given by $\hat{H}_0|n\rangle = E_n|n\rangle$ for $n = 1, 2, \ldots N$. With respect to this basis $\hat{H}_0$ will be a diagonal $N \times N$ Hermitian matrix given by

$$\hat{H}_0 = \sum_{n=1}^{N} E_n|n\rangle\langle n| \tag{2.5}$$

In an open system the system interacts with its environment, usually in an uncontrollable way by, for example, population relaxation or phase decoherence. The dissipative term $\mathcal{L}_D$ accounts for such behaviour. If the assumption is made that there is no dissipation i.e. we have a closed system then $\mathcal{L}_D = 0$ and the evolution of the system is Hamiltonian. In that case the initial state of the system is described by $\hat{\rho}(t_0) = \hat{\rho}_0$ then the state of the system at time $t$ will be given by $\hat{\rho}(t)$, where

$$\hat{\rho}(t) = \hat{U}(t, t_0)\hat{\rho}_0\hat{U}(t, t_0)^\dagger,$$

where $\hat{U}(t, t_0)$ is the Hilbert space evolution operator that satisfies the Schrödinger equation

$$i\hbar\frac{d}{dt}\hat{U}(t, t_0) = \hat{H}[\mathbf{f}(t)]\hat{U}(t, t_0), \tag{2.6}$$

and therefore $\hat{\rho}(t)$ will be determined by the unitary group $U(N)$ where $N$ is the dimension of $\mathcal{H}$.

For a Hamiltonian system we have the restriction that the only states that can be reached from the initial state $\hat{\rho}_0$ are those given by $\hat{U}\hat{\rho}_0\hat{U}^\dagger$ i.e. those attained by unitary evolution. This is referred to as the *kinematical constraint* [11]. Formally, a target state $\hat{\rho}_T$ can only be reached from an initial state $\hat{\rho}_0 \Leftrightarrow$ there exists a unitary operator $\hat{U}$ such that $\hat{\rho}_T = \hat{U}\hat{\rho}_0\hat{U}^\dagger$. This statement defines an equivalence relation on the set of density operators and the equivalence classes that the set is partitioned into are referred to as kinematical equivalence classes. So we have

$$\hat{\rho}_1 \text{ is kinematically related to } \hat{\rho}_2 \quad \Leftrightarrow \quad \hat{\rho}_2 = \hat{U}\hat{\rho}_1\hat{U}^\dagger$$

for some unitary operator $\hat{U}$. As a consequence of this two density matrices that are kinematically equivalent will have the same spectra or set of eigenvalues. This means that the density matrices representing pure states will form one equivalence class and that a pure state will only be attainable if the initial state was a pure state. Other restrictions that depend on constraints placed on the control fields are referred to as *dynamical constraints.* At this stage the term observable should be introduced. An observable is a quantity that can be measured experimentally. These are represented by Hermitian operators $\hat{A}$ on $\mathcal{H}$. The expectation value is

$$\langle\hat{A}(t)\rangle = \mathrm{Tr}\left[\hat{A}\hat{\rho}(t)\right]. \tag{2.7}$$

Maximising the expectation value of a selected observable is one of the aims of controlling a quantum system.

## 2.2 Degrees of Controllability for Hamiltonian Systems

In this section a non-dissipative quantum system, i.e $\mathcal{L}_D = 0$, is considered with the Hamiltonian given in (2.3). There are various degrees of controllability of quantum systems [12, 13, 14]. The degree of controllability depends on the nature of the initial and final states of the system and the dynamical Lie group of the system.

**Definition 6** Completely Controllable.

*A quantum system subject to the Hamiltonian given in* (2.3) *is said to be completely controllable if for any unitary operator, $\hat{U}$, there exists an admissible control-trajectory pair given by $(\mathbf{f}(t), \hat{U}(t, t_0))$ defined for $t_0 \leq t \leq t_F$ (for some $t_F < \infty$) such that $\hat{U} = \hat{U}(t_F, t_0)$ i.e. if any unitary operator is dynamically realizable.*

**Definition 7** Density matrix controllable.

*A quantum system subject to the Hamiltonian given in* (2.3) *is said to be density matrix controllable if for any pair of kinematically equivalent density matrices $\hat{\rho}_0$ and $\hat{\rho}_1$, there exists an admissible control-trajectory pair given by $(\mathbf{f}(t), \hat{U}(t, t_0))$ defined for $t_0 \leq t \leq t_F$ (for some $t_F < \infty$) such that $\hat{\rho}_1 = \hat{U}(t_F, t_0)\hat{\rho}_0\hat{U}(t_F, t_0)^\dagger$.*

**Definition 8** Pure-state controllable.

*A quantum system subject to the Hamiltonian given in* (2.3) *is said to be pure-state controllable if for any two pure states given by the (normalised) wave functions $|\Psi_0\rangle$, $|\Psi_1\rangle$, there exists an admissible control-trajectory pair $(\mathbf{f}(t), \hat{U}(t, t_0))$ defined for $t_0 \leq t \leq t_F$ (for some $t_F < \infty$) such that $|\Psi_1\rangle = \hat{U}(t_F, t_0)|\Psi_0\rangle$.*

**Definition 9** Observable controllable.

*A quantum system subject to the Hamiltonian given in* (2.3) *is said to be observable controllable if for any observable $\hat{A}$ and initial state $\hat{\rho}_0$ of the system, there exists an admissible control-trajectory pair $(\mathbf{f}(t), \hat{U}(t, t_0))$ defined for $t_0 \leq t \leq t_F$ (for some $t_F < \infty$) such that the ensemble average $\mathrm{Tr}[\hat{\rho}(t)\hat{A}]$ of $\hat{A}$ assumes any kinematically admissible value* [11].

## 2.3 Lie-algebraic Criteria for Controllability

It has been shown [15, 7] that the controllability of a closed quantum system subject to the Hamiltonian given in (2.3) depends on the Lie algebra, denoted $\mathcal{L}$, generated by the matrices $i\hat{H}_m$ for $m = 0 \ldots M$. Since $i\hat{H}_m$ are skew-Hermitian they generate a Lie algebra $\mathcal{L}$ which is a subalgebra of $u(N)$. This is called the dynamical Lie algebra of the control system. With reference to the basis of eigenstates $|n\rangle$ of $\hat{H}_0$, where $n = 1 \ldots N$, the matrices $\hat{H}_m$ for $m = 1 \ldots M$ are trace-zero as they contain off-diagonal entries representing transition dipole moments. In most control applications it is more convenient, but not essential, to work with trace-zero matrices. The matrix $\hat{H}_0$ is a diagonal matrix where the entries are the energy levels of the system. In general their sum, and hence the trace of $\hat{H}_0$, is not zero. As it is the differences between adjacent energy levels, and not their sum, which is important we define the trace-zero matrix

$$\tilde{H}_0 = \hat{H}_0 - \frac{1}{N}\mathrm{Tr}(\hat{H}_0)\hat{I} \tag{2.8}$$

which is equivalent to $\hat{H}_0$ up to the addition of a constant multiplier of $\hat{I}$ the $N \times N$ identity matrix.

It has been shown [16] that if trace-zero matrices are used we loose control of the global phase but in an application such as maximising the expectation of an observable this phase is immaterial in the calculations. Denote by $\tilde{\mathcal{L}}$ the Lie algebra generated by the trace-zero matrices $i\tilde{H}_0$ and $i\hat{H}_m$ for $m = 1 \ldots M$.

The theorem [13, 12] below gives the conditions under which the various degrees of controllability are obtainable.

**Theorem 1** *A necessary and sufficient condition for a quantum system with Hamiltonian (2.3) and dynamical Lie algebra $\mathcal{L}$ to be*

*(i) completely controllable is $\mathcal{L} \cong u(N)$;*

*(ii) density matrix controllable is $\mathcal{L} \cong su(N)$;*

*(iii) observable controllable is $\mathcal{L} \cong su(N)$;*

*(iv) pure-state controllable is* $\mathcal{L} \cong su(N)$,

*or if* $N$ *is even,* $\mathcal{L} \cong sp(N/2)$, *where sp denotes the symplectic Lie algebra.*

Pure-state controllability is equivalent to wave function controllability [17]. Systems satisfying (ii) and (iii) are sometimes simply called controllable.

## 2.4 Graph-Connectivity Criteria

Graph theory provides us with convenient criteria for controllability of a system with just one control field [18]. Before considering these criteria the concepts of *regular* and *strongly regular* need to be defined [14]. Consider the $N$-level quantum system where the Hamiltonian is of the form

$$\hat{H}[f(t)] = \hat{H}_0 + f(t)\hat{H}_1$$

and where

$$\hat{H}_0 = \sum_{n=1}^{N} E_n |n\rangle\langle n|$$

The $E_n$'s, which are real, represent the energy levels of the system and are the eigenvalues of $\hat{H}_0$.

**Definition 10** Regular.

*The internal system Hamiltonian,* $\hat{H}_0$, *is said to be regular if the energy levels are all different i.e the eigenvalues of* $\hat{H}_0$ *are unique. This is also referred to as a non-degenerate system.*

**Definition 11** Strongly regular.

*If* $\hat{H}_0$, *in addition to being regular, has the property that the difference between any pair of energy levels is unique i.e* $E_i - E_j \neq E_m - E_n$ *unless* $(i,j) = (m,n)$, $\hat{H}_0$ *is said to be strongly regular.*

**Definition 12** Adjacent.

*Consider a graph with* $N$ *vertices denoted* $v_1, v_2, \ldots, v_N$. *If two vertices* $v_i, v_j$ *for* $i, j = 1, 2, \ldots N, i \neq j$ *are connected by an edge then the vertices* $v_i, v_j$ *are said to be adjacent.*

Now we are ready to define a transition graph.

**Definition 13** Transition graph.

*A graph with $N$ nodes is said to be the transition graph determined by the matrix $\hat{H}_1 = [d_{ij}]$ if the existence of an edge is established by the following rule*

$$\text{if } d_{ij} \neq 0 \text{ then } v_i \text{ and } v_j \text{ are adjacent}$$

$$\text{if } d_{ij} = 0 \text{ then } v_i \text{ and } v_j \text{ are not adjacent.}$$

The relationship between the internal Hamiltonian $\hat{H}_0$, the transition graph and the controllability of the system is given by the following theorem [18].

**Theorem 2** *If the internal system Hamiltonian $\hat{H}_0$ is strongly regular and the transition graph determined by $\hat{H}_1$ is connected then the system is density matrix and observable controllable.*

An example in [14] shows why it is necessary for the Hamiltonian $\hat{H}_0$ to be regular. The following example demonstrates why the Hamiltonian $\hat{H}_0$ needs to be not just regular but strongly regular.

**Example 1** If we consider a system with four equally spaced energy levels and uniform dipole moments between adjacent energy levels then, as the matrix $\hat{H}_0$ is not strongly regular, the system is not completely controllable even though the graph represented by $\hat{H}_1$ is connected. By taking the uniform dipole moments to be equal to $d$, the spacings between the energy levels to be equal to $\omega$, setting

$$\tilde{H}_0 = \hat{H}_0 - \frac{1}{4}\mathrm{Tr}(\hat{H}_0)I_4$$

and employing the change of basis $\{|1\rangle, |2\rangle, |3\rangle, |4\rangle\} \mapsto \{|1\rangle, |2\rangle, -|4\rangle, |3\rangle\}$. The matrices $\tilde{H}_0$ and $\hat{H}_1$ will be given by:

$$\tilde{H}_0 = \frac{\omega}{2}\begin{pmatrix} -3 & 0 & 0 & 0 \\ 0 & -1 & 0 & 0 \\ 0 & 0 & 3 & 0 \\ 0 & 0 & 0 & 1 \end{pmatrix} \qquad \hat{H}_1 = \begin{pmatrix} 0 & d & 0 & 0 \\ d & 0 & 0 & d \\ 0 & 0 & 0 & -d \\ 0 & d & -d & 0 \end{pmatrix}$$

The dynamical Lie algebra, $\tilde{\mathcal{L}}$, generated by $i\tilde{H}_0$ and $i\hat{H}_1$ is given explicitly by

$$\begin{aligned}
h_1 &= (2\omega d^2)^{-1}[[i\tilde{H}_0, i\hat{H}_1], i\hat{H}_1] & h_2 &= -2(i\omega^{-1}\tilde{H}_0 + \tfrac{3}{2}h_1) \\
y_1 &= (\omega d)^{-1}[h_1, [i\tilde{H}_0, i\hat{H}_1]] & x_1 &= [h_1, y_1] \\
y_2 &= id^{-1}\hat{H}_1 - y_1 & x_2 &= x_1 + (\omega d)^{-1}[i\tilde{H}_0, i\hat{H}_1] \\
y_{\epsilon_1+\epsilon_2} &= d^{-1}[i\hat{H}_1, x_2] + 2h_2 & x_{\epsilon_1+\epsilon_2} &= [h_1, y_{\epsilon_1+\epsilon_2}] \\
x_{2\epsilon_1} &= 2^{-1}[x_{\epsilon_1+\epsilon_2}, x_1] & y_{2\epsilon_1} &= 2^{-1}[x_{2\epsilon_1}, h_1]
\end{aligned}$$

which shows that $sp(2)$, and not $su(4)$ (see Appendices A.3 and A.1), is generated by $i\tilde{H}_0$ and $i\hat{H}_1$; hence the system is not controllable. This shows that the regularity of $\hat{H}_0$ is not sufficient for the system to be controllable.

## 2.5 Systems with Nearest Neighbour Interaction

In this section we focus on N-level quantum systems subject to a single control field i.e $M = 1$, and where interactions are dominated by those between nearest neighbours. These two assumptions give rise to a sub-case which warrants special consideration as will be shown in Chapter 4. Hence, if the dipole moment of the transition from $|n\rangle$ to $|n+1\rangle$ is denoted by $d_n$ the single interaction Hamiltonian, $\hat{H}_1$ is written

$$\hat{H}_1 = \sum_{n=1}^{N-1} d_n(|n\rangle\langle n+1| + |n+1\rangle\langle n|). \tag{2.9}$$

With the $E_n$'s ordered in a non-decreasing sequence $E_1 \leq E_2 \leq \ldots \leq E_N$ the energy level spacings or frequencies, $\omega_n$, for the transitions $|n\rangle \rightarrow |n+1\rangle$ are non-negative and are given by

$$\omega_n \equiv E_{n+1} - E_n \geq 0, \qquad 1 \leq n \leq N-1.$$

The Lie algebra generated by $i\hat{H}_0$ and $i\hat{H}_1$ is denoted $\mathcal{L}$. For the reason given in Section 2.3 it is convenient to deal with trace-zero matrices and this is achieved by using Equation 2.8. Defined this way, $i\tilde{H}_0$ and $i\hat{H}_1$ are both trace-zero and skew-Hermitian. Hence, the Lie algebra generated by the operators $i\tilde{H}_0$ and $i\hat{H}_1$, denoted $\tilde{\mathcal{L}}$, is a real Lie algebra of trace-zero, skew-Hermitian matrices.

Our aim is to classify the degree of controllability of the systems above by identifying the dynamical Lie algebras generated. We are especially interested in those cases

where restrictions in the form of symmetrical relationships between the energy levels $E_n$ and the coupling strengths $d_n$ are imposed on the $i\tilde{H}_0$ and $i\tilde{H}_1$. Before we proceed to these cases, however, we will first summarise the conditions under which the Lie algebra generated by $i\tilde{H}_0$ and $i\tilde{H}_1$ has been shown to be $su(N)$ [19]:

**Theorem 3** *Let $d_0 = d_N = 0$ and $v_m = 2d_m^2 - d_{m+1}^2 - d_{m-1}^2$ for $1 \leq m \leq N-1$ and if, in addition, $N$ is even set $p = \frac{1}{2}N$ and suppose $d_{p-k} \neq \pm d_{p+k}$ for some $k > 0$. The dynamical Lie algebra $\hat{\mathcal{L}}$ generated by $i\tilde{H}_0$ and $i\hat{H}_1$ defined in (2.8) and (2.9) is $su(N)$ if $d_m \neq 0$, $E_m \neq 0$ for $1 \leq m \leq N-1$, and one of the following criteria applies:*

*(i) there exists $\omega_p \neq 0$ such that $\omega_m \neq \omega_p$ for $m \neq p$, or;*

*(ii) $\omega_m = \omega$ for $1 \leq m \leq N-1$ but there exists $v_p \neq 0$ such that $v_m \neq v_p$ for $m \neq p$.*

Roughly speaking this theorem says that the Lie algebra generated will be $su(N)$ if all the dipole couplings $d_n$ are non-zero, and

- there exists at least one frequency that is different from all others (and it is not the middle frequency if the dimension of the system is even), or
- if all the frequencies are the same then there exist three consecutively placed transition dipole moments such that the difference between the sum of the squares of the first and third, and twice the square of the middle, is not zero and is also different from all such differences between any other three consecutive transition dipole moments. If $N$ is even it is also required that there exists at least one pair of transition dipole moments, placed symmetrically either side of the middle dipole moment, whose squares are not equal.

In cases where the dynamical Lie algebra is not $su(N)$, we shall see that the Lie algebra generated depends on whether the Hilbert space dimension of the system is even or odd.

### 2.5.1 Odd-dimensional systems

In this section we are concerned with systems whose Hilbert space dimension is odd, i.e. $N = 2\ell + 1$. Consider systems of the form $\hat{H} = \hat{H}_0 + f(t)\hat{H}_1$, where

$$\hat{H}_0 = \sum_{n=1}^{2\ell+1} E_n |n\rangle\langle n| \qquad \hat{H}_1 = \sum_{n=1}^{2\ell} d_n \Big( |n\rangle\langle n+1| + |n+1\rangle\langle n| \Big). \tag{2.10}$$

Again it is assumed that the $E_n$'s are ordered in a non-decreasing sequence $E_1 \leq E_2 \leq \ldots \leq E_N$ where $E_1 \neq E_N$, none of the transition dipole moments, $d_n$'s, are zero and that the following symmetrical relations apply

$$\begin{aligned} & E_{n+1} - E_n = E_{N-n+1} - E_{N-n} \text{ i.e. } \omega_n = \omega_{N-n} \\ \text{and} \quad & d_n = d_{N-n} \qquad \text{for } 1 \leq n \leq N-1. \end{aligned} \tag{2.11}$$

In Appendix B.1.1 it is shown that the Lie algebra, $\tilde{\mathcal{L}}$ generated by $i\hat{H}_0$ and $i\hat{H}_1$ is a subalgebra of $so(2\ell+1)$. Whilst $i\hat{H}_0'$ (derived from $i\hat{H}_0$ by a change of basis) and $i\hat{H}_1$ are shown to be linear symplectic of generators of $so(2\ell+1)$ this is not sufficient for the generation of $so(2\ell+1)$. Further criteria are required and these are given by the three theorems that follow.

The result of the first theorem is effectively that the Lie algebra generated by $i\tilde{H}_0$ and $i\hat{H}_1$ is $so(2\ell+1)$ provided that the square of the central transition frequency (there are two but by (2.11) they are equal) is not equal to the square of any of the other transition frequencies. Note that the change of basis given in Appendix (B.1.1) is employed below.

Consider the system

$$i\hat{H}_0' = \sum_{m=1}^{\ell} \epsilon_m h_m \qquad i\hat{H}_1 = \sum_{m=1}^{\ell} \delta_m y_m \qquad \epsilon_m \neq 0 \quad \delta_m \neq 0 \quad \forall m \tag{2.12}$$

with $h_m$ and $y_m$ as defined in A.2 and A.4. The theorem is stated formally below [19].

**Theorem 4** *Let $\omega_m = \epsilon_{m+1} - \epsilon_m$ for $1 \leq m < \ell$ and $\omega_0 = \epsilon_1$. The dynamical Lie algebra $\tilde{\mathcal{L}}$ generated by the system $\hat{H} = \hat{H}_0' + f(t)\hat{H}_1$ with $i\hat{H}_0$ and $i\hat{H}_1$ as in (2.12) is $so(2\ell+1)$ if $\omega_m^2 \neq \omega_0^2$ for $1 \leq m \leq l$.*

The proof is given in Appendix B.1.3.

The condition, $\omega_m^2 \neq \omega_0^2$, on the transition frequencies can be relaxed and $so(2\ell+1)$ can still be generated provided there is a further restriction on the transition dipoles. Let $\mathcal{M}$ be the set of values of m for which $\omega_{l-m+1}^2 = \omega_l^2$ and let the transition dipoles, $d_n$'s, in $\hat{H}_1$ be replaced by $\tilde{\delta}_m$'s where, for $1 \leq m \leq l$, $\tilde{\delta}_m = d_{l-m+1}$ if $m \in \mathcal{M}$, $\tilde{\delta}_m$ is zero otherwise and $\tilde{\delta}_{l+1} = 0$. To aid explanations the notation $\tilde{\delta}_0 = \tilde{\delta}_1$ is introduced. As the energy levels form a non-decreasing sequence the transition frequencies, $\omega_n$'s,

are positive and $\omega_{l-m+1}^2 = \omega_l^2$ is the same as $\omega_{l-m+1} = \omega_l$ i.e. $\omega_{m-1} = \omega_0$ using the $\omega$ notation. Under these conditions $so(2\ell+1)$ will be generated provided that $2\tilde{\delta}_m^2 - \tilde{\delta}_{m+1}^2 - \tilde{\delta}_{m-1}^2 \neq 2\tilde{\delta}_1^2 - \tilde{\delta}_2^2 - \tilde{\delta}_0^2$ for all $m \in \mathcal{M}$ except for when $m$ is 1. This result is stated formally below [19].

**Theorem 5** *Let* $v_m \equiv 2\tilde{\delta}_m^2 - \tilde{\delta}_{m+1}^2 - \tilde{\delta}_{m-1}^2$ *for* $1 \leq m \leq l$, *where* $\tilde{\delta}_0 = \tilde{\delta}_1$, $\tilde{\delta}_{l+1} = 0$. *The dynamical Lie algebra* $\hat{\mathcal{L}}$ *generated by the system* $\hat{H} = \hat{H}_0' + f(t)\hat{H}_1$ *with* $i\hat{H}_0'$ *and* $i\hat{H}_1$ *as in* (2.12) *is* $so(2\ell+1)$ *if* $\omega_{m-1} = \omega_0$ *but* $v_m \neq v_1$ *for all* $m \in \mathcal{M} - \{1\}$.

The proof is given in Appendix B.1.4.

It is also possible to generate $so(2\ell+1)$ when all the energy levels are equally spaced, this gives $\omega_m = \omega_1$ for $2 \leq m \leq l$, and when all the transition dipole moments are equal i.e. $d_m = d$ for $1 \leq m \leq l$. Again using the notation employed so far this result is stated below [19].

**Theorem 6** *The dynamical Lie algebra* $\hat{\mathcal{L}}$ *generated by the system* $H = \tilde{H}_0 + f(t)\hat{H}_1$ *with* $N = 2\ell + 1$ *equally spaced energy levels* $\omega_m = \omega_1$ *and uniform dipole moments* $d_m = d$ *is* $so(2\ell+1)$.

The proof is given in Appendix B.1.5.

The following example shows that the full Lie algebra $u(N)$ is not always generated by the system and the importance of the results set out in Theorems 4, 5 and 6.

**Example 2** Consider a system with Hamiltonian $\hat{H} = \hat{H}_0 + f(t)\hat{H}_1$, where

$$\hat{H}_0 = \sum_{n=1}^{7} E_n(|n\rangle\langle n|) \qquad \hat{H}_1 = \sum_{n=1}^{6} d_n(|n\rangle\langle n+1| + |n+1\rangle\langle n|),$$

$E_n = n$ for $n = 1 \ldots 7$ and $d_1 = d_6 = \sqrt{3}$, $d_2 = d_5 = \sqrt{5}$ and $d_3 = d_4 = \sqrt{6}$ then the change of basis $\{|1\rangle, |2\rangle, |3\rangle, |4\rangle, |5\rangle, |6\rangle, |7\rangle\} \mapsto \{|4\rangle, |3\rangle, |2\rangle, |1\rangle, -|5\rangle, |6\rangle, -|7\rangle\}$ leads to

$$i\hat{H}_0' = -h_1 - 2h_2 - 3h_3 \qquad i\hat{H}_1 = \sqrt{6}y_1 + \sqrt{5}y_2 + \sqrt{3}y_3$$

with $h_m$ and $y_m$ as defined in appendices B1 and B3 respectively. Therefore, the Lie algebra $\tilde{\mathcal{L}}$ generated by $i\hat{H}_0'$ and $i\hat{H}_1$ is a subalgebra of $so(7)$. However it is easy to verify that $\tilde{\mathcal{L}} \not\cong so(7)$. Indeed, in this particular case $\tilde{\mathcal{L}}$ is a three-dimensional subalgebra of $so(7)$ and a higher order representation of $su(3)$ spanned by $i\hat{H}_0'$, $i\hat{H}_1$ and $[i\hat{H}_0', i\hat{H}_1] = \sqrt{6}x_1 + \sqrt{5}x_2 + \sqrt{3}x_3$ with $x_m$ also as defined in appendix B3. This

shows that for certain choices of the parameters $E_n$ and $d_n$, the Lie algebra $\tilde{\mathcal{L}}$ is a *proper* subalgebra of $so(7)$.

### 2.5.2 Even dimensional systems

In this section we are concerned with systems whose Hilbert space dimension is even, i.e. $N = 2\ell$. Consider systems of the form $\hat{H} = \hat{H}_0 + f(t)\hat{H}_1$, where

$$\hat{H}_0 = \sum_{n=1}^{2\ell} E_n |n\rangle\langle n| \qquad \hat{H}_1 = \sum_{n=1}^{2\ell-1} d_n \Big( |n\rangle\langle n+1| + |n+1\rangle\langle n| \Big). \tag{2.13}$$

Again it is assumed that the $E_n$'s are ordered in a non-decreasing sequence $E_1 \leq E_2 \leq \ldots \leq E_{2\ell}$ where $E_1 \neq E_{2\ell}$, none of the transition dipole moments, $d_n$'s, are zero and that the following symmetrical relations apply

$$\begin{aligned} & E_{n+1} - E_n = E_{2\ell-n+1} - E_{2\ell-n} \text{ i.e. } \omega_n = \omega_{2\ell-n} \\ \text{and} \qquad & d_n = d_{2\ell-n} \qquad \text{for } 1 \leq n \leq 2\ell - 1. \end{aligned} \tag{2.14}$$

Note that Theorem 3 does not apply to this system as $N = 2\ell$ and there is no $k$ such that $d_{\ell-k} \neq \pm d_{\ell+k}$. In Appendix B.2.1 it is shown that the Lie algebra, $\tilde{\mathcal{L}}$ generated by $i\hat{H}_0$ and $i\hat{H}_1$ is a subalgebra of $sp(\ell)$. Whilst $i\hat{H}_0'$ (derived from $i\hat{H}_0$ by a change of basis) and $i\hat{H}_1$ are shown to be linear combination of generators of $sp(\ell)$ this is not sufficient for the generation of $sp(\ell)$. Further criteria are required and these are given by the three theorems that follow.

The result of the first theorem is effectively that the Lie algebra generated by $i\tilde{H}_0$ and $i\hat{H}_1$ is $so(2\ell + 1)$ provided that the square of the central transition frequency is not equal to the square of any of the other transition frequencies. Note that the change of basis given in Appendix B.2.1 is employed below.

Consider the system

$$i\hat{H}_0' = \sum_{m=1}^{\ell} \epsilon_m h_m \qquad i\hat{H}_1 = \sum_{m=1}^{\ell} \delta_m y_m \qquad \epsilon_m \neq 0 \quad \delta_m \neq 0 \quad \forall m \tag{2.15}$$

with $h_m$ and $y_m$ as defined in A.5 and A.7. The theorem is stated formally below [19].

**Theorem 7** *Let $\omega_m = \epsilon_{m+1} - \epsilon_m$ for $1 \leq m < \ell$ and $\omega_\ell = 2\epsilon_\ell$. The dynamical Lie algebra $\hat{\mathcal{L}}$ generated by $i\hat{H}_0'$ and $i\hat{H}_1$ as in* (2.15) *and with the symmetrical relations given in* (2.11) *is $sp(\ell)$ if $\omega_m^2 \neq \omega_\ell^2$ for $m < \ell$.*

The proof is given in Appendix B.2.3.

As with Theorem 4 the condition on the transition frequencies in the theorem above can be relaxed and $sp(\ell)$ can still be generated provided there is a further restriction on the transition dipoles. Let $\mathcal{M}$ be the set of values of $m$ for which $\omega_{m-1}^2 = \omega_1^2$ and let the transition dipoles, $d_n$'s, in $\hat{H}_1$ be replaced by $\tilde{\delta}_m$'s where $\tilde{\delta}_m = d_m$ if $m \in \mathcal{M}$ and $\tilde{\delta}_m$ is zero otherwise. To aid explanations the notation $\tilde{\delta}_0$ is included and set to zero and it is noted as a consequence of (2.11) that $\tilde{\delta}_{\ell+1} = \tilde{\delta}_{\ell-1}$. As the energy levels, $E_n$'s, form a non-decreasing sequence the transition frequencies, $\omega_n$'s, are positive and $\omega_m^2 = \omega_\ell^2$ is the same as $\omega_m = \omega_\ell$. Under these conditions $sp(\ell)$ will be generated provided that $2\tilde{\delta}_m^2 - \tilde{\delta}_{m+1}^2 - \tilde{\delta}_{m-1}^2 \neq 2\tilde{\delta}_\ell^2 - \tilde{\delta}_{\ell+1}^2 - \tilde{\delta}_{l-1}^2$ for all $m \in \mathcal{M}$ except for when $m = \ell$. This result is stated formally as follows [19]

**Theorem 8** *Let $v_m = 2\tilde{\delta}_m^2 - \tilde{\delta}_{m+1}^2 - \tilde{\delta}_{m-1}^2$ for $1 \leq m \leq \ell$ and $\tilde{\delta}_{\ell+1} = \tilde{\delta}_{\ell-1}$, $\tilde{\delta}_0 = 0$. The dynamical Lie algebra $\hat{\mathcal{L}}$ generated by the system $H = \tilde{H}_0 + f(t)\hat{H}_1$ with $i\tilde{H}_0$ and $i\hat{H}_1$ as in* (2.8) *and* (2.9) *and with the symmetrical relations given in* (2.11) *is $sp(\ell)$ if $\omega_m = \omega_\ell$ but $v_m \neq v_l$ for all $m \in \mathcal{M} - \{\ell\}$.*

The proof is given in Appendix B.2.4.

It is also possible to generate $sp(\ell)$ when all the energy levels are equally spaced, this gives $\omega_m = \omega_1$ for $2 \leq m \leq \ell$, and when all the transition dipole moments are equal i.e. $d_m = d$ for $1 \leq m \leq \ell$. This result is given below [19].

**Theorem 9** *The dynamical Lie algebra $\hat{\mathcal{L}}$ generated by a system $H = \tilde{H}_0 + f(t)\hat{H}_1$ with $N = 2\ell$ equally spaced energy levels and uniform dipole moments is $sp(\ell)$.*

To show that the complete Lie algebra is not always generated by the system the example below is included. It demonstrates the importance of the results set out in Theorems 7, 8 and 9.

**Example 3** Consider a system with Hamiltonian $\hat{H} = \hat{H}_0 + f(t)\hat{H}_1$, where

$$\hat{H}_0 = \sum_{n=1}^{6} E_n(|n\rangle\langle n|) \qquad \hat{H}_1 = \sum_{n=1}^{5} d_n(|n\rangle\langle n+1| + |n+1\rangle\langle n|),$$

$E_n = n$ for $n = 1 \ldots 7$ and $d_1 = d_5 = \sqrt{5}$, $d_2 = d_4 = 2\sqrt{2}$ and $d_3$ then the change of basis $\{|1\rangle, |2\rangle, |3\rangle, |4\rangle, |5\rangle, |6\rangle\} \mapsto \{|1\rangle, |2\rangle, |3\rangle, |6\rangle, -|5\rangle, |4\rangle\}$ leads to

$$i\tilde{H}_0 = -(5h_1 + 3h_2 + 1h_3)/2, \qquad i\hat{H}_1 = \sqrt{5}y_1 + 2\sqrt{2}y_2 + 3y_3$$

with $h_m$ and $y_m$ as defined in appendix C1 and C3 respectively. Therefore, the Lie algebra $\tilde{\mathcal{L}}$ generated by $i\tilde{H}_0$ and $i\hat{H}_1$ is a subalgebra of $sp(3)$. However it is easy to verify that $\tilde{\mathcal{L}} \not\cong sp(3)$. Indeed, in this particular case $\tilde{\mathcal{L}}$ is a three-dimensional subalgebra of $sp(3)$ spanned by $i\tilde{H}_0$, $i\hat{H}_1$ and $[i\tilde{H}_0, i\hat{H}_1] = -(\sqrt{5}x_1 + 2\sqrt{2}x_2 + 3x_3)$ with $x_m$ as defined in appendix C3. This shows that for certain choices of the parameters $E_n$ and $d_n$, the Lie algebra $\tilde{\mathcal{L}}$ is a *proper* subalgebra of $sp(3)$.

### 2.5.3 Systems with direct control limited to single transition

So far we have been concerned with systems where all the transition dipole moments are modulated by the time dependent control field. In this section a system where the control field drives just one transition is considered. The Hamiltonian is of the form

$$\hat{V} = \hat{V}_0 + f(t)\hat{V}_1 \tag{2.16}$$

where

$$\begin{aligned} \hat{V}_0 &= \sum_{n=1}^{N} E_n |n\rangle\langle n| + \sum_{n=1, n\neq r}^{N-1} d_n(|n\rangle\langle n+1| + |n+1\rangle\langle n|) \\ \hat{V}_1 &= d_r(|r\rangle\langle r+1| + |r+1\rangle\langle r|) \end{aligned} \tag{2.17}$$

Defined this way $i\hat{V}_0$ and $i\hat{V}_1$ generate the Lie algebra $su(N)$ and hence systems of this kind are completely controllable provided that the squares of the transition dipole moments either side of the modulated transition are not equal i.e $d_{r+1}^2 \neq d_{r-1}^2$, the corresponding transition frequency is not zero i.e $\omega_r \neq 0$ and that none of the transition dipole moments are zero i.e $d_n \neq 0$. This result is given below.

**Theorem 10** *A quantum system with Hamiltonian* (2.16) *and* (2.17) *is completely controllable if* $d_n \neq 0$ *for* $1 \leq n \leq N-1$, $\omega_r \neq 0$ *and* $d_{r+1}^2 \neq d_{r-1}^2$.

The proof of this is given in Appendix B.3. The strategy employed is to show that the iterated commutators of the skew-Hermitian matrices $i\tilde{V}_0$ and $i\hat{V}_1$ as defined in 2.17, and their linear combinations, generate the Lie algebra $su(N)$. Fortunately, however, it suffices to show that the Lie algebra generated by $i\tilde{V}_0$ and $i\hat{V}_1$ contains all the generators of $su(N)$, i.e. $x_n \equiv x_{n,n+1}$ and $y_n \equiv y_{n,n+1}$ for $1 \leq n \leq N-1$.

**Example 4** Consider a 5-level system of this type as described in (2.17) where $E_n = n$ for $1 \leq n \leq 5$, $r = 2$, $d_1 = d_2 = d_4 = 1$ and $d_3 = 2$. The matrices $\hat{V}_0$ and $\hat{V}_1$ will be given by:

$$\hat{V}_0 = \begin{pmatrix} 1 & 1 & 0 & 0 & 0 \\ 1 & 2 & 0 & 0 & 0 \\ 0 & 0 & 3 & 2 & 0 \\ 0 & 0 & 2 & 4 & 1 \\ 0 & 0 & 0 & 1 & 5 \end{pmatrix} \qquad \hat{V}_1 = \begin{pmatrix} 0 & 0 & 0 & 0 & 0 \\ 0 & 0 & 1 & 0 & 0 \\ 0 & 1 & 0 & 0 & 0 \\ 0 & 0 & 0 & 0 & 0 \\ 0 & 0 & 0 & 0 & 0 \end{pmatrix}$$

To show that this system is completely controllable we need to show that the dynamical Lie algebra $\tilde{\mathcal{L}}$ generated by $i\hat{V}_0$ and $i\hat{V}_1$ is $su(5)$. A basis for $su(N)$ is given in Appendix A.1. To do this it is sufficient to show that $\tilde{\mathcal{L}}$ contains the generators of $su(5)$ i.e. $x_n \equiv |n\rangle\langle n+1| - |n+1\rangle\langle n|$ and $y_n \equiv i(|n\rangle\langle n+1| + |n+1\rangle\langle n|)$ for $1 \leq n \leq 4$. Firstly we note that $i\hat{V}_1 = y_2$ and we obtain $x_2$ by:

$$X_0 \equiv [y_2, i\hat{V}_0] \quad Y_0 \equiv [X_0, y_2] \quad X_0' \equiv [Y_0, y_2] \quad Y_0' \equiv [X_0', y_2]$$

$$x_2 = 3^{-1}(X_0 - X_0')$$

Now we move on to $x_1$, $y_1$, $x_3$ and $y_3$.

$$h_2 = 2^{-1}[x_2, y_2] \quad Y_1 \equiv 3^{-1}(4Y_0 + Y_0') \quad X_1 \equiv [[x_2, Y_1], y_2]$$
$$Z_1 \equiv 2^{-1}[X_1, Y_1] \quad Y_1' \equiv 2^{-1}[Y_1, Z_1] \qquad X_1' \equiv 2^{-1}[Y_1, Z_1]$$

$$y_1 = 3^{-1}(4Y_1 - Y_1') \quad x_1 = 3^{-1}(4X_1 - X_1') \quad y_3 = 6^{-1}(Y_1' - Y_1) \quad x_3 = 6^{-1}(X_1' - X_1)$$

Finally we obtain $x_4$ and $y_4$

$$h_3 = 2^{-1}[x_3, y_3] \quad W_0 \equiv i\hat{V}_0 - y_1 - 2y_3$$

$$x_4 = [h_3, W_0] \quad y_4 = [x_4, h_3]$$

We have shown that at least $su(5)$ can be generated by $i\hat{V}_0$ and $i\hat{V}_1$. Additionally since there is a non trace-zero matrix present the system generates $u(N)$ and is completely controllable.

## 2.6 Simultaneous Controllability

Theorem 1 in Section 2.3 defines degrees of controllability that apply to any quantum system. In this section we turn our attention to composite or multi-particle systems. Consider a system made up of $L$ particles or quantum units. Quantum dots [20] provide an example of such a system. Denoting the Hilbert space of the quantum unit $\ell$ as $\mathcal{H}_\ell$, the Hilbert space of the composite system is usually the tensor product space $\mathcal{H}_S = \mathcal{H}_1 \otimes \ldots \otimes \mathcal{H}_L$. If the dimension of $\mathcal{H}_\ell$ is $N_\ell$ then the dimension of $\mathcal{H}_S$ will be $N$ where $N = N_1 \times \ldots \times N_P$. If we take the Hamiltonian to be defined as in Equation (2.3) and $\tilde{H}_m$ for $m = 0 \ldots M$ as given by Equation (2.8) then, by Theorem 1, we know that the degree of controllability of this multi-particle system depends on either the dynamical Lie algebra $\mathcal{L}$ generated by the skew-Hermitian matrices $i\hat{H}_m$ for $m = 1 \ldots M$, or the dynamical Lie algebra $\tilde{\mathcal{L}}$ generated by trace-zero skew-Hermitian matrices $i\tilde{H}_m$ for $m = 0 \ldots M$ i.e the multi-particle system is

- *completely controllable* if and only if $\mathcal{L} \cong u(N)$;
- *mixed-state controllable* if and only if $\tilde{\mathcal{L}} \cong su(N)$;
- *pure-state controllable* if and only if $\tilde{\mathcal{L}} \cong su(N)$, *or if* $N$ *is even,* $\tilde{\mathcal{L}} \cong sp(N/2)$.

However, the dimension of $\mathcal{H}_P$ is potentially very large, and $\mathcal{H}_P$ is not the most appropriate Hilbert space for modelling systems where, for instance, the quantum units do not interact with each other. This situation often arises in Chemistry, where the intention is to control a number of different types of molecules, in a dilute solution, which interact simultaneously with an applied external laser pulse, but where interactions between molecules are insignificant [21]. Another example is given by ensembles of quantum dots that are close enough together so that they can be collectively addressed by the same laser pulse, but where interactions between the dots are negligible, e.g. due to weak coupling or differing dot sizes [22]. A quantum system made up of multiple non-interacting quantum units will be referred to as *decomposable* or *separable.* Placing this restriction on a multi-particle system means that it will neither be completely controllable nor mixed-state controllable nor pure-state controllable in the sense defined above. However we can consider the controllability of each quantum unit separately. Also we can consider the control of all the individual quantum units with

the same sequence of control pulses. This will be referred to as *simultaneously* controllable. Note that the ability to completely control individually each quantum unit in a multi-particle system does not necessarily mean that the multi-particle system is *simultaneously* controllable.

If we consider that each of the $L$ non-interacting quantum units is an independent subsystem represented by the Hilbert space, $\mathcal{H}_\ell$, for $\ell = 1, \ldots, L$, then an appropriate Hilbert space of the decomposable quantum system is the direct sum $\mathcal{H} = \mathcal{H}_1 \oplus \ldots \oplus \mathcal{H}_L$. With respect to a suitable basis the state of the system, $\hat{\rho}$, and the Hamiltonians, $\hat{H}_m$, for $m = 0, \ldots, M$, have a block-diagonal structure and are given by

$$\begin{aligned} \hat{\rho}(t) &= \mathrm{diag}\left(\hat{\rho}_1(t), \ldots, \hat{\rho}_L(t)\right), \\ \hat{H}_m &= \mathrm{diag}(\hat{H}_{m,1}, \ldots, \hat{H}_{m,L}), \quad m = 1, \ldots, M \end{aligned} \tag{2.18}$$

where $\hat{\rho}_\ell(t)$ and $\hat{H}_{m,\ell}$ are $N_\ell \times N_\ell$ matrices and $N_\ell = \dim(\mathcal{H}_\ell)$. From the structure of the Hamiltonian matrices (2.18) it can be seen that the dynamical Lie group of the system must be contained in $U(N_1) \times \ldots \times U(N_L)$ and that maximal orbits for a generic mixed state under the action of this Lie group are homeomorphic to $U(N_1) \times \ldots \times U(N_L)/[U(1) \times \ldots U(1)]$, where there are $N$ terms in the denominator. The latter is equivalent to $SU(N_1) \times \ldots \times SU(N_L)/[U(1) \times \ldots U(1)]$ where there are $N - L$ terms in the denominator. Setting $\alpha_{m,\ell} = \mathrm{Tr}(\hat{H}_{m,\ell})$ and defining the matrix $A$ as follows

$$A = \begin{pmatrix} \alpha_{0,1} & \cdots & \alpha_{0,L} \\ \vdots & & \vdots \\ \alpha_{M,1} & \cdots & \alpha_{M,L} \end{pmatrix} \tag{2.19}$$

we have [22, 23]

**Theorem 11 (Simultaneous Controllability).** *The independent components of a decomposable system with Hamiltonian (2.3) of the form (2.18) are* simultaneously mixed-state controllable *if and only if the dimension of the dynamical Lie algebra $\mathcal{L}$ is*

$$dim\, \mathcal{L} = r + \sum_{\ell=1}^{L} (N_\ell^2 - 1)$$

*where $r$ is the rank of the matrix $A$.*

A proof of this is given in Appendix B.4.

### 2.6.1 Simultaneous controllability of ensemble of 2-level dots

An interesting example of a system where the notion of simultaneous controllability is relevant is an ensemble of $L$ quantum dots. Suppose each dot is itself an $N_\ell$-dimensional quantum system. The results of Theorem 1 in Section 2.3 show that each of the dots is individually controllable if its associated dynamical Lie algebra $\mathcal{L}_\ell$ has dimension $N_\ell^2 - 1$ at least, and the entire ensemble is controllable as an $N$-dimensional composite system, where $N = N_1 \times \ldots \times N_L$, if the Lie algebra of the system has dimension $N^2 - 1$ at least. If inter-dot coupling is negligible then the system is decomposable, and hence not controllable as a composite system. However its components are simultaneously controllable if the Lie algebra of the system satisfies Theorem 11 in Section 2.6.

Suppose each dot can be represented as a two-level system with Hamiltonian

$$\hat{H}^{(\ell)}[f(t)] = \epsilon_\ell \hat{\sigma}_z + f(t) d_\ell \hat{\sigma}_x, \tag{2.20}$$

where $\hat{\sigma}_x$ and $\hat{\sigma}_z$ are the Pauli matrices. We can now use Theorem 11 to give explicit conditions for simultaneous controllability. If $\epsilon_\ell \neq 0$ and $d_\ell \neq 0$ then, as $[\hat{\sigma}_x, \hat{\sigma}_z] = -2i\hat{\sigma}_y$, the $\ell^{th}$ dot is individually controllable. However this is not sufficient for simultaneous controllability. If, for example, two or more dots in the ensemble have exactly the same system parameters then the Lie subalgebra they generate is a higher dimensional representation of su(2) and the dots are not simultaneously controllable. The difference between individual and simultaneous controllability can be made explicit by considering two non-interacting two-level systems simultaneously driven by a coherent control field. We can write the Hamiltonian of the composite system as $\hat{H} = \hat{H}_0 + f(t)\hat{H}_1$, where

$$\hat{H}_0 = \mathrm{diag}(E_0^{(1)}, E_1^{(1)}) \oplus \mathrm{diag}(E_0^{(2)}, E_1^{(2)})$$
$$\hat{H}_1 = d_1\hat{\sigma}_x \oplus d_2\hat{\sigma}_x.$$

$\hat{H}_0$ can further be split into a trace-zero part $\tilde{H}_0 = \epsilon_1\hat{\sigma}_z \oplus \epsilon_2\hat{\sigma}_z$, where $\epsilon_\ell = (E_1^{(\ell)} - E_0^{(\ell)})/2$ and a diagonal part $\hat{D}_0 = \alpha_1\hat{I} \oplus \alpha_2\hat{I}$, where $\alpha_\ell = (E_0^{(\ell)} - E_1^{(\ell)})/2$. If $\epsilon_\ell = 0$ and $d_\ell = 0$ then subsystem $\ell$ is not individually controllable. Hence we shall assume that $\epsilon_\ell \neq 0$ and $d_\ell \neq 0$ for $\ell = 1, 2$.

The diagonal generator $\hat{D}_0$ is not relevant for our controllability analysis. The trace-zero generators $W_1 = i\tilde{H}_0/\epsilon_1$, $W_2 = i\hat{H}_1/d_1$ give rise to the following Lie algebra:

$$W_3 = [W_2, W_1]/2 = -i(\hat{\sigma}_y \oplus ab\hat{\sigma}_y) \qquad W_4 = [W_3, W_1]/2 = -i(\hat{\sigma}_x \oplus a^2 b\hat{\sigma}_x)$$
$$W_5 = [W_3, W_2]/2 = i(\hat{\sigma}_z \oplus ab^2\hat{\sigma}_z) \qquad W_6 = [W_4, W_1]/2 = i(\hat{\sigma}_y \oplus a^3 b\hat{\sigma}_y)$$
$$W_7 = [W_3, W_4]/2 = -i(\hat{\sigma}_z \oplus a^3 b^2\hat{\sigma}_z)$$

where $a = \epsilon_2/\epsilon_1$ and $b = d_2/d_1$. Combining these terms yields

$$W_2 + W_4 = 0 \oplus (1-a^2)bi\hat{\sigma}_x \qquad a^2W_2 + W_4 = (a^2-1)i\hat{\sigma}_x \oplus 0$$
$$W_3 + W_6 = 0 \oplus ab(a^2-1)i\hat{\sigma}_y \qquad a^2W_3 + W_6 = (1-a^2)i\hat{\sigma}_y \oplus 0$$
$$W_5 + W_7 = 0 \oplus ab^2(1-a^2)i\hat{\sigma}_z \qquad a^2W_5 + W_7 = (a^2-1)i\hat{\sigma}_z \oplus 0.$$

This shows that if $a, b \neq 0, \pm 1$ then the relevant Lie algebra $\tilde{\mathcal{L}}$ of the system is $\mathrm{su}(2) \oplus \mathrm{su}(2)$.

For $\alpha = \pm 1$ we can similarly show that $V_k = W_k$ for $k = 1, 2, 3, 4$ and

$$V_5 = [V_2, V_4]/2 = \hat{\sigma}_y \oplus ab^3\hat{\sigma}_y \qquad V_6 = [V_4, V_3]/2 = i(\hat{\sigma}_x \oplus b^3\hat{\sigma}_x)$$
$$V_7 = [V_2, V_5]/2 = i(\hat{\sigma}_z \oplus ab^4\hat{\sigma}_z)$$

Combining these terms leads to

$$W_6 - W_2 = 0 \oplus b(b^2-1)i\hat{\sigma}_x \qquad b^2W_2 - W_6 = (b^2-1)i\hat{\sigma}_x \oplus 0$$
$$W_5 + W_3 = 0 \oplus ab(b^2-1)\hat{\sigma}_y \qquad b^2W_3 - W_5 = (a^2-1)\hat{\sigma}_y \oplus 0$$
$$W_7 - W_4 = 0 \oplus ab^2(b^2-1)i\hat{\sigma}_z \qquad b^2W_5 - W_7 = (b^2-1)i\hat{\sigma}_z \oplus 0.$$

This shows that if $a \neq 0, b \neq 0, \pm 1$, then the relevant Lie algebra $\tilde{\mathcal{L}}$ of the system is still $\mathrm{su}(2) \oplus \mathrm{su}(2)$, and the two subsystems are therefore simultaneously controllable.

On the other hand, if $a = \pm 1$ and $b = \pm 1$, then $V_4 = V_6 = V_2$, $V_5 = V_3$, $V_7 = V_1$, i.e., the Lie algebra is three dimensional, and since $V_3 = [V_2, V_1]$, a representation of $su(2)$. The non-interacting two-level systems are therefore individually but not simultaneously controllable.

However, even if two or more dots in the ensembles are identical, we can often recover simultaneous controllability if we can divide the ensemble into (possibly overlapping) regions that can be selectively addressed. For example, consider a five-dot ensemble

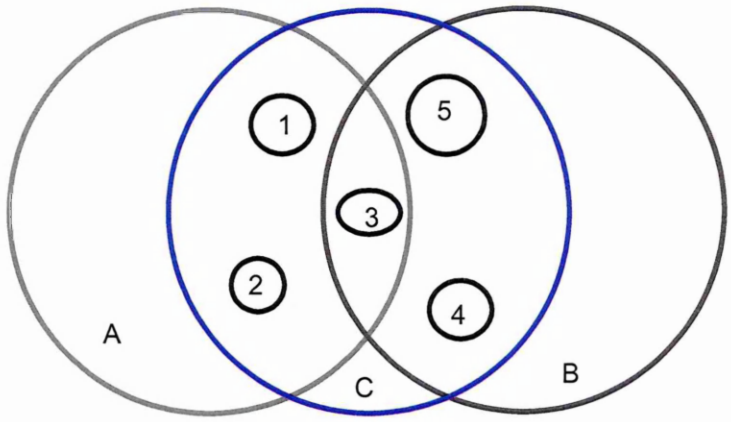


Figure 2.1: Ensemble of five quantum dots: If dots 1 and 4 are identical and the laser is addressing all the five dots within the region C then the ensemble is not simultaneously controllable. However, if we can create two regions A and B, which can be separately addressed by the laser, then the ensemble becomes simultaneously controllable despite the fact that the regions overlap.

where dots 1 and 4 are identical but all the other dots are distinct, i.e., $(\epsilon_1, d_1) = (\epsilon_4, d_4)$, but $(\epsilon_\ell, d_\ell) \neq (\pm\epsilon_{\ell'}, \pm d_{\ell'})$ for $\ell \neq \ell'$ and $\ell, \ell' \in \{1, 2, 3, 5\}$. As dots 1 and 4 have the same characteristics, $\hat{H}^{(1)} = \hat{H}^{(4)}$, the Lie algebra generated by

$$\hat{H}_0 = \epsilon_1\hat{\sigma}_z \oplus \epsilon_2\hat{\sigma}_z \oplus \epsilon_3\hat{\sigma}_z \oplus \epsilon_1\hat{\sigma}_z \oplus \epsilon_5\hat{\sigma}_z \quad \hat{H}_C = d_1\hat{\sigma}_x \oplus d_2\hat{\sigma}_x \oplus d_3\hat{\sigma}_x \oplus d_1\hat{\sigma}_x \oplus d_5\hat{\sigma}_x$$

has dimension 12, and the ensemble is *not* simultaneously controllable. However, if we can adjust the laser to create two regions A and B, encompassing dots $\{1, 2, 3\}$ and $\{3, 4, 5\}$, respectively, as shown in Fig. 2.1, for instance, simultaneously controllability can be recovered as the Lie algebra generated by $\{\hat{H}_0, \hat{H}_A, \hat{H}_B\}$ with

$$\hat{H}_0 = \epsilon_1\hat{\sigma}_z \oplus \epsilon_2\hat{\sigma}_z \oplus \epsilon_3\hat{\sigma}_z \oplus \epsilon_1\hat{\sigma}_z \oplus \epsilon_5\hat{\sigma}_z$$

$$\hat{H}_A = d_1\hat{\sigma}_x \oplus d_2\hat{\sigma}_x \oplus d_3\hat{\sigma}_x \oplus 0 \oplus 0 \qquad \hat{H}_B = 0 \oplus 0 \oplus d_3\hat{\sigma}_x \oplus d_1\hat{\sigma}_x \oplus d_5\hat{\sigma}_x$$

has dimension 15 as required.

### 2.6.2 Simultaneous controllability of ensemble of 3-level dots

We can also apply the controllability results to dots with a more complicated internal structure. For instance, consider an ensemble of $P$ dots with a twofold-degenerate internal ground state and an excited state in a $\Lambda$ configuration as shown in Fig. 2.2.

Let $\epsilon_\ell$ denote the energy gap between the degenerate ground states and the excited state, and $d_\ell^+$, $d_\ell^-$ be the dipole moments of the $\sigma_+$ and $\sigma_-$ transition, respectively, for the $\ell^{th}$ dot. Without loss of generality we can assume $\hat{H}_m = \oplus_{\ell=1}^P \hat{H}_{m,\ell}$ for $m = 0, 1, 2$, $\ell = 1, \ldots, P$, and

$$\hat{H}_{0,\ell} = \frac{\epsilon_\ell}{3}\begin{pmatrix} -1 & 0 & 0 \\ 0 & -1 & 0 \\ 0 & 0 & +2 \end{pmatrix}, \quad \hat{H}_{1,\ell} = d_\ell^+\begin{pmatrix} 0 & 0 & 1 \\ 0 & 0 & 0 \\ 1 & 0 & 0 \end{pmatrix}, \quad \hat{H}_{2,\ell} = d_\ell^-\begin{pmatrix} 0 & 0 & 0 \\ 0 & 0 & 1 \\ 0 & 1 & 0 \end{pmatrix}.$$

The ensemble is simultaneously (mixed-state) controllable exactly if the Lie algebra generated by $\{\hat{H}_m\}$ is $\oplus_{\ell=1}^P \mathrm{su}(3)$. Again, this is usually the case unless two or more dots in the ensemble are effectively identical. For example, we verified that even if $d_\ell^+ = 1$ and $d_\ell^- = -1$ for all $\ell$, the Lie algebra for a five-dot ensemble with $\epsilon_\ell = 1 + \Delta\epsilon_\ell \geq 0$ and $\Delta\epsilon_\ell \neq \Delta\epsilon_{\ell'}$ unless $\ell = \ell'$ did indeed have dimension $40 = 5 \times (3^2 - 1)$. However, if two dots have the same energy gap $\epsilon_\ell$ and the same (absolute) values of dipole moments $d_\ell^\pm$ then simultaneous controllability is lost, e.g., if we have $\epsilon_1 = \epsilon_4$ and $d_4^\pm = d_1^\pm$ or $d_4^\pm = -d_1^\pm$ then the Lie algebra dimension is only $32 = 4 \times (3^2 - 1)$. However, if $\epsilon_1 = \epsilon_4$ but $d_4^+ \neq \pm d_1^+$, for instance, then simultaneous controllability is maintained.

In the previous example, we can also ask what about controllability if we can apply a single pulse consisting of a mixture of $\sigma_+$ and $\sigma_-$ polarised light. In this case we replace $\hat{H}_1$ and $\hat{H}_2$ by the composite control Hamiltonian $\hat{H}_C = \cos\alpha \hat{H}_1 + \sin\alpha \hat{H}_2$ with $\alpha \in [0, \pi/2]$, so the single dot Hamiltonians are

$$\hat{H}_{0,\ell} = \frac{\epsilon_\ell}{3}\begin{pmatrix} -1 & 0 & 0 \\ 0 & -1 & 0 \\ 0 & 0 & +2 \end{pmatrix}, \quad \hat{H}_{C,\ell} = \begin{pmatrix} 0 & 0 & d_\ell^+ \cos\alpha \\ 0 & 0 & d_\ell^- \sin\alpha \\ d_\ell^+ \cos\alpha & d_\ell^- \sin\alpha & 0 \end{pmatrix}.$$

We see clearly that the system cannot be simultaneously controllable for $\alpha = 0$ or $\alpha = \pi/2$ as in this case none of the dots are individually controllable, their Lie algebras being contained in u(2). However, if we assume $d_\ell^- = -d_\ell^+$, which is often the case in practice, then even for $\alpha \in (0, \pi/4)$, the Lie algebra generated by $\hat{H}_{0,\ell}$ and $\hat{H}_{C,\ell}$ above is a unitary representation of $\mathrm{so}(3) \oplus \mathrm{u}(1)$. Hence, the dots are not individually controllable, and the ensemble is thus not simultaneously controllable. The Lie algebra of an ensemble of $L$ (non-identical) dots of this form is a unitary representation of $(\oplus_{\ell=1}^P \mathrm{so}(3)) \oplus \mathrm{u}(1)$. Note that so(3) is not even sufficient for pure-state controllability. If $d_\ell^- \neq \pm d_\ell^+$ then the $\ell^{th}$ dot is generally individually controllable for $\alpha \in (0, \pi/2)$

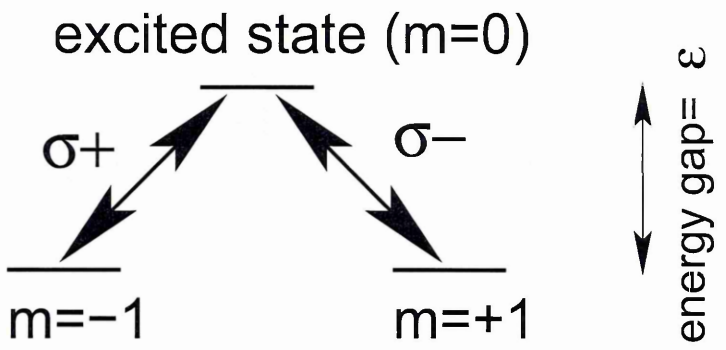


Figure 2.2: Energy level structure for three-state dot in $\Lambda$ configuration

and any ensemble of non-identical dots would be simultaneously controllable with a mixed-polarisation control pulse.

# Chapter 3

# Theory of Optimal Control of Quantum Systems

## 3.1 Overview of key techniques

There are a number of methods that have been devised to attempt control of quantum systems [24, 25, 26, 27]. These include pulse timing and multi-path interference control in the realm of chemical reaction dynamics, stimulated Raman scattering involving adiabatic passage (STIRAP) in atomic and molecular physics, and constructive geometric control, which has been used extensively in the fields of Nuclear Magnetic Resonance (NMR) [28] and Electron Spin Resonance (ESR). More recently other techniques such as learning algorithms, closed-loop feedback control and optimal control techniques [29, 30] have been introduced. It is the last of these, optimal control pulse design based on variational techniques, which will be the main focus of this chapter.

Pulse timing, also referred to as pump/dump and the Tannor-Rice method [31], is based on finding the best timing for a sequence of two coherent pulses in order to select a particular chemical reaction for instance. The laser pulses are ultra-short and are typically of the order of femto seconds. The selection of the chemical reaction is controlled by the choice of the length of time between the two pulses [32].

Multi-path interference control, or the Brumer-Shapiro control method [33, 27], attempts to steer a chemical reaction towards attaining a specified product from the

possible outcomes by modulating independent pathways from an initial state to a selected final state. The probabilities of following these pathways are typically not equal as they are proportional to the square of the sum of the amplitudes linked to the separate transitions along the individual pathways. There are two stages to the procedure. The first stage is to prepare the molecule in a linear superposition of bound eigenstates with distinct energy levels by employing a pulsed or continuous wave laser. The second stage is to use two lasers with frequencies tuned to the appropriate transitions to dissociate the superposition state [34].

STIRAP is a form of adiabatic control [35] that relies on Raman scattering for the transfer of population between two specified quantum states via other states. Scattering occurs when, for example, a molecule absorbs radiation of frequency $\nu$ and goes into an excited state. If the molecule returns to another energy state, which must be one level above or below the initial state, then energy of a different frequency from $\nu$ will be re-radiated. This is called *Raman scattering.* If the molecule returns to an energy state one level above the initial state the frequency of the re-radiated energy is referred to as the *Stokes line*; if one level below, the *anti-Stokes line* [36].

The simplest example is population transfer from an initial state to a final state via an intermediate state in three-level system, where the difference between the transition frequencies is a Stokes line. Two appropriately timed coherent pulses couple the three states. The first, or pump pulse, couples the first and intermediate states and the second, or Stokes pulse, couples the intermediate and final states. These pulses are of sufficient strength to induce many cycles of Rabi oscillations between the initial and intermediate states and also between the intermediate and final states. Experiments have shown that efficient transfer of population from the initial to the final state with negligible population of the intermediate state takes place when the Stokes pulse precedes (but overlaps with) the pump pulse, in what is known as a counter-intuitive pulse sequence. Robust extensions to higher-dimensional systems have also been proposed [37].

Geometric control techniques [38] attempt to engineer the evolution of the system by applying sequences of simple pulses. For two-level systems the pulses can be interpreted as effecting rotations about the $x$, $y$ or $z$ axis, for instance, where the rotation angle is determined by the total pulse area, whence the name geometric control. For

more complex systems or tasks the pulse sequences can be determined using Lie group decomposition techniques (see e.g. [39, 40, 41, 42, 43]). Geometric control approaches are particularly useful for control of spin dynamics [44], and systems with long relaxation times and well-separated transition frequencies, which allow frequency selective addressing of individual transitions.

Learning control techniques [45, 46] rely on genetic or evolutionary search algorithms to explore a parameter space to find control pulses that optimise a certain fitness function. Their main advantage is that they can be implemented in the laboratory without the need for a model of the system, as feedback from repeated experiments can be used to directly evaluate the fitness function [47, 48].

Although learning control techniques typically use feedback from repeated experiments to optimise the fitness of the pulses, they must not be confused with closed-loop feedback control. The latter typically rely on continuous monitoring of a system using weak measurements [49, 50, 51, 52], and the application of control fields conditional on the results of the measurement record although some schemes for fully-coherent quantum feedback have also been proposed [53]. Closed-loop feedback control has been demonstrated in cavity QED (quantum electrodynamics) experiments, but presents significant challenges in general. For instance, the back-action of the measurement on the system results in non-unitary evolution and complicated conditional dynamics. Furthermore, the need for very high detection efficiency and fast response times, appear limiting factors for other applications in quantum physics or chemistry.

Having concluded this brief overview of other control techniques, the remainder of the chapter will be devoted exclusively to variational techniques for optimal control pulse design. We will introduce the optimal control problem and describe a class of iterative solution algorithms. We then investigate their convergence properties, the optimality of the solutions obtained, and numerical implementations.

## 3.2 Optimal Control Problem

The aim of optimal control is to find a solution to the equation of motion at a specified time $t_F$ which also optimises the value of a chosen objective at $t_F$. The solution we

seek consists of a control function, $\mathbf{f}(t)$, defined for a specified time interval $[t_0, t_F]$ and the corresponding density matrix, $\hat{\rho}(t)$, solution to the quantum Liouville equation (2.2).

The basic objective is to maximise is the expectation of the chosen observable at the target time $t_F$

$$\mathcal{A} = \langle \hat{A}(t_F) \rangle = \mathrm{Tr}\left[\hat{A}\hat{\rho}(t_F)\right] \tag{3.1}$$

where $\hat{A}$ is the Hermitian operator representing the objective acting on the Hilbert space $\mathcal{H}$ and $\hat{\rho}(t_F)$ is the density operator that describes the state of the system at time $t_F$. Although this may seem to constrain the problems that can be solved it is in fact general enough to encompass the simultaneous optimisation of independent observables as these can be defined by a composite observable [54]. An alternative approach, which we will not consider here, is time-optimal control [55].

The most general problems that can be considered are those where there are dissipative effects, such as relaxation processes. However, there are a number of physical situations where dissipation is insignificant on the control time scale and so in this work we will limit ourselves to problems where these effects are assumed to negligible, that is where $\mathcal{L}_D = 0$ in (2.2). Hence, the systems we are now concerned with are Hamiltonian, although the algorithm developed can be adapted to dissipative systems as well. To maximise the value of the objective functional (3.1) a unitary operator, $\hat{U}(t)$, needs to be found that maps the eigenstates of the density operator representing the initial state so that they overlap the eigenstates of the observable at time $t_F$. Suppose we take the density operator of the initial state to be

$$\hat{\rho}(t_0) = \sum_{n=1}^{N} w_n |\Psi_n\rangle\langle\Psi_n|$$

where the eigenvalues are ordered in the following way $w_N > w_{N-1} \ldots > w_1$, and we suppose the observable at time $t_F$ is given by

$$\hat{A}(t_F) = \sum_{n=1}^{N} \alpha_n |a_n\rangle\langle a_n|$$

and with eigenvalues ordered $\alpha_N > \alpha_{N-1} > \ldots \alpha_1$. The required unitary operator $\hat{U}(t)$ must then simultaneously transform each eigenstate of $\hat{\rho}(t_0)$ i.e one of the $|\Psi\rangle$'s onto the corresponding eigenstate, $|a_n\rangle$, of $\hat{A}$ at time $t_F$, that is

$$\hat{U}(t_F)|\Psi_n\rangle \equiv |a_n\rangle$$

for all $n$ such that $1 \leq n \leq N$. It has been shown that the above is also true when the eigenvalues occur with multiplicity greater than one [11].

To return now to the two elements of the solution to the optimal control problem i.e. $\mathbf{f}(t)$ and $\hat{\rho}(t)$. We know that $\rho(\hat{t})$ is a solution to the quantum Liouville equation (2.2) and the Hamiltonian (2.3) is a functional of $\mathbf{f}(t)$. The individual components, $f_m(t)$ for $m = 1 \ldots M$, of the control field $\mathbf{f}(t)$ have the properties that they are real-valued, continuous, have continuous first derivatives and are bounded for $t \in [t_0, t_F]$, i.e.

$$\| f_m \| = \max_{t_0 \leq t \leq t_F} |f_m(t)| < \infty \tag{3.2}$$

In a practical situation the total energy of the control fields will be a *cost*, which needs to be limited as too much energy in the system could lead to dissipative effects becoming significant or to destruction of the system such as the breaking of molecular bonds or the ionisation of an atom and we are assuming that dissipative effects are negligible.

The total energy of each control field, or pulse, is given by

$$\frac{p_0^2}{h} \| f_m \|_2^2 = \frac{p_0^2}{h} \int_{t_0}^{t_F} |f_m(t)|^2 dt$$

and is finite. $p_0$ is referred to as the characteristic dipole moment of the system. It has dimensions L T I and can be measured in m C or Debye. Choosing a constant in this way allows for calculations to be independent of a particular system. The control fields, $f_m$, for $m = 1 \ldots M$, have dimensions M L $T^{-3}$ $I^{-1}$ and can be measured in N $C^{-1}$ or eV $m^{-1}$ $C^{-1}$.

The unitary operator $\hat{U}$ satisfies the Schrödinger equation (2.6) and hence is equivalent to the time-ordered exponential

$$\exp_+ \left[ -\frac{i}{\hbar} \int_{t_0}^{t_F} \left( \hat{H}_0 + \sum_{m=0}^{M} f_m(t) \hat{H}_m \right) dt \right]$$

To find an optimal solution we need then to both maximise the value of the observable at time $t_F$ and minimise the cost $\mathcal{C}$ over the time interval, where $\mathcal{C}$ is given by

$$\mathcal{C} = \sum_{m=1}^{M} \frac{\lambda_m}{2\hbar} \| f_m \|_2^2 \tag{3.3}$$

The $\lambda_m$'s are real, positive parameters with dimensions $[\hat{A}]$ $M^{-1}$ $T^4$ $I^2$, where $[\hat{A}]$ is the dimensions of the observable. This will ensure that $\mathcal{C}$ and $\mathcal{A}$ will have the same

dimensions. These $\lambda_m$'s determine the penalties associated with each control function. This will be achieved by maximising the functional $\mathcal{A}$ - $\mathcal{C}$ which is a function of, and hence depends directly on, $\hat{A}$, $\rho(\hat{t_F})$, $\lambda_m$ and $\mathbf{f}$.

From this point on it will be more convenient to employ Liouville space notation. In this notation the $N \times N$ matrix $\hat{\rho}$ is written as an $N^2 \times 1$ vector by stacking the columns and it is denoted by $|\hat{\rho}\rangle\rangle$ using the Liouville ket notation. The quantum Liouville equation is written

$$i\hbar\frac{\partial}{\partial t}|\hat{\rho}(t)\rangle\rangle = (\hat{\mathcal{L}}_0 + \sum_{m=1}^{M} f_m(t)\hat{\mathcal{L}}_m)|\hat{\rho}(t)\rangle\rangle \tag{3.4}$$

where $\hat{\mathcal{L}}_0$ is the Liouville operator representing the internal Hamiltonian, $\hat{H}_0$, and $\hat{\mathcal{L}}_m$ is the Liouville operator representing the interaction Hamiltonian, $\hat{H}_m$ associated with the control field $f_m$. These operators are represented by $N^2 \times N^2$ matrices.

## 3.3 Iterative solution algorithms

As discussed in Section 3.2 a solution consists of a control function, $\mathbf{f}(t)$, and the corresponding solution, $\hat{\rho}(t)$, to the quantum Liouville equation (3.4). Therefore an optimal solution consists of a pair $(\mathbf{f}(t), \hat{\rho}(t))$, which maximises the functional $\mathcal{A}$ - $\mathcal{C}$ and satisfies the dynamical constraints. A new functional $J$, which depends on $\mathbf{f}(t)$ and two variational trial functions, $\hat{\rho}_v$, the state of the system, and $\hat{A}_v$, the observable, can be defined which will include dynamical constraints.

$$J = \mathcal{A} - \mathcal{D} - \mathcal{C} \tag{3.5}$$

The dynamical term, $\mathcal{D}$ is given by

$$\mathcal{D} = \int_{t_0}^{t_F} \langle\langle \hat{A}_v(t)|\frac{\partial}{\partial t} + \frac{i}{\hbar}\mathcal{L}_{tot}[\mathbf{f}(t)]|\hat{\rho}_v(t)\rangle\rangle dt$$

where

$$\hat{\mathcal{L}}_{tot} = \hat{\mathcal{L}}_0 + \sum_{m=1}^{M} f_m(t)\mathcal{L}_m \quad \text{and} \quad \mathbf{f}(t) = (f_1(t), f_2(t), \ldots, f_M(t))^T$$

Among other things, $\mathcal{D}$ ensures that the quantum Liouville equation (3.4) is satisfied [56]. For $J$ to have a stationary path the variation of $J$ under independent

variations of $\hat{A}_v$, $\hat{\rho}_v$ and $\mathbf{f}(t)$ will be zero. This will be shown in Appendix C.1 to lead to the Euler-Lagrange Equations given by (3.6), (3.7) and (3.8).

$$\lambda_m f_m(t) = -i\langle\langle \hat{A}_v(t)|\mathcal{L}_m|\hat{\rho}_v(t)\rangle\rangle \tag{3.6}$$

$$i\hbar\frac{\partial}{\partial t}|\hat{\rho}_v(t)\rangle\rangle = \Big[\hat{\mathcal{L}}_0 + \sum_{m=1}^{M} f_m(t)\hat{\mathcal{L}}_m\Big]|\hat{\rho}_v(t)\rangle\rangle \tag{3.7}$$

$$i\hbar\frac{\partial}{\partial t}|\hat{A}_v(t)\rangle\rangle = \Big[\hat{\mathcal{L}}_0 + \sum_{m=1}^{M} f_m(t)\hat{\mathcal{L}}_m\Big]|\hat{A}_v(t)\rangle\rangle \tag{3.8}$$

In addition to satisfying the Euler-Lagrange equations the variational trial functions need to meet the boundary conditions

$$\hat{\rho}_v(t_0) = \hat{\rho}_0 \quad \text{and} \quad \hat{A}_v(t_F) = \hat{A}$$

As analytical solutions to sets of coupled differential equations with mixed boundary conditions such as these can usually not be found, iterative numerical methods are crucial to solve this kind of problem. These often have a common structure [27].

**Procedure 1**

1. Set $n = 0$.
2. Choose an initial trial field $\mathbf{f}^{(n)}(t) = (f_1^{(n)}(t), f_2^{(n)}(t), \ldots, f_M^{(n)}(t))^T$ satisfying (3.2).
3. Find $\hat{\rho}_v^{(n)}$ by solving the initial value problem

$$i\hbar\frac{\partial}{\partial t}|\hat{\rho}_v(t)\rangle\rangle = (\hat{\mathcal{L}}_0 + \sum_{m=1}^{M} f_m(t)\hat{\mathcal{L}}_m)|\hat{\rho}_v(t)\rangle\rangle, \qquad |\hat{\rho}_v(t_0)\rangle\rangle = |\hat{\rho}_0\rangle\rangle, \tag{3.9}$$

   integrating from $t_0$ to $t_F$.
4. Find $\hat{A}_v^{(n)}$ by solving the final value problem

$$i\hbar\frac{\partial}{\partial t}|\hat{A}_v(t)\rangle\rangle = (\hat{\mathcal{L}}_0 + \sum_{m=1}^{M} \tilde{f}_m(t)\hat{\mathcal{L}}_m)|\hat{A}_v(t)\rangle\rangle, \qquad |\hat{A}_v(t_F)\rangle\rangle = |\hat{A}\rangle\rangle \tag{3.10}$$

   integrating from $t_F$ to $t_0$.
5. Update the control field.
6. Test if convergence conditions have been achieved. If yes, then stop, otherwise increment $n$ by 1 and goto Step 3.

Among the oldest and most popular type of iterative solution algorithms are conjugate gradient methods [27], which have also recently been adapted to study optimal coherent control of dissipative N-level systems [57].

However, we will concentrate on a newer class of algorithms, which vary slightly from the above both in structure and in that two control functions, $\mathbf{f}^{(n)}(t)$ and $\tilde{\mathbf{f}}^{(n)}(t)$ are used. The first, $\mathbf{f}^{(n)}(t)$, is used in Step 3. Between Step 3 and Step 4 $\tilde{\mathbf{f}}^{(n)}(t)$ is updated using $\hat{\rho}_v^{(n)}$ and $\mathbf{f}^{(n)}(t)$ and the test for convergence is made. This class of algorithms has the advantage of strong convergence properties, in the sense that it guarantees not only convergence of the functional $J$ but convergence of the control pulses and trajectories to a solution of the Euler-Lagrange equations, as we will prove in the following sections.

Following [58, 59], the sequences of control fields $f_m^{(n+1)}(t)$ and $\tilde{f}_m^{(n)}(t)$ are generated using the following iterative formulae

$$f_m^{(n+1)}(t) = (1-\alpha)\tilde{f}_m^{(n-1)}(t) - \frac{i\alpha}{\lambda_m}\langle\langle A_v^{(n)}(t)|\mathcal{L}_m|\rho_v^{(n+1)}(t)\rangle\rangle \tag{3.11}$$

$$\tilde{f}_m^{(n)}(t) = (1-\beta)f_m^{(n)}(t) - \frac{i\beta}{\lambda_m}\langle\langle A_v^{(n)}(t)|\mathcal{L}_m|\rho_v^{(n)}(t)\rangle\rangle \tag{3.12}$$

In each case the new control field, $\tilde{f}_m^{(n)}(t)$ or $f_m^{(n+1)}(t)$, is calculated using a proportion, $1-\alpha$ and $1-\beta$ respectively, of the control field $\tilde{f}_m^{(n)}(t)$ from the previous iteration or of the control field $f_m^{(n)}(t)$ calculated earlier in the same iteration and a proportion, $\alpha$ and $\beta$ respectively, of the value of $\tilde{f}_m^{(n)}(t)$ or $f_m^{(n)}(t)$ given by the relationship (3.6) of the Euler-Lagrange equations. If $\alpha$ and $\beta$ are both equal to 1 then we have precisely that relationship. This special case is the one proposed by Zhu and Rabitz [60] and generalized in [61, 62]. For $\alpha = 1$ and $\beta = 0$ we obtain the Krotov method [27].

Since Eqs. (3.11) and (3.12) are satisfied after each iteration $\mathcal{D}$ is zero and the value of the functional $J$ after $n$ iterations is be given by

$$J^{(n)} = \langle\langle \hat{A}|\hat{\rho}_v^{(n)}(t_F)\rangle\rangle - \sum_{m=1}^{M}\frac{\lambda_m}{2\hbar}\parallel f_m^{(n)} \parallel_2^2 . \tag{3.13}$$

## 3.4 Convergence of the algorithm

The aim of this section is to show that the sequence $J^{(0)}, J^{(1)}, \ldots, J^{(n)}, \ldots$ is both increasing monotonically and bounded above and is hence convergent. Firstly a lemma

is required and this is then followed by two theorems.

**Lemma 1** *Suppose $U(t,t_0)$ is such that $U(t,t_0)^{-1}$ exists for $t \in [t_0,t_F]$ and $U(t,t_0)$ satisfies*

$$i\hbar\frac{\partial}{\partial t}\Big(U(t,t_0)\Big) = \tilde{\mathcal{L}}U(t,t_0) \tag{3.14}$$

*then*

$$|\delta\rho_v^{(n)}(t)\rangle\rangle = -\frac{i}{\hbar}\tilde{U}^{(n)}(t,t_0)\int_{t_0}^{t}\tilde{U}^{(n)}(t',t_0)^{-1}|\Delta^{(n)}(t')\rangle\rangle dt' \tag{3.15}$$

*is a solution of*

$$i\hbar\frac{\partial}{\partial t}|\delta\rho_v^{(n)}(t)\rangle\rangle = \tilde{\mathcal{L}}|\delta\rho_v^{(n)}(t)\rangle\rangle + |\Delta^{(n)}(t)\rangle\rangle. \tag{3.16}$$

*where*

$$\tilde{\mathcal{L}}^{(n)} \;=\; (\mathcal{L}_0 + \sum_{m=1}^{M}\tilde{f}_m^{(n)}\mathcal{L}_m)$$

*and*

$$|\Delta^{(n)}(t)\rangle\rangle = \sum_{m=1}^{M}[f_m^{(n+1)} - \tilde{f}_m^{(n)}]\mathcal{L}_m|\rho_v^{(n+1)}(t)\rangle\rangle + \sum_{m=1}^{M}[\tilde{f}_m^{(n)} - f_m^{(n)}]\mathcal{L}_m|\rho_v^{(n)}(t)\rangle\rangle$$

The proof of this lemma is given in Appendix C.2.

We wish to show that the sequence $J^{(0)}, J^{(1)}, \ldots, J^{(n)}, \ldots$ is convergent. This is achieved using the following theorem.

**Theorem 12** *For any bounded initial field $\mathbf{f}^{(0)}(t)$, with individual components, $f_m(t)$, that have the properties that they are real-valued, continuous, have continuous first derivatives and for $\alpha,\beta \in [0,2]$ we have*

$$\delta J^{(n)} = J^{(n+1)} - J^{(n)} \geq 0, \tag{3.17}$$

*and $J^{(n)}$ is bounded above. Hence as the sequence $J^{(n)}$ is monotonically increasing and bounded above it is convergent. Moreover, $\delta J^{(n)} = 0$ if $(\alpha,\beta) \in \{(0,0),(0,2),(2,0),(2,2)\}$.*

The proof is given in Appendix C.3.

We now wish to show that the sequence of control functions $f_m^{(n)}$ and $\tilde{f}_m^{(n)}$ converge. To do these we need to consider 4 cases and use results associated with each case from the proof to Theorem 12. Before we start with the cases we note that $f_m^{(n+1)}$, $\tilde{f}_m^{(n)}$ and

$f_m^{(n)}$ are real valued functions and that $\lambda_m > 0$ for all $m$ such that $0 \leq m \leq M$ and $\hbar \geq 0$. Also from the Theorem 12 we have that $\delta J^{(n)} \searrow 0$, i.e. $\delta J^{(n)}$ converges to 0 from above, for $\alpha, \beta \in [0, 2]$

**Case 1:** $0 < \alpha < 2$ and $0 < \beta < 2$. For this case $\delta J^{(n)}$ is defined in by C.14

$$\delta J^{(n)} = \sum_{m=1}^{M} \frac{\lambda_m}{2\hbar} \Big[ (\frac{2}{\alpha} - 1) \parallel f_m^{(n+1)} - \tilde{f}_m^{(n)} \parallel_2^2 + (\frac{2}{\beta} - 1) \parallel \tilde{f}_m^{(n)} - f_m^{(n)} \parallel_2^2 \Big]$$

$\delta J^{(n)} \searrow 0$ implies that

$$\lim_{n\to\infty} \parallel f_m^{(n+1)} - \tilde{f}_m^{(n)} \parallel_2^2 = 0 \quad \text{and} \quad \lim_{n\to\infty} \parallel \tilde{f}_m^{(n)} - f_m^{(n)} \parallel_2^2 = 0$$

hence

$$\begin{aligned} \parallel f_m^{(n+1)} - f_m^{(n)} \parallel_2^2 &\leq \Big[ \parallel f_m^{(n+1)} - \tilde{f}_m^{(n)} \parallel_2 + \parallel f_m^{(n)} - \tilde{f}_m^{(n)} \parallel_2 \Big]^2 \\ &\leq 2 \Big[ \parallel f_m^{(n+1)} - \tilde{f}_m^{(n)} \parallel_2^2 + \parallel f_m^{(n)} - \tilde{f}_m^{(n)} \parallel_2^2 \Big] \end{aligned}$$

and therefore

$$\lim_{n\to\infty} \parallel f_m^{(n+1)} - f_m^{(n)} \parallel_2^2 = 0$$

**Case 2:** $\alpha = 0$ and $0 < \beta < 2$.

For this case we know from 3.11 that $f_m^{(n+1)} = \tilde{f}_m^{(n)}$ and from C.15 that

$$\delta J^{(n)} = \sum_{m=1}^{M} \frac{\lambda_m}{2\hbar} (\frac{2}{\beta} - 1) \parallel \tilde{f}_m^{(n)} - f_m^{(n)} \parallel_2^2$$

$\delta J^{(n)} \searrow 0$ implies that $\lim_{n\to\infty} \parallel \tilde{f}_m^{(n)} - f_m^{(n)} \parallel_2^2 = 0$ and hence that

$$\lim_{n\to\infty} \parallel f_m^{(n+1)} - f_m^{(n)} \parallel_2^2 = 0$$

**Case 3:** $0 < \alpha < 2$ and $\beta = 0$.

For this case we know from 3.12 that $\tilde{f}_m^{(n)} = f_m^{(n)}$ and from C.16 that

$$\delta J^{(n)} = \sum_{m=1}^{M} \frac{\lambda_m}{2\hbar} (\frac{2}{\alpha} - 1) \parallel f_m^{(n+1)} - \tilde{f}_m^{(n)} \parallel_2^2$$

$\delta J^{(n)} \searrow 0$ implies that $\lim_{n\to\infty} \parallel f_m^{(n+1)} - \tilde{f}_m^{(n)} \parallel_2^2 = 0$ and hence that

$$\lim_{n\to\infty} \parallel f_m^{(n+1)} - f_m^{(n)} \parallel_2^2 = 0$$

**Case 4:** $\alpha = 0$ and $\beta = 0$.

For this case we know from 3.11 and 3.12 that $f_m^{(n+1)} = \tilde{f}_m^{(n)}$ and $\tilde{f}_m^{(n)} = f_m^{(n)}$ i.e. $f_m^{(n+1)} = f_m^{(n)}$ for all $n \in \mathbb{N}$. Hence

$$\lim_{n\to\infty} \| f_m^{(n+1)} - f_m^{(n)} \|_2^2 = 0$$

Thus, in all 4 cases we have

$$\lim_{n\to\infty} \| f_m^{(n+1)} - f_m^{(n)} \|_2^2 = 0$$

i.e the sequence of functions $f_m^{(n)}$ converge. Suppose this sequence converges to $f_m$. Then

$$\| \tilde{f}_m^{(n)} - f_m \|_2 \leq \| \tilde{f}_m^{(n)} - f_m^{(n+1)} \|_2 + \| \tilde{f}_m^{(n+1)} - f_m \|_2$$

shows that the sequence $\tilde{f}_m^{(n)}$ also converges to $f_m$. This is expressed in the following theorem

**Theorem 13** *The sequences of control fields $f_m^{(n)}(t)$ and $\tilde{f}_m^{(n)}(t)$ converge quadratically to a function $f_m(t)$ for each $m$ for any bounded initial field $\mathbf{f}^{(0)}(t)$ and $\alpha, \beta \in [0, 2)$.*

Notice that convergence of the field does not follow for $\alpha = 2$ and $\beta = 2$.

## 3.5 Optimality of solutions

For $\alpha, \beta \in [0, 2)$ Theorem 12 implies that $f_m^{(n)}(t)$ converges point wise to $f_m(t)$ for all $t \in [t_0, t_F]$. Hence, let $\mathbf{f}(t) = (f_1(t), \ldots, f_M(t))$ be the vector of control fields that the algorithm converges to for a given initial vector of control fields $\mathbf{f}^{(0)}$, suppose $\alpha, \beta \in [0, 2)$, and let $\hat{\rho}(t)$ and $\hat{A}(t)$ be the corresponding solutions of the initial value and final value equations

$$i\hbar \frac{\partial}{\partial t} \hat{\rho}(t)\rangle\rangle = (\hat{\mathcal{L}}_0 + \sum_{m=1}^{M} f_m(t)\hat{\mathcal{L}}_m)|\hat{\rho}(t)\rangle\rangle \quad \hat{\rho}(t_0) = \hat{\rho}_0 \tag{3.18}$$

$$i\hbar \frac{\partial}{\partial t} \hat{A}(t)\rangle\rangle = (\hat{\mathcal{L}}_0 + \sum_{m=1}^{M} f_m(t)\hat{\mathcal{L}}_m)|\hat{A}(t)\rangle\rangle \quad \hat{A}(t_F) = \hat{A} \tag{3.19}$$

Furthermore, $\delta\hat{\rho}^{(n)}(t) = \hat{\rho}(t) - \hat{\rho}_v^{(n)}(t)$ satisfies the differential equation

$$i\hbar \frac{\partial}{\partial t} \delta\hat{\rho}^{(n)}(t) = (\hat{\mathcal{L}}_0 + \sum_{m=1}^{M} f_m^{(n)}(t)\hat{\mathcal{L}}_m)|\delta\hat{\rho}^{(n)}(t)\rangle\rangle + \Delta^{(n)}(t) \tag{3.20}$$

with $\delta\hat{\rho}^{(n)}(t_0) = 0$ and

$$\Delta^{(n)}(t) = \sum_{m=1}^{M} [f_m^{(n)}(t) - f_m(t)]\mathcal{L}_m|\hat{\rho}(t)\rangle\rangle. \tag{3.21}$$

Hence, we have the formal solution

$$|\delta\hat{\rho}^{(n)}(t)\rangle\rangle = -\frac{i}{\hbar}\mathfrak{U}^{(n)}(t,t_0)\int_{t_0}^{t}\mathfrak{U}^{(n)}(t',t_0)^{-1}|\Delta^{(n)}(t')\rangle\rangle dt' \tag{3.22}$$

where $\mathfrak{U}^{(n)}(t,t_0)$ is the Liouville space propagator satisfying the homogeneous different equation

$$i\hbar\frac{\partial}{\partial t}\mathfrak{U}^{(n)}(t,t_0) = \left[\mathcal{L}_0 + \sum_{m=1}^{M} f_m^{(n)}(t)\mathcal{L}_m\right]\mathfrak{U}^{(n)}(t,t_0), \tag{3.23}$$

with $\mathfrak{U}^{(n)}(t,t_0) = \hat{I}$. Since $\lim_{n\to\infty}|\Delta^{(n)}(t)\rangle\rangle = 0$ for all $t \in [t_0,t_F]$, we thus conclude that $\delta\hat{\rho}^{(n)}(t) \to 0$, i.e. $\hat{\rho}^{(n)}(t)$ converges to $\hat{\rho}(t)$ for all $t \in [t_0,t_F]$. Similarly we can conclude that $\hat{A}_v^{(n)}(t) \to \hat{A}$ for all $t \in [t_0,t_F]$.

In addition, noting that $f_m^{(n)}(t) \to f_m(t)$ and $\tilde{f}_m^{(n)}(t) \to f_m(t)$ for all $t \in [t_0,t_F]$, we have

$$\begin{aligned} f_m(t) &= \lim_{n\to\infty} f_m^{(n)}(t) \\ &= (1-\alpha)\lim_{n\to\infty}\tilde{f}_m^{(n)}(t) - \frac{i\alpha}{\lambda_m}\lim_{n\to\infty}\langle\langle\hat{A}_v^{(n-1)}(t)|\mathcal{L}_m|\hat{\rho}_v^{(n)}(t)\rangle\rangle \\ &= (1-\alpha)f_m(t) - \frac{i\alpha}{\lambda_m}\langle\langle\hat{A}(t)|\mathcal{L}_m|\hat{\rho}(t)\rangle\rangle \end{aligned}$$

which implies the first Euler-Lagrange Equation (3.6) for $\alpha \neq 0$. For $\alpha = 0$ we can similarly conclude

$$\begin{aligned} f_m(t) &= \lim_{n\to\infty}\tilde{f}_m^{(n)}(t) \\ &= (1-\beta)\lim_{n\to\infty}\tilde{f}_m^{(n)}(t) - \frac{i\beta}{\lambda_m}\lim_{n\to\infty}\langle\langle\hat{A}_v^{(n)}(t)|\mathcal{L}_m|\hat{\rho}_v^{(n)}(t)\rangle\rangle \\ &= (1-\beta)f_m(t) - \frac{i\alpha}{\lambda_m}\langle\langle\hat{A}(t)|\mathcal{L}_m|\hat{\rho}(t)\rangle\rangle \end{aligned}$$

which also implies the first Euler-Lagrange Equation (3.6) but this time for $\beta \neq 0$. For $\alpha = \beta = 0$ we have trivially $f_m(t) = f_m^{(0)}(t)$. This proves the following:

**Theorem 14** *For $0 \leq \alpha,\beta < 2$ the solutions $\hat{\rho}^{(n)}(t)$ and $\hat{A}^{(n)}(t)$ of Equations (3.18) and (3.19) converge to functions $\hat{\rho}(t)$ and $\hat{A}(t)$, respectively, for all $t \in [t_0,t_F]$. Also for $(\alpha,\beta) \neq (0,0)$ the solution $(\hat{\rho}(t),\hat{A}(t),f_m(t))$ satisfies the Euler-Lagrange Equations (3.6), (3.7) and (3.8).*

This may seem to suggest that the choices made for the algorithm parameters $\alpha$ and $\beta$ and for the initial fields are irrelevant. However this is not necessarily so as the variational function $J$ will generally have many critical points, some of which will be close to the global maximum, while others may correspond to minima, saddle points or local maxima far from the global maximum and the choice of the parameters and initial field can influence which critical point the algorithm converges to.

## 3.6 Critical points, local vs global maxima

We have shown in Section 3.4 that the generalised algorithm described in Procedure 3.3 converges to the Euler-Lagrange equations even for $(\alpha, \beta) \neq (1, 1)$, which is a necessary condition for the solution to be a *local* maximum of the functional $J$. However it is *not* sufficient to ensure that the solution is a local *maximum* much less to ensure *global* optimality. We now address the question of how to assess the actual "degree of optimality" of a solution found by the algorithm.

In principle, we can determine if a particular solution (critical point) corresponds to a local minimum, local maximum or saddle point of the functional $J$ by computing its Jacobian matrix at the critical point and determining if it is positive definite, negative definite or indefinite. However, even this information may not be useful in practice. Indeed, a critical point for which the value of the functional $J$ is close to its global maximum *may* be more useful for practical purposes than a local maximum for which the value is far less than the global maximum, even if the former is a local minimum or saddle point. The problem is complicated by the fact that the actual value of the global maximum of $J$ is generally unknown.

We can simplify the problem by considering only the value of the objective functional $\mathcal{A}$ at the target time, or rather the *relative yield*

$$\nu_A(t_F - t_0) = \frac{\langle \hat{A}(t_F) \rangle}{\max_{\hat{\rho}(t_F)} \{ \langle \hat{A}(t_F) \rangle : \hat{\rho}(t_0) = \hat{\rho}_0 \}}, \tag{3.24}$$

where the denominator is the maximum of $\langle \hat{A}(t_F) \rangle$ over all possible final states $\hat{\rho}(t_F)$, subject to the constraint that the system is initially in the state $\hat{\rho}_0$. The global maximum of $\langle \hat{A}(t_F) \rangle$ is given by the maximum eigenvalue $a_{max}$ of $\hat{A}$, and is assumed exact if the system is in an eigenstate corresponding to $a_{max}$ at time $t_F$. However,

the global maximum $a_{max}$ is not usually attainable even if the system is completely controllable and there are no constraints on the controls.

For Hamiltonian systems the evolution of the system must be unitary, which restricts the set of states that are reachable from the initial state, and leads to tighter kinematical bounds on the expectation value of all observables. Concretely, if $w_n$ are the eigenvalues of the initial density operator $\hat{\rho}_0$ and $a_n$ those of the observable $\hat{A}$, in both cases counted with multiplicity and ordered in a non-increasing sequence, then we have

$$\sum_{n=1}^{N} w_n a_{N+1-n} \leq \langle \hat{A}(t) \rangle \leq \sum_{n=1}^{N} w_n a_n, \quad \forall t. \tag{3.25}$$

For a completely controllable (finite-dimensional) Hamiltonian system there always exists a target time $T < \infty$ such that these bounds are dynamically attainable for $t_F \leq T$ but the value of $T$ is usually unknown.

It is very important to realise that the functionals $\mathrm{Tr}[\hat{A}\hat{\rho}(t_F)]$ and $J$ have different critical points and global extrema, and that the class of algorithms described here are designed to find critical points of the functional $J$, not the unconstrained objective functional alone, i.e. we are in fact searching for the best trade-off between maximising the observable and minimising the cost while satisfying certain dynamical constraints. Note that the algorithm actually *requires* $\lambda_m > 0$ for all $m = 1 \ldots M$, and fails for $\lambda_m = 0$ as the magnitude of the control field will tend to $\infty$ as $\lambda_m \to 0$.

## 3.7 Numerical Implementation

In each step the iterative algorithm requires the solution of an initial and a final value problem, which requires numerical methods. In general, a variety of numerical techniques can be used to solve the equations. Among the most popular in the literature are Runge-Kutta and Runge-Kutta-Felberg methods such as the 4/5th order ODE routines implemented in matlab. However, for systems subject to essentially Hamiltonian dynamics it is desirable to use numerical discretisations that preserve the Lie group structure, in our case the geometry of the unitary group.

A number of very sophisticated Lie group techniques have been developed [63], and we implemented and tested some higher-order Lie group methods. However, for the

applications we studied these techniques did not appear to result in significant improvements of the numerical solutions, while increasing the complexity and execution times of the algorithm. Rather, we obtained good results with a simple Euler-type discretisation, where the time interval, $[t_0, t_F]$ was divided into $J$ equal parts of length $\Delta t = (t_F - t_0)/J$, hence the end of the $j^{th}$ time subinterval is given by $t_j = t_0 + j\Delta t$.

Only one control field was to be employed, hence $\mathbf{f} = f$ and $\tilde{\mathbf{f}} = \tilde{f}$. The values of $f$, $\tilde{f}$, $\hat{\rho}_v$ and $\hat{A}_v$ after time $t_j$ of the $n^{th}$ iteration are given by $f_j^{(n)}$, $\tilde{f}_j^{(n)}$,$\hat{\rho}_j^{(n)}$ and $\hat{A}_j^{(n)}$ respectively. The algorithm developed is as follows:

1. Choose an initial field, $f^{(0)}$.
2. Set $\hat{\rho}_0^{(n)} = \hat{\rho}_0$ for all $n$.
3. Set $\hat{A}_J^{(n)} = \hat{A}$ for all $n$.
4. Set maximum number of iterations to be performed.
5. Set a tolerance value for the change in $W$.
6. Set $n = 0$
7. If $n > 0$ calculate the field $f_j^{(n)}(t)$ for $j$ from 0 to $J-1$ using
$$f_j^{(n)}(t) = (1-\alpha)\tilde{f}_j^{(n-1)} - \frac{i\alpha}{\lambda}\langle\langle \hat{A}_j^{(n-1)}(t)|\mathcal{L}|\hat{\rho}_j^{(n)}(t)\rangle\rangle \tag{3.26}$$
8. Calculate the Hilbert space propagator $U_j^{(n)}$ and $\hat{\rho}_j^{(n)}$ for $j$ from 0 to $J-1$ using
$$\hat{U}_j^{(n)} = \exp\left\{-\frac{i}{\hbar}\Delta t\left[\hat{H}_0 + f_j^{(n)}\hat{H}_1\right]\right\}$$
$$\hat{\rho}_{j+1}^{(n)} = \hat{U}_j^{(n)}\hat{\rho}_j^{(n)}[\hat{U}_j^{(n)}]^\dagger$$
9. If $n > 0$ calculate the last component of the field, $f_J^{(n)}(t)$ using
$$f_J^{(n)}(t) = (1-\alpha)\tilde{f}_J^{(n-1)} - \frac{i\alpha}{\lambda}\langle\langle \hat{A}_J^{(n-1)}(t)|\mathcal{L}|\hat{\rho}_J^{(n)}(t)\rangle\rangle$$
10. Test to see if maximum number of iterations have been performed. If so stop, else continue.
11. Calculate the value of functional, $W^{(n)}$ using
$$W^{(n)} = \mathrm{Tr}\left(\hat{A}\hat{\rho}_J^{(n)}\right) - \frac{\Delta t\lambda}{2\hbar}\left\{\frac{[f_0^{(n)}]^2 + [f_J^{(n)}]^2}{2} + \sum_{j=1}^{J-1}[f_j^{(n)}]^2\right\}$$

12. If $n > 0$ calculate $W^{(n)} - W^{(n-1)}$. If this value is less than the tolerance chosen in Step 5 then stop.

13. Calculate the field $\tilde{f}^{(n)}(t)$, the Hilbert space propagator $U_j^{(n)}$ and $\hat{A}_j^{(n)}$ for $j$ from $J$ through to 1 using

$$\begin{aligned} \tilde{f}_j^{(n)}(t) &= (1-\beta) f_j^{(n)} - \frac{i\beta}{\lambda} \langle\langle \hat{A}_j^{(n)}(t) | \mathcal{L} | \hat{\rho}_j^{(n)}(t) \rangle\rangle \\ \hat{U}_j^{(n)} &= \exp\left\{ -\frac{i}{\hbar} \Delta t \left[ \hat{H}_0 + \tilde{f}_j^{(n)} \hat{H}_1 \right] \right\} \\ \hat{A}_{j-1}^{(n)} &= [\hat{U}_j^{(n)}]^\dagger \hat{A}_j^{(n)} \hat{U}_j^{(n)} \end{aligned} \tag{3.27}$$

14. Calculate the first component of the field, $\tilde{f}_0^{(n)}(t)$ using

$$\tilde{f}_0^{(n)}(t) = (1-\beta) f_0^{(n)} - \frac{i\beta}{\lambda} \langle\langle \hat{A}_0^{(n)}(t) | \mathcal{L} | \hat{\rho}_0^{(n)}(t) \rangle\rangle$$

15. Increment $n$ by 1 and go to Step 7.

## 3.8 Realisation of optimal pulses in the laboratory

The procedure we have followed so far was to start with a physical situation, make simplifying assumptions, formulate a model and find a method for solving the resulting optimal control problem. Although the latter is usually a complicated inverse problem, we have shown that there is a particular class of iterative algorithms, which have good convergence properties and yield control pulses that are at least weakly optimal in the sense that the converged field and corresponding trajectory satisfy the Euler-Lagrange equations. We shall now discuss briefly how the optimal control pulses obtained theoretically can be implemented in practice using pulse shaping technology.

A standard experimental setup for creating shaped pulses, consisting of a pulsed laser, diffraction gratings (DE), an acoustic optical modulator (AOM) and a phase shifter (PS) is shown in Fig. 3.1. The (Gaussian) wave packet emitted by the pulsed laser passes through a diffraction grating, which effectively Fourier-transforms the pulse, turning a narrow time-domain wave packet into a broad frequency-domain wave packet. The different Fourier components are then individually manipulated, e.g., using an acoustic optical modulator to attenuate the values of certain frequency components as

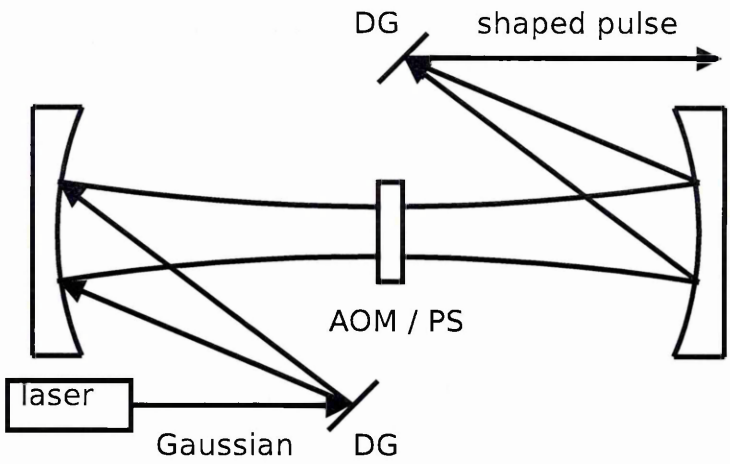


Figure 3.1: Schematic of experimental pulse shaping setup

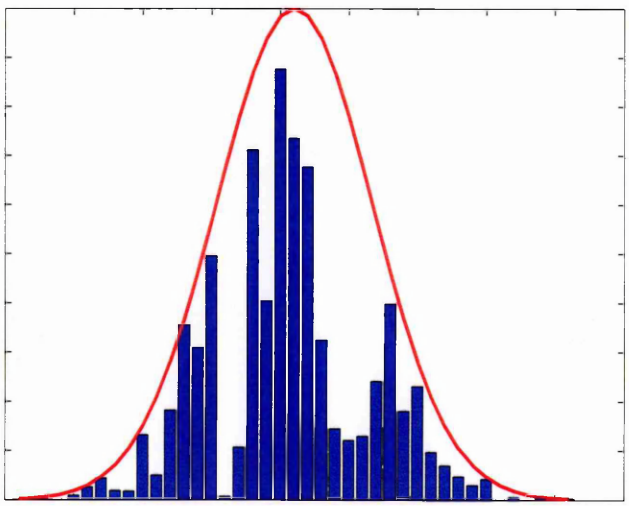

Figure 3.2: Attenuation of the frequency components of a Gaussian pulse using AOM

shown in Fig. 3.2, followed by a phase shifter to change the phase of each component. Finally, the modulated frequency components are recombined with a second diffraction grating, resulting in a complex time-domain pulse.

To utilise this setup to implement our control pulses, all we have to do is to convert our time-domain pulses to the Fourier domain by taking the Fourier transform. Since we compute the values of the field only at discrete times, it is natural to use the discrete Fourier transform. Taking discrete Fourier transform of the (real) vector representing our optimal pulse results in a complex vector. The absolute values of the components of this vector correspond to the magnitudes of the frequency components of the pulse; the polar angle to the phase.

Knowledge of the shape and magnitude of the time-domain pulse produced by the pulsed laser and the parameters of the diffraction grating allows us, in principle, to calculate the frequency domain wave packet. If the incoming pulse is Gaussian then the Fourier-transformed pulse will have also have a Gaussian profile, and we can calculate its width and height from the width and height of the original pulse. The information about the amplitude and phase of the Fourier components can therefore be used directly to calculate the necessary attenuations and phase shifts to implement the desired pulse with the pulse shaping setup shown.

The accuracy with which we can reproduce complicated pulses depends on the bandwidth and frequency resolution, which are determined by the number and width of the cells of the AOM/PS, respectively, and of course, the spectrum of the input pulse and the details of diffraction gratings used.

# Chapter 4

# Application of Optimal Control of Quantum Systems

Having shown how to calculate optimal pulse shapes and how to implement them in the laboratory, the next logical step is to apply the technique to problems of practical interest. We will mainly focus on selective excitation of a particular mode for complex multi-level systems, which is a central problem in atomic and molecular physics, mode-selective chemistry, and more recently, solid-state quantum technology. Among the specific examples we consider are the excitation of a certain mode in a generic three-level $\Lambda$ system, the selective excitation of a particular quantum dot in an ensemble of dots that is globally addressed by a single laser field, and the selective excitation of a vibrational mode for a simple molecule.

## 4.1 Generic 3-level system

In Section 2.6.2 a two-fold-degenerate internal ground state and an excited state in a $\Lambda$ configuration (see Figure 2.2) was introduced and shown not to be controllable when driven by a single mixed-polarisation field. In particular, one can show that, if the system is driven by a single field which contains an equal mixture of $\sigma^+$ and $\sigma^-$ polarisation, then it can be decomposed into a two-level system comprised of the superposition state $(|1\rangle + |3\rangle)/\sqrt{2}$ and the upper state $|2\rangle$, as well as a decoupled 'dark state' $(|1\rangle - |3\rangle)/\sqrt{2}$.

With respect to the basis $\{|1\rangle, |3\rangle, |2\rangle\}$ the internal Hamiltonian $\hat{H}_0$ and external Hamiltonian $\hat{H}_1$ are given by

$$\hat{H}_0 = \frac{\epsilon}{3}\begin{pmatrix} -1 & 0 & 0 \\ 0 & -1 & 0 \\ 0 & 0 & +2 \end{pmatrix}, \quad \hat{H}_1 = d\begin{pmatrix} 0 & 0 & 1 \\ 0 & 0 & 1 \\ 1 & 1 & 0 \end{pmatrix}.$$

For generic systems in general we define characteristic or base units for the angular frequency and for the dipole moments. Take these to be $\omega_0$ for the angular frequency and $p_0$ for the dipole moment. For this system put $\epsilon = \hbar\omega_0$ and $d = p_0$. The control fields will then be in units of $\frac{\hbar\omega_0}{p_0}$.

The decomposition is achieved by applying the change of basis

$$\{|1\rangle, |3\rangle, |2\rangle\} \rightarrow \{(|1\rangle + |3\rangle)/\sqrt{2}, (|1\rangle - |3\rangle)/\sqrt{2}, |2\rangle\}$$

. With respect to this basis the Hamiltonian matrices are given by

$$\hat{H}_0 = \frac{\epsilon}{3}\begin{pmatrix} -1 & 0 & 0 \\ 0 & -1 & 0 \\ 0 & 0 & +2 \end{pmatrix}, \quad \hat{H}_1 = d\begin{pmatrix} 0 & 0 & \sqrt{2} \\ 0 & 0 & 0 \\ \sqrt{2} & 0 & 0 \end{pmatrix}.$$

There is no change in the internal Hamiltonian but the entries in the external Hamiltonian show that the only possible transitions are between the 'light state' $(|1\rangle + |3\rangle)/\sqrt{2}$ and the excited state $|2\rangle$. Thus the 'dark state' has become decoupled from the system.

Therefore, if the system is initially in the superposition state $(|1\rangle + |3\rangle)/\sqrt{2}$ we can transfer 100% of the population to the upper level $|2\rangle$. Figure 4.1 shows that this can almost be achieved using the algorithm. However, because of the decoupling, if the system is initially in the dark state $(|1\rangle - |3\rangle)/\sqrt{2}$ then it is not possible to get any population in the upper state $|2\rangle$. Calculations using the algorithm verify this. Whatever values of the parameters $\alpha$, $\beta$ and $\lambda$ are tried, the algorithm always converges to the zero control field, regardless of the initial field used to start the iteration.

If the system is initially in the left ground state $|1\rangle$ then the maximum population that the upper state $|2\rangle$ can attain is 50% as $|1\rangle = \left[(|1\rangle + |3\rangle)/\sqrt{2} + (|1\rangle - |3\rangle)/\sqrt{2}\right]/\sqrt{2}$. Figure 4.2 shows the result of using the algorithm to find a control field to effect this population transfer and demonstrates that a value of very close to the 50% limit can

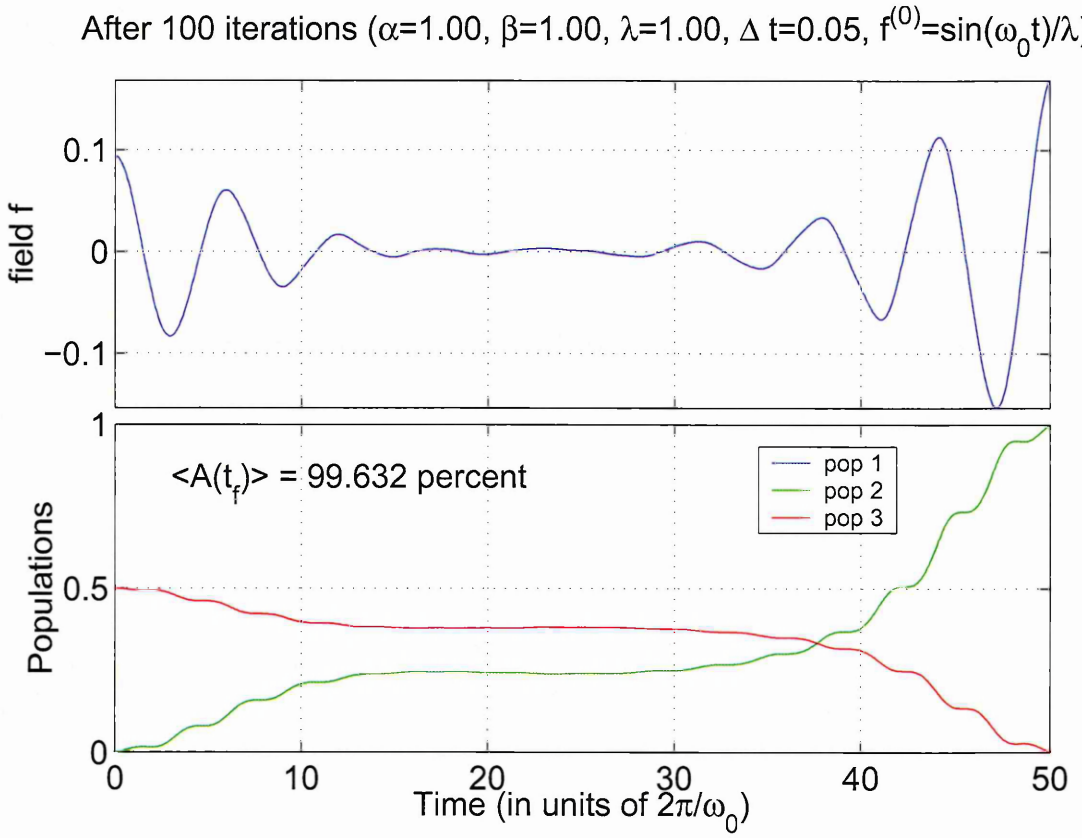


Figure 4.1: Excitation of upper level $|2\rangle$ for a $\Lambda$ system, initially in the superposition state $(|1\rangle + |3\rangle)/\sqrt{2}$, driven by a single mixed-polarisation pulse. The shaped pulse achieves almost 100% population transfer. $\omega_0$ is the characteristic frequency of the system. The control field is measured in units of $\hbar\omega_0/p_0$ where $p_0$ is the characteristic dipole moment of the system.

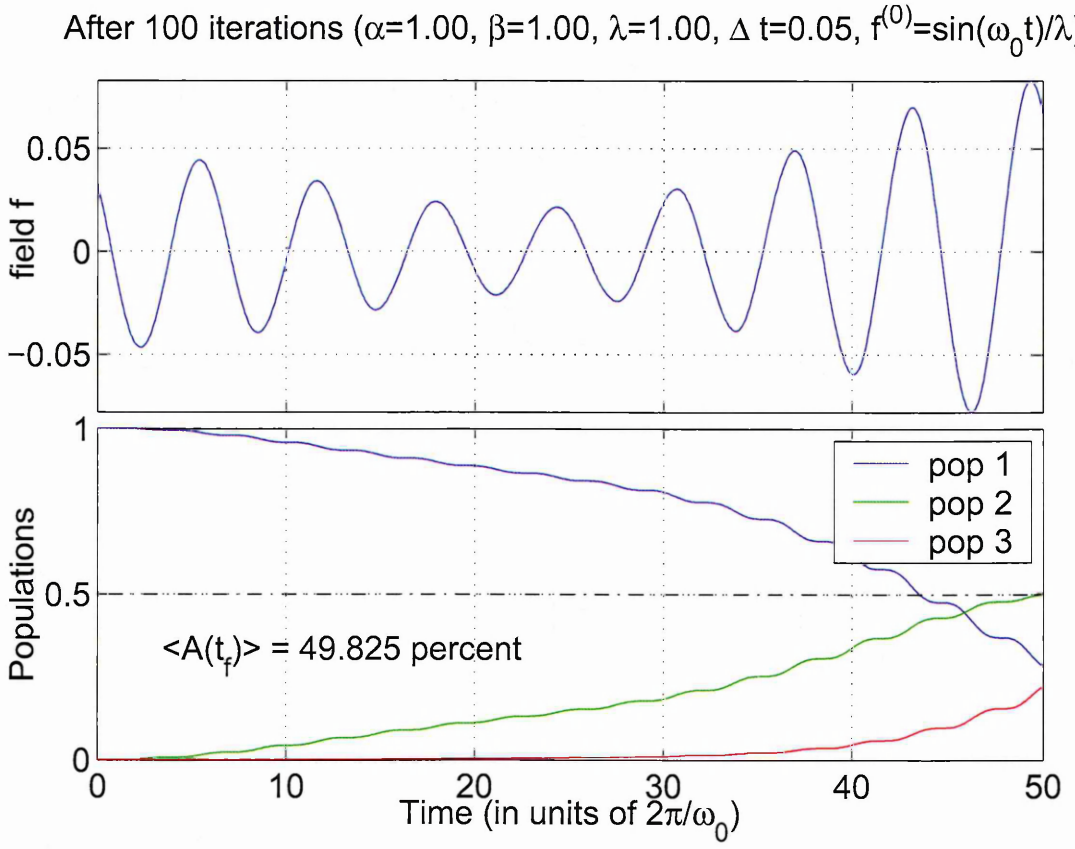


Figure 4.2: Excitation of upper level $|2\rangle$ for a $\Lambda$ system, initially in the left ground state $|1\rangle$, driven by a single mixed-polarisation pulse. The shaped pulse achieves close to the optimum of 50% population transfer. $\omega_0$ is the characteristic frequency of the system. The control field is measured in units of $\hbar\omega_0/p_0$ where $p_0$ is the characteristic dipole moment of the system.

be obtained this way. This scheme could be used to directly distinguish between the superposition states $(|1\rangle + |3\rangle)/\sqrt{2}$ and $(|1\rangle - |3\rangle)/\sqrt{2}$ by continuously driving the system with a resonant field which is an equal mixture of $\sigma^+$ and $\sigma^-$ polarisation. Suppose the system is initially in the light state $(|1\rangle + |3\rangle)/\sqrt{2}$. When driven by the field described there will be population transfer to the excited state which, in time, will decay and fluorescence will be seen. However if the system is initially in the dark state the field will not transfer population to the excited state, as they are decoupled, and there will be no fluorescence.

It was also demonstrated in Section 2.6.2 that when two (independent) fields with suitable polarisation are applied the system is controllable. Figure 4.3 shows two optimal fields calculated by the algorithm. The effect of these fields is to transfer population, initially in equal amounts in the two ground states, completely to the upper state.

## 4.2 Control of ensembles of quantum dots

Simultaneous controllability of an ensemble of non-interacting quantum dots implies in particular that it is possible to selectively excite a particular dot with a single laser pulse without the need for selective addressing. If the energy level of the dots, and hence their resonance frequencies, are different, a standard approach would be to use frequency-selective addressing using simple, e.g., Gaussian pulses resonant with the transition frequency of the dots to be excited. However, this may be less than optimal, especially when the pulse length is kept to a minimum to achieve fast operations, which would be crucial in quantum information processing applications. The question therefore naturally arises as to whether, or not, the results could be improved using optimally shaped pulses.

### 4.2.1 Selective excitation, the benefit of pulse-shaping for 2-level systems of dots

To address this question, we consider an ensemble of five quantum dots, modelled as two-level systems with energy differences $\epsilon_\ell$ of 1.32, 1.35, 1.375, 1.38, and 1.397 eV. If

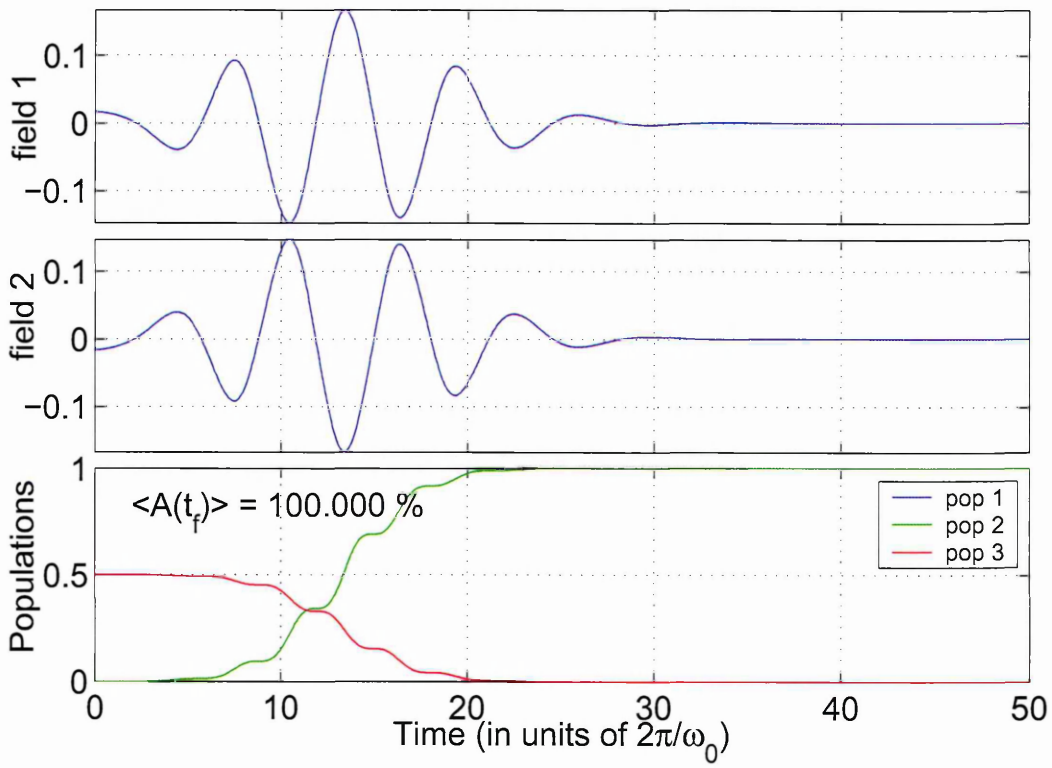


Figure 4.3: Excitation of upper level $|2\rangle$ for a $\Lambda$ system, initially in state $(|1\rangle - |3\rangle)/\sqrt{2}$, simultaneously driven with two independent control fields with $\sigma^+$ and $\sigma^-$ polarization, respectively. As expected, 100% population transfer is achieved. The algorithm parameters used are $\alpha = 1$, $\beta = 1$, $\lambda_1 = 1$ and $\lambda_2 = 1$. The initial trial fields were $f_1^{(0)} = \sin(\omega_0 t)/\lambda_1$ and $f_2^{(0)} = \sin(\omega_0 t)/\lambda_2$. $\omega_0$ is the characteristic frequency of the system. The control fields are measured in units of $\hbar\omega_0/p_0$ where $p_0$ is the characteristic dipole moment of the system. The figure shows the results after 100 iterations.

inter-dot coupling is negligible, the internal system Hamiltonian is

$$\hat{H}_0 = \mathrm{diag}(\hat{H}_{0,1}, \ldots, \hat{H}_{0,5}), \qquad \hat{H}_{0,\ell} = \epsilon_\ell \hat{\sigma}_z/2, \tag{4.1}$$

and the Hamiltonian that describes the coupling to the external driving field is

$$\hat{H}_1 = \mathrm{diag}(\hat{H}_{1,1}, \ldots, \hat{H}_{1,5}), \qquad \hat{H}_{1,\ell} = d_\ell \hat{\sigma}_x/2, \tag{4.2}$$

where $d_\ell$ is the dipole coupling of the $\ell^{th}$ dot to the field. Even if we assume, for simplicity, that all the dipole couplings are equal $d_\ell = 1$ for $\ell = 1, \ldots, 5$, the dots are still simultaneously controllable, and in particular we can selectively excite a single dot without spatial addressing.

Selective excitation of a particular dot requires sufficient frequency resolution. In particular, the frequency resolution $\Delta\omega$ should be less than the difference between the transition energy of the target dot and the next closest transition energy (divided by $\hbar$). Thus for selective excitation of the first dot we need $\Delta\omega \leq 0.03$ [eV/$\hbar$], and thus a pulse of length $t_F \geq 2\pi/0.03 \approx 200$ time units. However, the selectivity of population transfer achieved by a 200 time unit pulse depends significantly on the pulse shape.

Figure 4.4 shows the evolution of the ground and excited state populations of the dots if we simply apply a $\pi$-pulse, resonant with the transition frequency of the first dot with Gaussian envelope $A(t) = q\sqrt{\pi}\exp[-q^2(t - t_F/2)^2]$, where $q = 4/t_F$ and the target time is $t_F = 200$ time units ($\approx$ 130 fs). Although the pulse achieves almost 100% population transfer from the ground to the excited state for the target dot, it also leads to significant unwanted excitation of energetically adjacent dots. This effect becomes even more pronounced as the pulses become shorter, or the differences in transition frequencies of the dots smaller.

Figure 4.5 shows that we can considerably improve the results in this case using shaped pulses. The shaped pulse still achieves near perfect excitation of the target dot but considerably reduces the overall excitation of the other dots. More importantly though, while there is some remaining transient excitation of the other dots, the shaped pulse ensures that the populations of the excited states return to (almost) zero at the target time, except for the target dot, for which the excited state population is almost 1.

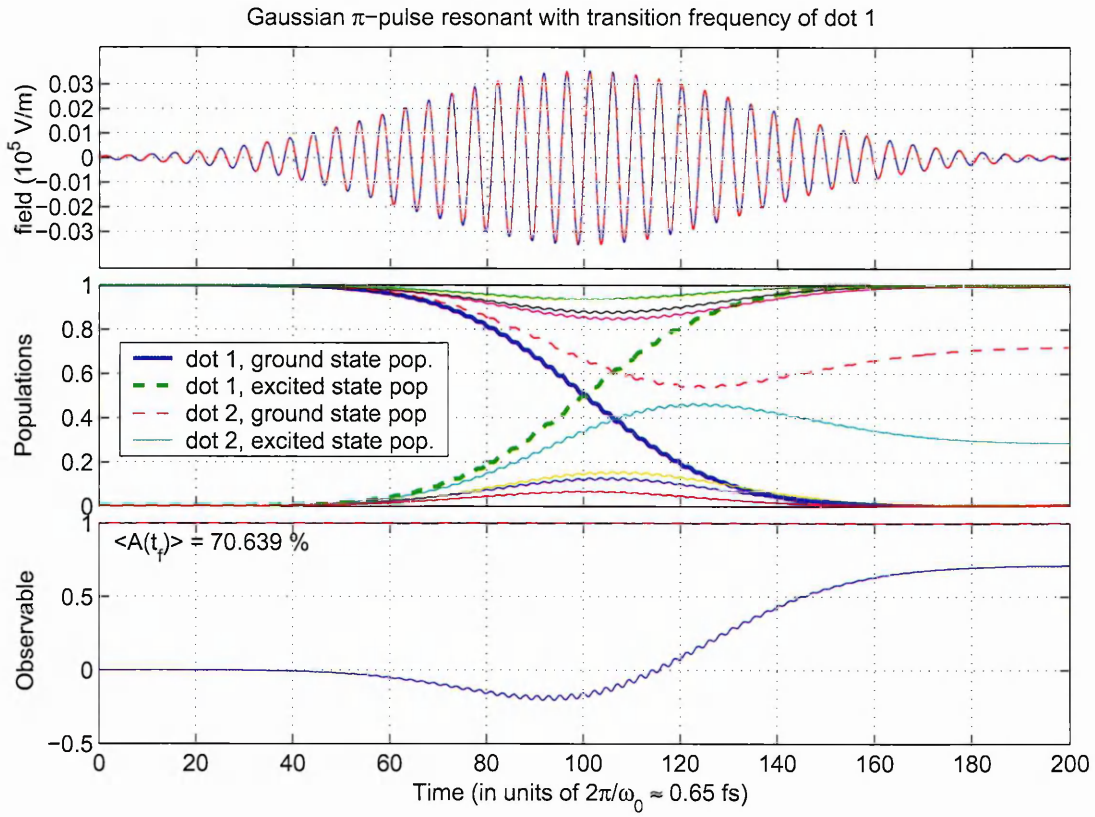


Figure 4.4: Selective excitation of dot 1: control field (in units of $10^5$ V m$^{-1}$) and evolution of the populations for a frequency-selective Gaussian pulse.
$\omega_0 = 9.67 \times 10^{15}$rad s$^{-1}$. Control field $f = (1/50)\sqrt{\pi}\exp(-(1/5)^2(t-100)^2)\sin(\omega_0 t)/\lambda$.

The pulse shown in Figure 4.5 was obtained using the iterative optimal control algorithm developed in Section 3.7. The starting point for the algorithm was the Gaussian pulse shown in Figure 4.4. The observable to be optimised was chosen to be $\hat{A} = \mathrm{diag}(\hat{P}, \hat{Q}, \hat{Q}, \hat{Q}, \hat{Q})$, where $\hat{P} = |1\rangle\langle 1|$ is the projection onto the upper level and $\hat{Q} = -\hat{P}$ to reflect our objective of simultaneously maximising the excited state population of the first dot and minimising the excitation of all other dots. Note that this is not the only possible choice of the observable but the results of the algorithm depend significantly on the choice of the target observable. For example, choosing $\hat{A}' = \mathrm{diag}(\hat{P}, \hat{0}, \hat{0}, \hat{0}, \hat{0})$ is a bad choice and does not improve results because, although the initial Gaussian pulse accomplishes the objective of achieving 100% population transfer for the target dot, the populations of the other dots do not affect the expectation value of $\hat{A}'$ and hence the algorithm does nothing to alter the pulse shape in an attempt to suppress the off-resonant excitation of the other dots.

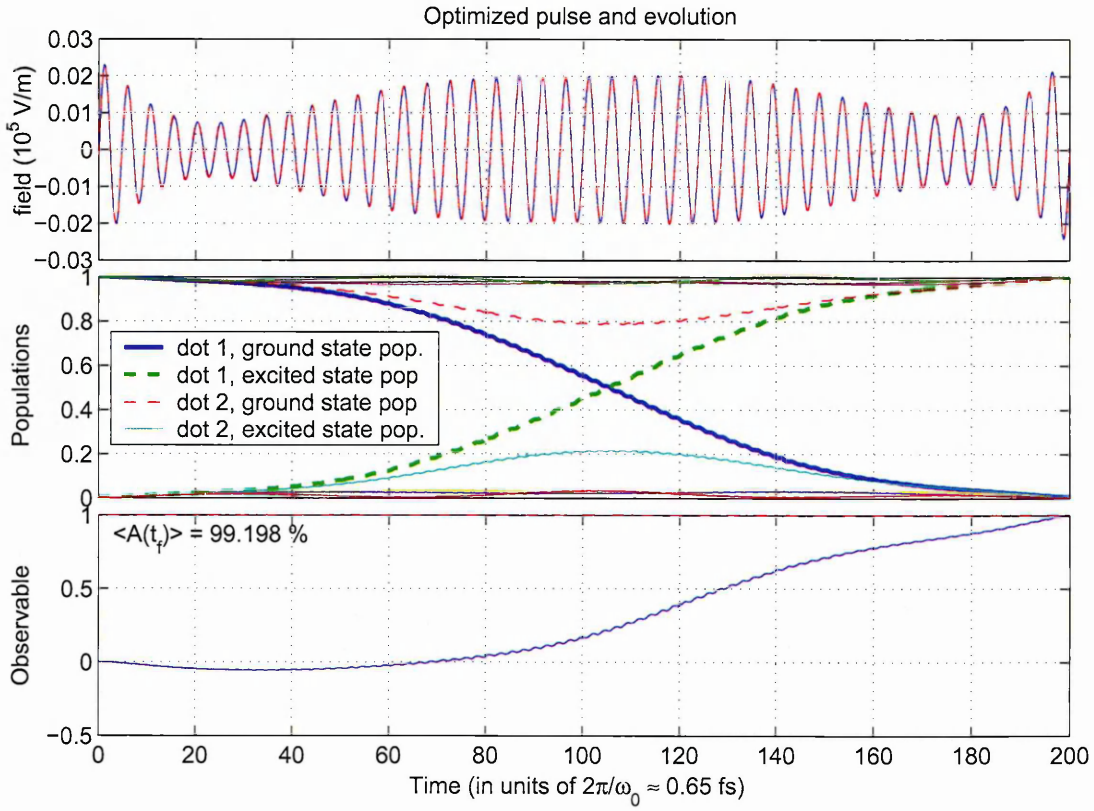


Figure 4.5: Selective excitation of dot 1: control field (in units of $10^5$ V m$^{-1}$) and evolution of the populations for an optimally shaped pulse after 200 iterations. $\omega_0 = 9.67 \times 10^{15}$ rad s$^{-1}$.
Initial trial control field $f^{(0)} = (1/50)\sqrt{\pi}\exp(-(1/5)^2(t-100)^2)\sin(\omega_0 t)/\lambda$.
Algorithm parameters are $\alpha = 1$, $\beta = 1$ and $\lambda = 4$.

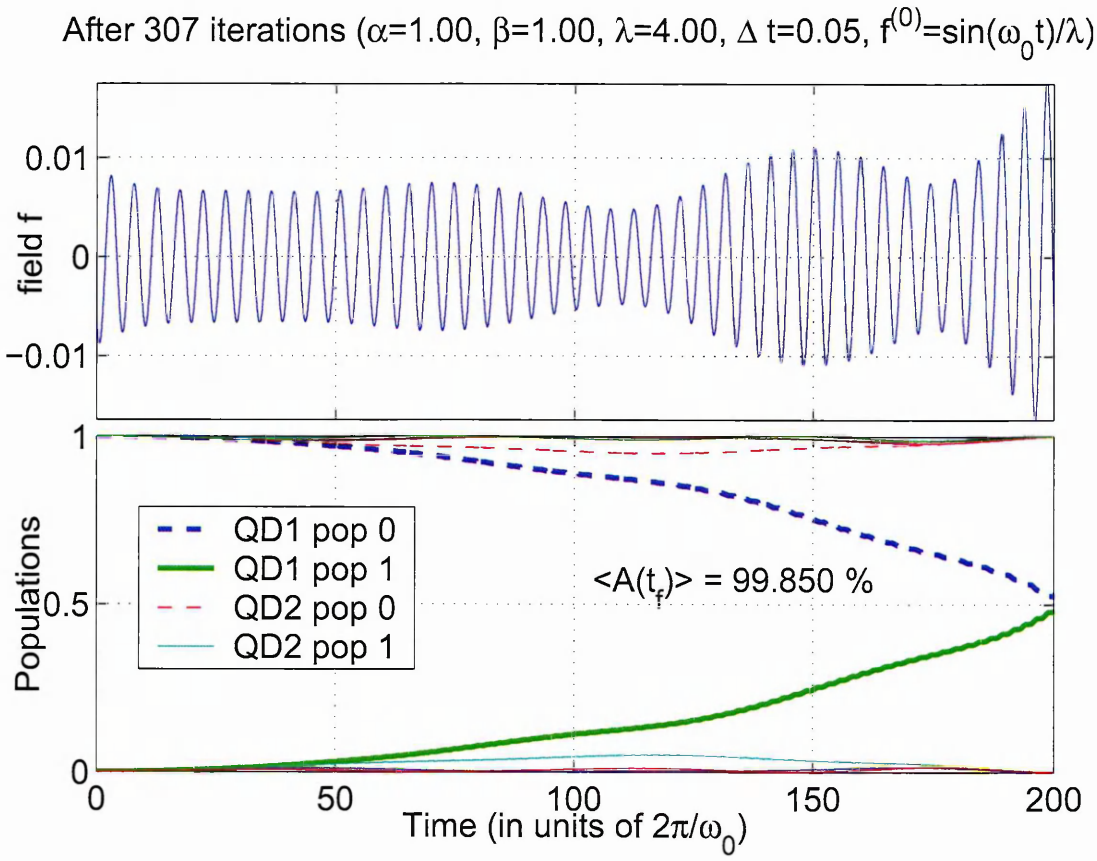


Figure 4.6: Selective preparation of superposition state $(|0\rangle+|1\rangle)/\sqrt{2}$ in dot 1: optimal control field (in units of $10^5$ V m$^{-1}$) and corresponding evolutions of the populations. $\omega_0 = 9.67 \times 10^{15}$ rad s$^{-1}$.

### 4.2.2 Selective preparation of a superposition state

A more interesting application than selective population inversion is the selective preparation of superposition states in one or more dots. As a specific example we consider the case of preparing dot 1 in the superposition state $|\Psi\rangle = (|0\rangle + |1\rangle)/\sqrt{2}$. To compute the optimal pulse we choose the observable $\hat{A} = \mathrm{diag}(\hat{S}, \hat{Q}, \hat{Q}, \hat{Q}, \hat{Q})$ where $\hat{S}$ is the projector onto the desired superposition state $|\Psi\rangle\langle\Psi|$, and $\hat{Q} = -|1\rangle\langle 1|$ as before. The results are shown in Figure 4.6.

### 4.2.3 Simultaneous excitation of two dots

We can also design pulses that perform certain operations on more than one dot simultaneously. A simple example is simultaneous population inversion in dots 1 and

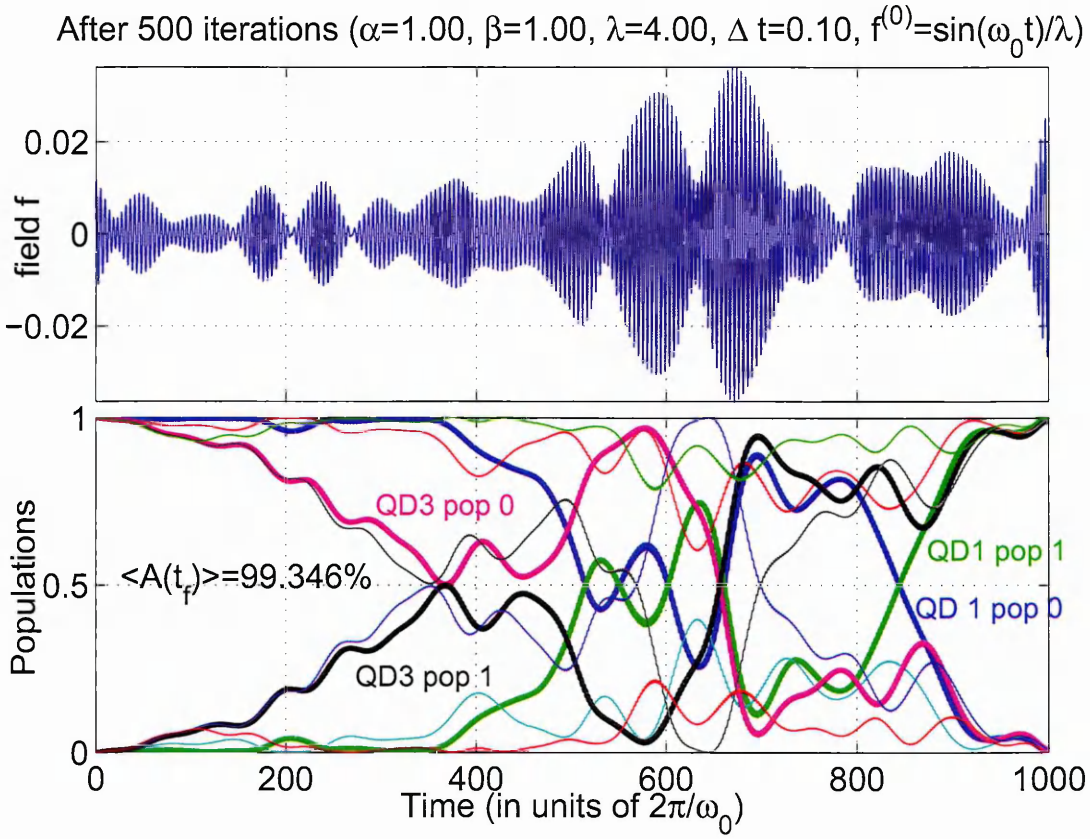


Figure 4.7: Simultaneous excitation of dots 1 and 3 for five-dot ensemble. Applying the optimal control pulse (top) leads to complicated system dynamics (bottom) but the net effect is a simultaneous population inversion in dots 1 and 3, while the excited state populations of all other dots return to 0 at the final time (and the their ground state populations return to 1). Both control fields in units of $10^5$ V m$^{-1}$. $\omega_0 = 9.67 \times 10^{15}$ rad s$^{-1}$.

3 without excitation of the other dots in the ensemble. Note that we have to choose a longer pulse to selectively excite dot 3 because the energetically closest dot (No. 4) is only detuned by $\Delta\omega = 0.005$ [eV/$\hbar$], which suggests a pulse of length $t_F \geq 2\pi/0.005 \approx$ 1250 time units to ensure sufficient frequency resolution. However, Figure 4.7 shows that we still achieve very good results using optimally shaped pulses that are only 1000 time units long.

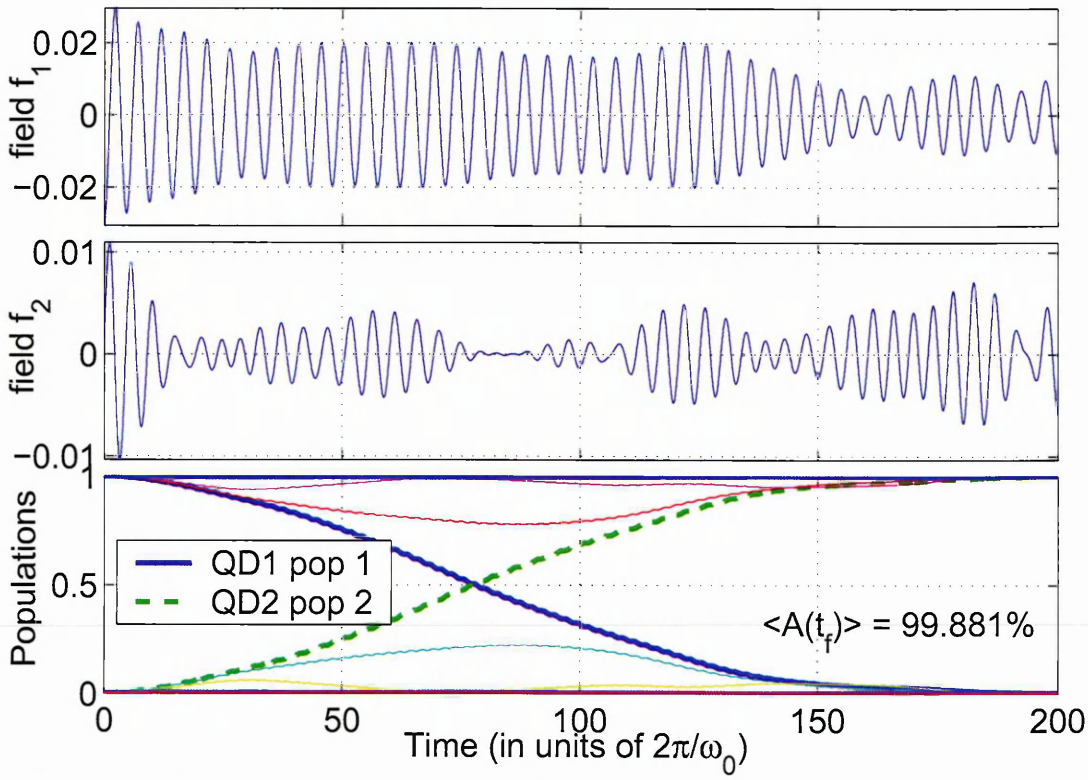


Figure 4.8: The top and middle graphs show the two independent applied fields (both in units of $10^5$ V m$^{-1}$) calculated by the algorithm for the selective excitation of dot 1. The bottom graph shows that the effect is to transfer the population in the ground state of dot 1 to the excited state. $\omega_0 = 9.67 \times 10^{15}$ rad s$^{-1}$. Algorithm parameters are $\alpha = 1$, $\beta = 1$, $\lambda_1 = 4$ and $\lambda_2 = 4$.

### 4.2.4 Control of ensemble containing two identical dots

In this section we return to the 5-dot ensemble, considered in Section 2.6.1, where dots 1 and 4 are the same. It was shown that this ensemble is not simultaneously controllable with a single field but if two lasers are employed then it is. Figure 4.8 shows the result of applying two optimised control fields to get selective excitation of dot 1. The population of dot 1 is initially in the ground state and is transferred to the excited state with a yield of 99.881%.

## 4.3 Control of vibrational states

### 4.3.1 Hydrogen Fluoride Model

The hydrogen fluoride molecule is a polarised linear molecule with 24 vibrational states each associated with different energy levels. However, we shall consider only the first ten vibrational states as the probabilities of achieving the energy levels required for the next fourteen vibrational states are small and ignoring these states will have little effect on the activity at the lower levels. A further modelling assumption is that the only dipole moments taken into account are those between neighbouring energy levels as the matrix elements for non-adjacent energy levels are comparatively small. To model this situation the values of the energy levels and the values of the dipole moments are required. We shall assume a Morse Oscillator model where the energy levels are given in [64] by:

$$E_n = \hbar\omega_0\Big(n-\frac{1}{2}\Big)\Big[1-\frac{B}{2}\Big(n-\frac{1}{2}\Big)\Big]$$

where $B = 0.0419$. In terms of $\hbar\omega_0 = 7.882 \times 10^{-20} J = 0.492\ eV$ the values of $E_n$ are 0.4948, 1.4529, 2.3691, 3.2434, 4.0758, 4.8663, 5.6149, 6.3216, 6.9864 and 7.6093 for $n = 1 \ldots 10$ respectively. A Hilbert space $\mathcal{H}$ of dimension 10 is employed. With respect to the standard basis $\{|1\rangle, |2\rangle, \ldots, |10\rangle\}$ the internal Hamiltonian, $\hat{H}_0$ will be given by a 10 by 10 diagonal matrix with these values of $E_n$ on the leading diagonal. $|1\rangle$ is the ground state.

Using the Morse Oscillator model the dipole moment for transition from level $n$ to $n+1$ is $p_0\sqrt{n}$ where $p_0 = 3.24 \times 10^{-31}$ mC $= 0.097$ Debye. In terms of $p_0$ and with respect

to the standard basis for $\mathcal{H}$ the interaction Hamiltonian is given by $\hat{H}_1$, where

$$\hat{H}_1 = \sum_{n=1}^{9} \sqrt{n}\Big(|n\rangle\langle n+1| + |n+1\rangle\langle n|\Big)$$

For convenience we shall use the standard units $\hbar\omega_0$ for the energy, $2\pi\omega_0^{-1} = 8.41$ fs for the time and $\hbar\omega_0 p_0^{-1} = 2.4327 \times 10^{11}$ Vm$^{-1}$ for the electric field strength.

To be able to selectively address individual transitions, the frequency resolution of the pulse should be better than $2\pi/(\omega_n - \omega_{n+1})$. Noting that the frequencies for transitions between adjacent energy levels are $\omega_n = (E_{n+1} - E_n)/\hbar = \omega_0(1 - Bn)$ and the detuning is $\Delta = \hbar(\omega_n - \omega_{n+1}) = \hbar\omega_0 B$ for all $n$, this implies that the target time $t_F$ should be greater than $2\pi(\omega_0 B)^{-1} \approx 200$fs ($1/B$ time units), and we shall see that the yield, i.e., expectation value of the observable at the target time, generally increases for larger $t_F$ as long as dissipative processes are negligible.

We must also choose a sufficiently small time step $\Delta t$ to be able to resolve all relevant frequencies when we numerically solve the differential equations. In general, $\Delta t$ should be sufficiently smaller than the inverse of the largest frequency $\nu_{max}$ we wish to resolve. For instance in our example, we want to resolve at least frequencies up to $\nu_{max} = \omega_0/(2\pi)$, if possible, and thus $\Delta t$ should be less than $1/10$ time units, and a smaller time step will be required if the system is driven hard. However choosing a larger $\Delta t$ can be useful in avoiding solutions with high-frequency components.

Next we must choose the penalty weight [1] $\lambda$, which determines the trade-offs between maximising the objective and minimising the costs. The choice of $\lambda$ is very important. If, on the one hand, we choose $\lambda$ small we may theoretically achieve high yields but we are likely to obtain control pulses that are more complex and energetic than necessary, and hence may be harder to reproduce in the laboratory, or may result in unnecessarily complex dynamics with possible undesirable side effects. Also, very small values of $\lambda$ and the resulting hard pulses will require a very small time step to ensure convergence of the numerical algorithm, and may also result in pulses with unwanted high-frequency components. On the other hand large $\lambda$ will over emphasise the cost and tend to result in low yield solutions. Unfortunately, there does not appear to be any simple rule for choosing $\lambda$.

[1] Since we are dealing with only a single field, we shall drop the index $m$ for the remainder of this section.

Lastly we turn to the question of how to choose the initial trial fields to start the algorithm and the algorithm parameters $\alpha$ and $\beta$. Again the choices made can significantly influence the solution that the algorithm converges to, but there is simple rule for making good choices. Sine and cosine waves of fixed frequency and magnitude, Gaussian wave packets or even random noise are popular choices for the initial trial field. Our extensive trials suggest that, given that the frequencies and magnitudes of the initial fields are reasonable for the problem, most of these choices will work, although the resulting solutions tend to differ widely. The most important aspect regarding the choice of the initial fields seems to be to ensure that the magnitudes are large enough to prevent convergence to the zero-field solution, which can occur if the first few fields result in zero yield of the observable but not so large that they either result in convergence to unnecessarily hard pulses, or that they lead to numerical instabilities.

### 4.3.2 Selective excitation of mode $|7\rangle$

The first problem to be attempted is to assume that initially the total population is in the ground state and to find a shaped pulse that will transfer the total population to the seventh level, i.e. $\hat{\rho}_0 = |1\rangle\langle 1|$ and $\hat{A} = |7\rangle\langle 7|$.

A number of choices of algorithm parameters have to be made. These include the initial trial field, $\alpha$, $\beta$ and $\lambda$. A sine wave was chosen for the initial trial field and after some experimentation a value of 5.5 was chosen for $\lambda$. It is shown in Chapter 3, section 3.4 that the values of $\alpha$ and $\beta$ must be in the following range $0 \leq \alpha, \beta \leq 2$.

Experimentation is used again in finding suitable values of $\alpha$ and $\beta$. Figure 4.9 shows the % yield given by various values of $\alpha$ and $\beta$. From this we can see that many different pairs of values can give a high yield and the shape of the fields are also quite different. From among all the possible pairs of values $\alpha = 0.6$ and $\beta = 1.2$ were chosen. Figure 4.10 shows the resultant field, the evolutions of the various the populations and the behaviour of the observable from $t_0$ to $t_F$. The pair of values for $\alpha$ and $\beta$ were chosen because the yields they gave were high.

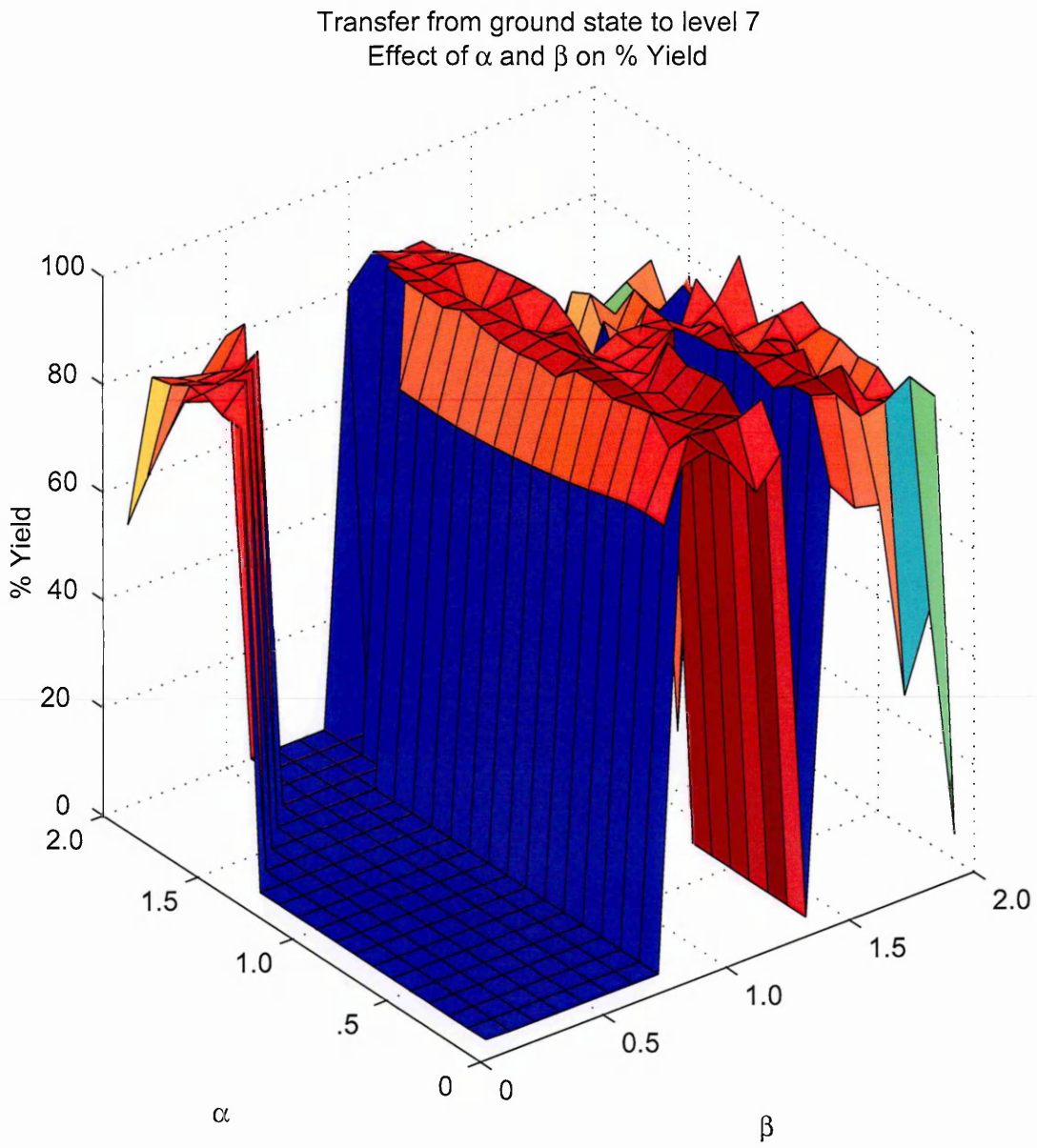


Figure 4.9: Graph of yield against $\alpha$ and $\beta$ for transfer of population from $|1\rangle$ to $|7\rangle$

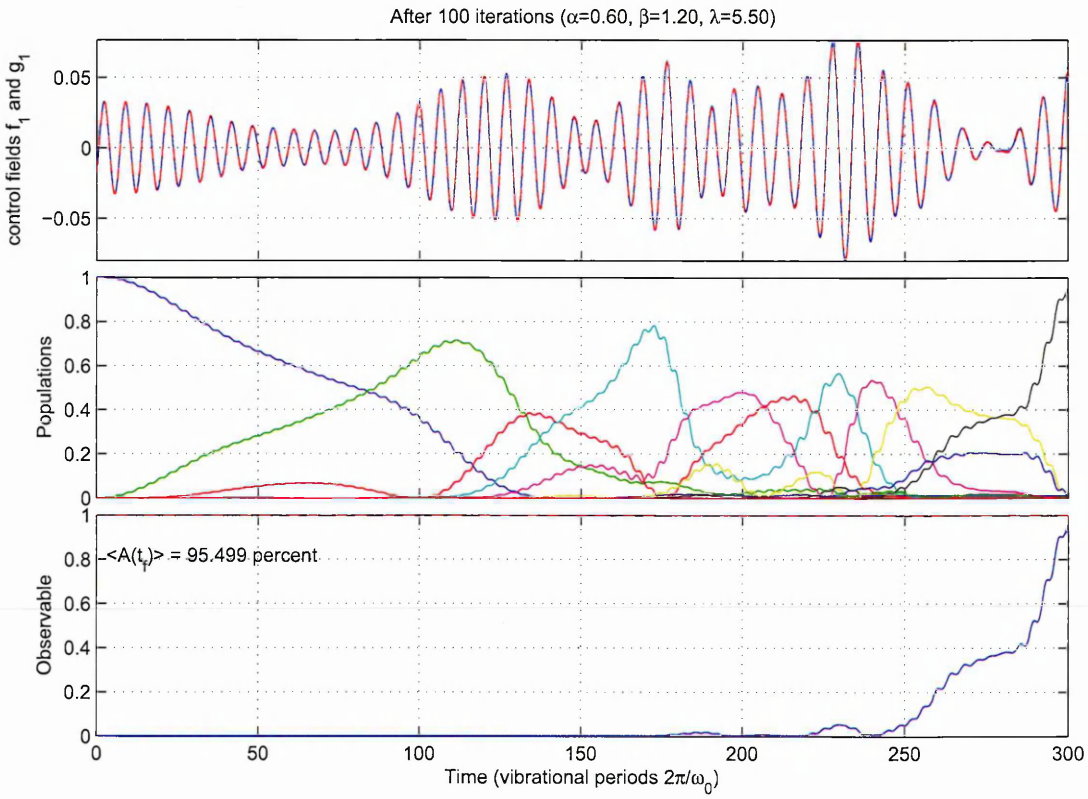


Figure 4.10: Top graph shows the optimal control field. The middle shows the evolutions of the populations. The bottom graph shows the evolution of the observable. $\omega_0 = 7.47 \times 10^{14}$. Initial trial field $f^{(0)} = \sin(\omega_0 t)/\lambda$. Field strength measured in units of $\hbar\omega_0 p_0^{-1} = 2.4327 \times 10^{11}\text{V m}^{-1}$.

### 4.3.3 Inversion of thermal equilibrium

The second problem was to find a shaped pulse that would invert the population. Thus the population that is initially in level $n$ is transferred to level $11-n$ for $1 \leq n \leq 10$. Initially the system was in thermal equilibrium. That is the population in each level is proportional to the negative exponential of its energy level. Hence, in this case,

$$\rho_0 = \sum_{n=1}^{10} \left( \frac{e^{-E_n}}{\sum_{n=1}^{10} e^{-E_n}} \right) e_{n,n}$$

where $P_n$ is the population of level $n$ and $E_n$ is the energy of level $n$ and

$$A = \sum_{n=1}^{10} \left( \frac{e^{-E_n}}{\sum_{n=1}^{10} e^{-E_n}} \right) e_{11-n,11-n}$$

The initial trial field was again chosen to be a sine function. However after some experimentation the value of $\lambda$ chosen for this problem was 1.5. Having fixed these the yield was calculated for values of $\alpha$ and $\beta$ in the range $0 \leq \alpha, \beta \leq 2$. Figure 4.12 shows the results of these calculations. Again there were many pairs of values for $\alpha$ and $\beta$ which gave high yields. $\alpha = 0.20$ and $\beta = 1.10$ were chosen.

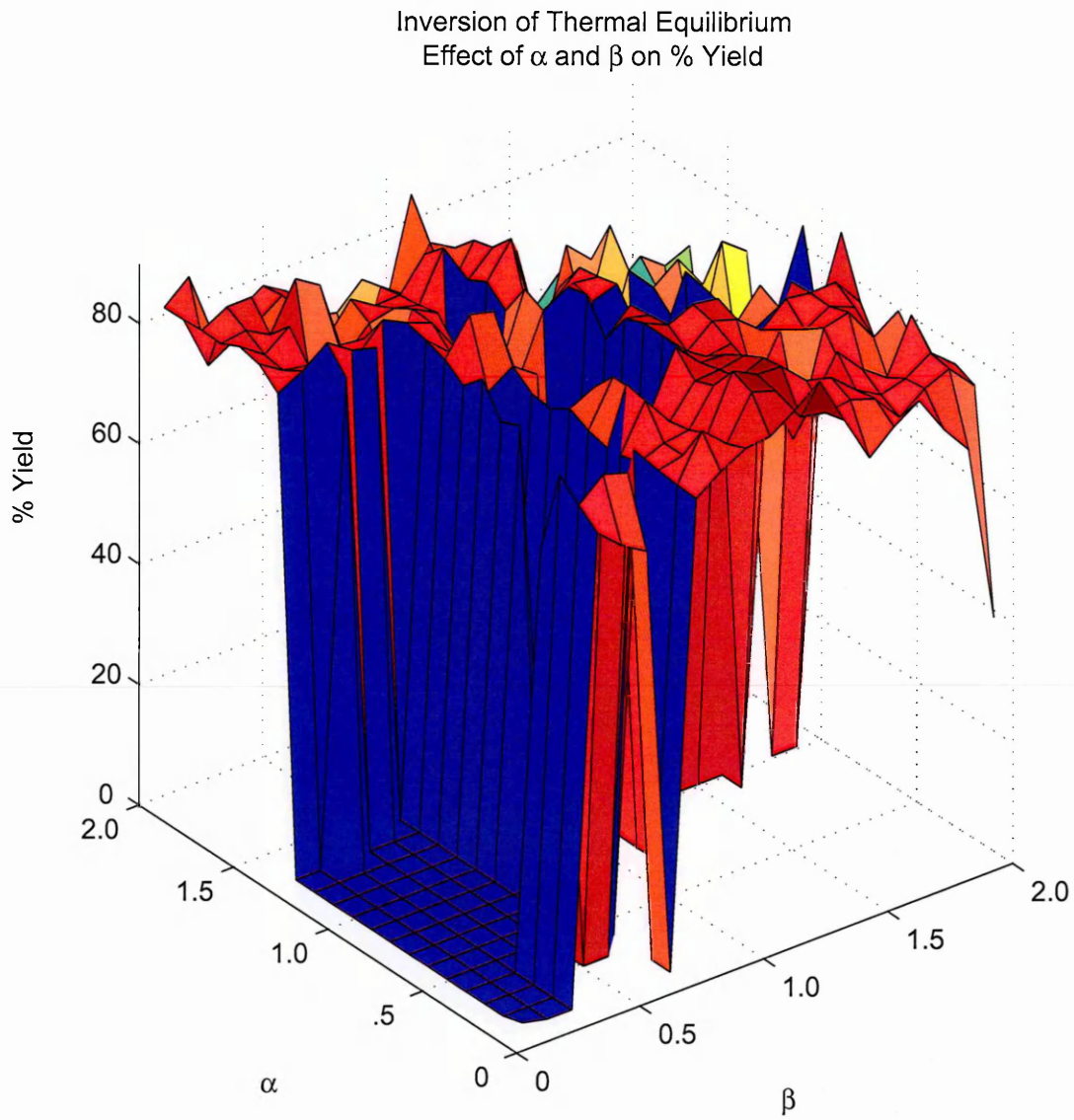


Figure 4.11: Graph of yield against $\alpha$ and $\beta$ for inversion of thermal equilibrium

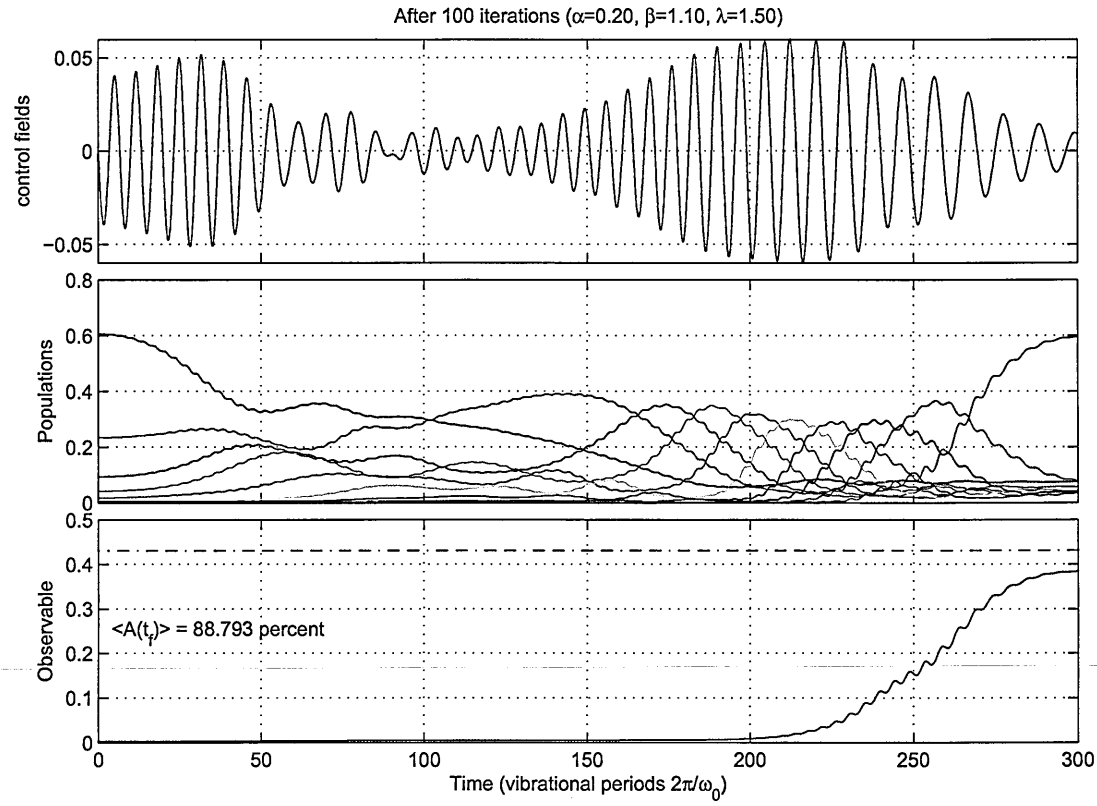


Figure 4.12: Top graph shows the optimal control field. The middle shows the evolutions of the populations. The bottom graph shows the evolution of the observable. $\omega_0 = 7.47 \times 10^{14}$. Initial trial field $f^{(0)} = \sin(\omega_0 t)/\lambda$. Field strength measured in units of $\hbar\omega_0 p_0^{-1} = 2.4327 \times 10^{11}\text{V m}^{-1}$. In the bottom graph the dotted red line represents the upper kinematical bound of the observable. The observable attains 88.793% of this value at the final time.

# Chapter 5

# Robustness

## 5.1 Introduction

One of the problems we set out to solve in Section 4.3.1 was to find an optimal control field that would achieve a population transfer from the ground state to the seventh level i.e. $\hat{\rho}_0 = |1\rangle\langle 1|$ and $\hat{A} = |7\rangle\langle 7|$, using the notation from that section. The value of the observable, as a percentage, referred to as the yield, gives the measure of success for a given solution. It turns out that there are many possible solutions. However, firstly the solutions are calculated based on a model, usually imperfect, of the physical system, and secondly it may not be possible to replicate physically calculated solutions to a high degree of accuracy. For these reasons it is of interest to investigate how good an approximation to a calculated solution is in practice.

It has been argued qualitatively that optimal control solutions are generally insensitive to minor perturbations [65]. However, we would like to quantify the robustness of various solutions with regard to their sensitivity to noise, and see if some solutions can be regarded as better than others. Furthermore, we would also like to know how sensitive a given optimal field is with regard to inaccuracies in values of the system parameters such as uncertainty in values used for the energy levels and dipole couplings.

Our general approach to measure the robustness of the solutions is to add noise in some way to the field $f(t)$, or to perturb the values of certain system parameters in our model, and to see in each case what difference this makes to the value of the

| Solution No. | 1 | 2 | 3 | 4 | 5 | 6 | 7 | 8 | 9 | 10 |
|---|---|---|---|---|---|---|---|---|---|---|
| $\alpha$ | 0 | 0.2 | 0.5 | 0.6 | 0.8 | 1 | 1.2 | 1.4 | 1.6 | 1.7 |
| $\beta$ | 0.8 | 1.6 | 1 | 1.2 | 1.4 | 1.8 | 1.2 | 0 | 0.2 | 1 |
| yield % | 93 | 92 | 90 | 95 | 88 | 91 | 89 | 89 | 80 | 86 |
| marker | $\triangleright$ | $\star$ | $\triangle$ | $\triangledown$ | $\Diamond$ | $\square$ | $\times$ | $*$ | $\circ$ | $+$ |

Table 5.1: Characteristic parameters of optimal fields chosen for robustness analysis. Given are the values of the algorithmic parameters $\alpha$, $\beta$, the yield and the markers used to indicated the results for the respective solution in subsequent graphs.

yield. In the following we consider the effect of both temporal and spectral noise, as well as uncertainties in the values of the dipole moments and the energy levels, respectively.

The types of noise or modulation were added randomly up to a set incremental level. This was performed 100 times for each incremental level and the yield obtained. The means and standard deviations of these samples were calculated. Plots were made of the sample yields against the incremental increases in noise or modulation. The product moment correlation coefficient was calculated and was found to be significant in many cases. In these cases the line of linear regression was determined and its gradient used as a measure of robustness. The closer the gradient is to zero the less sensitive the field is to noise or modulation and the more robust the field is as a solution.

## 5.2 Fields selected for robustness analysis

In the algorithm choices of the trial control field and the parameters $\alpha$, $\beta$ and $\lambda$ give rise to different solutions. After some experimentation $\lambda$ as 5.5 and sine as the trial control function were chosen. Ten different pairs of values were selected for $\alpha$ and $\beta$ which gave solutions with approximately the same yield. Further sections will contain a number of graphs comparing these solutions. Markers are used to help identify the line corresponding to a given solution. Table 5.1 gives the values of $\alpha$ and $\beta$ chosen, the yield and the marker for the ten chosen solutions. For the ten solutions the shape of the control field and the observable over the time interval were quite different

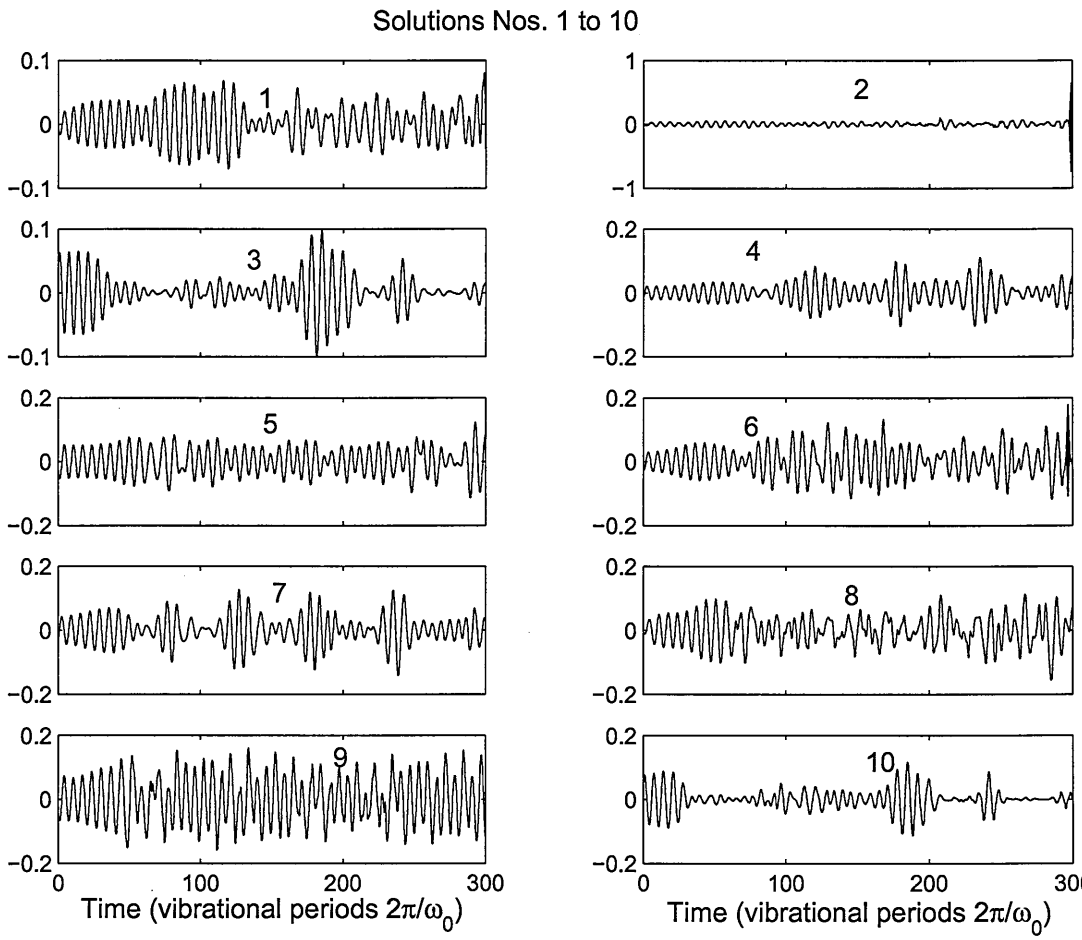


Figure 5.1: Optimal control fields chosen for robustness analysis (arbitrary units)

even though the values of the yields were similar. Figure 5.1 shows the shapes of the control fields and Figure 5.2 observables. The following features, which we can observe from Figs 5.1 and 5.2 may give some indication of the degree of robustness of the solutions.

**Solution 1.** The control field has comparatively low amplitude and no high frequencies. the observable oscillates towards the end of the time interval and rises rapidly to the maximum at the final time. The observable climbs fairly gently to its maximum although it does oscillate towards the final time.

**Solution 2.** The control field has low amplitude except for the end where the amplitude is comparatively very high and the frequency appears high. The observable oscillates towards the end of the time interval and rises rapidly to its maximum.

**Solution 3.** The control field has low amplitude although the amplitude does vary

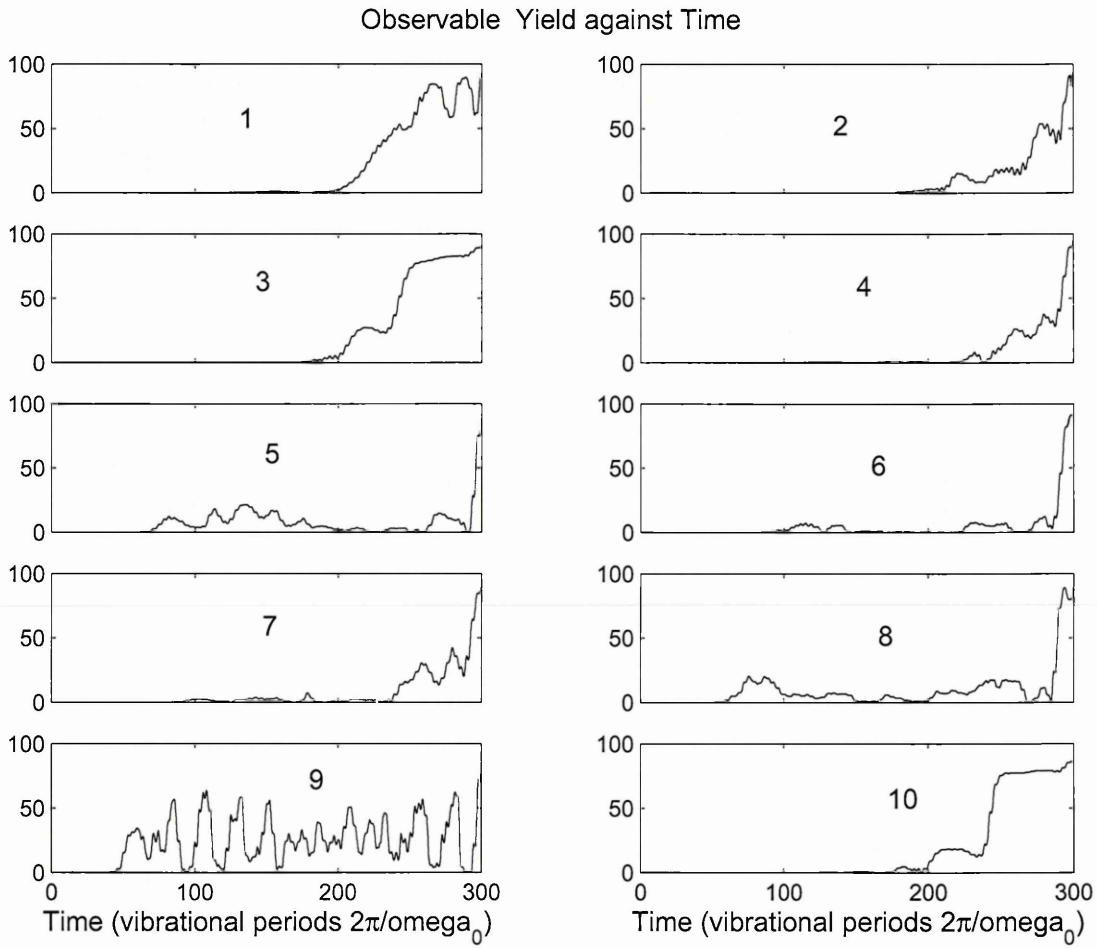


Figure 5.2: Evolution of observable for selected optimal control fields (yield in %)

widely. The observable moves towards its maximum well before the final time and the gradient at the final time is gentle.

**Solution 4.** The amplitude of the control field has a slightly higher maximum than for fields 1 and 3 for most of the time interval. However right at the end it has a final flourish with some high frequencies. This is difficult to see from this small graph but in Section 5.6 this solution will be looked at more closely. The observable rises to its maximum close to the end of the time interval.

**Solution 5.** The amplitude is fairly stable and has a maximum close to that of field 4. The observable rises and then falls early in the time interval and then rapidly ascends to its maximum at the final time.

**Solution 6.** The amplitude of the control field is fairly stable throughout the time interval except at the end where the frequency and amplitude both increase rapidly. The value of the observable climbs steeply to its maximum right at the end of the time interval.

**Solution 7.** The amplitude of the control field varies in a periodic, rhythmic manner. The observable has a couple of attempts at reaching it maximum before its final steep ascent close to the final time.

**Solution 8.** The control field has relatively small amplitude with little variation over the time interval.The observable rises just above zero on a few occasion throughout the time interval before rising steeply to its maximum at the end of the time interval.

**Solution 9.** The amplitude of the control field is relatively large and varies little throughout the time interval. The observable fluctuates widely throughout the time interval and the final time is at one of its many high points.

**Solution 10.** The amplitude of the control field varies from small to very small. The observable climbs to close to its maximum about three quarters of the way through the time interval and gently approaches its maximum at the final time.

## 5.3 Effect of Noise

### 5.3.1 Temporal Noise

In practice it is difficult to reproduce a pulse to match a calculated control field function $f(t)$. To simulate the physical realities the value of $f(t)$ was modulated at each point $t$ by adding a given percentage $\eta\%$ of the maximum value of $|f(t)|$. This means that the quantity of noise added at each moment in time was not dependent on the instantaneous value of $f(t)$. Thus, for a given control field, the amount of noise added was the same throughout the time interval and the effect was greatest when the value of $f(t)$ was least.

### 5.3.2 Spectral Noise

It is unlikely that a control field with precisely the calculated spectral profile can be produced. To anticipate these fluctuations the Fourier transform of the field, $f(t)$, was found. The value of both the amplitude and phase for each point of the time interval were perturbed by a random amount of up to $\eta\%$ of its size at that point. The inverse Fourier transform was then performed to reassemble the field. Hence in this case the quantity of noise depended on and was proportional to the value of the spectral parameters of the field at each point in the time interval.

## 5.4 Effect of Uncertainty in System Parameters

### 5.4.1 Modulation of values of Dipole Moments

The model requires values of the dipole moments. These are difficult to obtain from experiment so they are calculated using the Morse Oscillator model. To simulate uncertainty in these all the values of the dipole moments were simultaneously modulated by a random percentage of up to $\eta\%$. Thus the level of error is proportional to the value of each dipole moment.

### 5.4.2 Error in Energy Levels

Approximations for the energy levels of the system are also required by the model. The method used to test the sensitivity of the pulses to the energy levels was to modulate all the energy levels simultaneously by a random percentage of up to $\eta\%$. Initial calculations showed that the yield in all cases was extremely sensitive to changes in energy levels and to take this into account a range of valves for $\eta\%$ of much smaller than the size of those employed for the other types of error had to used to give commensurate changes in yield. However, this is offset by the fact that values for the energy levels can be obtained very accurately in comparison to those of dipole moments.

## 5.5 Combined Effect of Noise and Uncertainty

The final approach was to bring together the methods of adding noise to the control fields and modulating the system parameters employed so far. To take into account the greater sensitive of the yields to uncertainties in the energy levels a weighting was used. A common percentage level for each type of noise and system parameter modulation was used except that of energy level modulation which was $1/100^{th}$ that of the others. The range of percentage temporal noise, spectral noise and dipole moment modulation used was from 2.5% to 25% in increments of 2.5% whereas the energy levels were modulated by percentages ranging from 0.025% to 0.25% in increments of 0.025%.

All the values of $r$ are close to negative 1 indicating strong negative correlation in each case. We can see that the gradient of the line of regression for Solution 2 stands outs as large indicating that this solution is not robust with respect to temporal noise. The other gradients are particularly close to zero with that of Solution 1 being the closest.

## 5.6 Central Value and Symmetrical Bandwidth Limiting

To get an idea of the bandwidth of the solutions Figure 5.8 shows the magnitudes and gives the means of the magnitudes of the Fourier components for all ten solutions.

In each case the mean does not look like a good central value to use to symmetrically limit the frequencies. This is because each field, to a differing extent, includes some higher frequencies with small magnitude which significantly increase the mean frequency. In order to find a better central value than that given by the mean the magnitude of all frequencies contributing less than 5% of the maximum magnitude are set to zero. The mean frequency is then calculated using the remaining part of each distribution and is used as the central value for bandwidth limiting. Table 5.7 shows the means before and after this process. Apart from Solution 4, which is discussed below, we can see that the means are significantly reduced and this method gives a better central value for our purposes.

Figure 5.10 shows the effect on the yield of symmetrically limiting the bandwidth of the the ten solutions using % increments of the central value either side of their central values. From this it can be seen that up to at least a 50% symmetrical cut off either side of the central value there is, perhaps surprisingly, little effect on the yield with one exception. If we look at the mean of this exceptional case (Solution 4) we see that it is 13.5 which is greatly above where the centre of the distribution appears to be and indeed the value of the mean rises after the values 5% less than the maximum are removed. However, if look at Figure 5.9 which shows the distribution for this solution with a large range of frequencies we can see that there is a significant amount of the distribution at high values for frequency. This shows that this distribution is bimodal and hence a symmetrical bandwidth restriction about a central value with incremental narrowing soon sets most of the distribution to zero. Barring this solution it seems extraordinary how robust the solutions are. Only the middle 50% of the distribution actually seems necessary to attain a yield almost the same as the whole distribution.

## 5.7 Effect of other experimental limitations

As we know the pulse to be robust it is likely that we can discard such values without having a significant effect on the yield. Hence we set to zero any values, and their associated arguments, that are less than $k$% of the maximum value. $k$ could typically be 5. The mean and standard deviation of the remaining values are then calculated. These, along with the maximum value, are used to form a Gaussian curve. A new distribution is formed using either the known value or the value from the Gaussian curve, whichever is the minimum. As the acoustic optical modulator might have typically 128 channels, the greatest 128 values are taken. These values, as magnitudes, and their associated arguments, form a complex distribution. The inverse Fourier transform is then taken to form the pulse. The yield that this pulse would give is then calculated. The results for each field using a value of 5% for $k$ are given in Table 5.8. From the results it can be seen that 6 of the Solutions (Solutions 1, 2, 3, 5, 8, 9) the yield drops by less than 5% and the yield of two other Solutions drop by 6% and 11%. This leaves just two Solutions that are seriously affected.

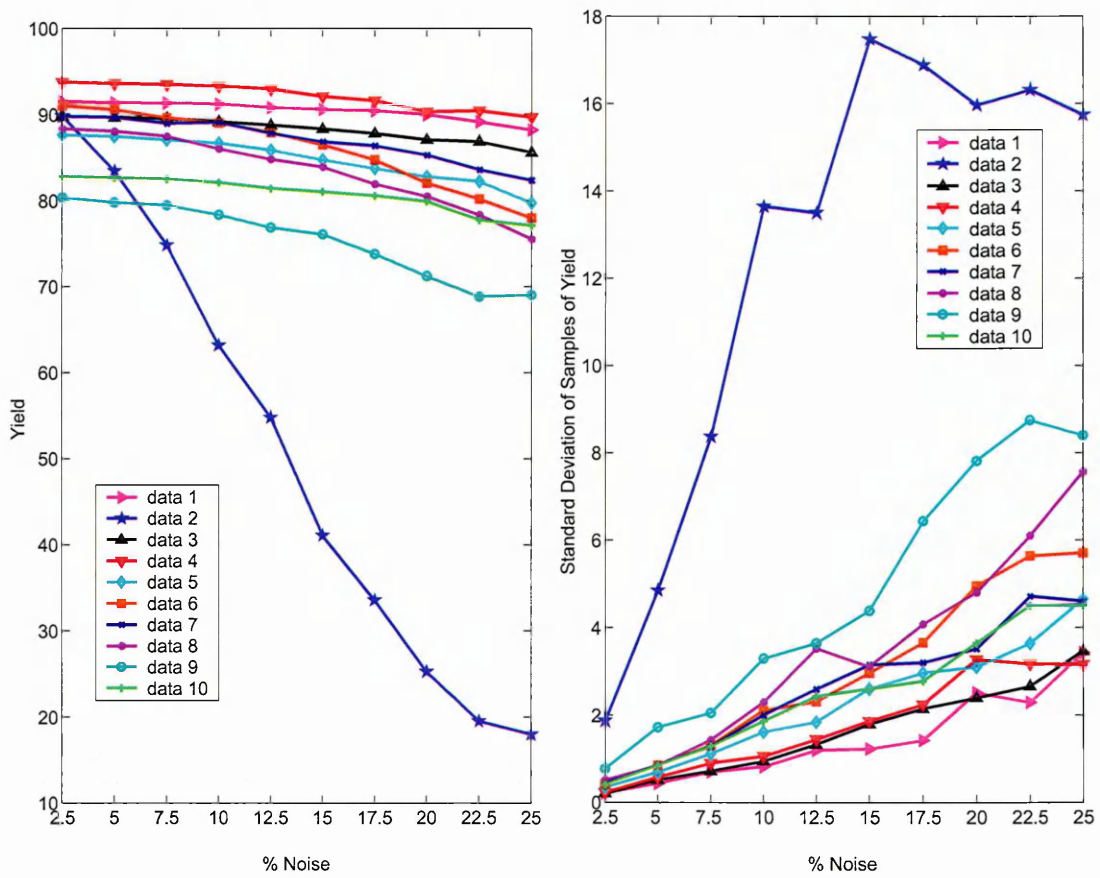


Figure 5.3: Average yield (left) and standard deviation of yield (right) versus magnitude of temporal noise for selected control fields.

| | 1 | 2 | 3 | 4 | 5 | 6 | 7 | 8 | 9 | 10 |
|---|---|---|---|---|---|---|---|---|---|---|
| $r$ | −0.93 | −0.99 | −0.97 | −0.97 | −0.97 | −0.97 | −0.97 | −0.98 | −0.97 | −0.95 |
| $m$ | −0.13 | −3.5 | −0.18 | −0.20 | −0.34 | −0.59 | −0.33 | −0.56 | −0.57 | −0.25 |
| $r'$ | 0.95 | 0.86 | 0.99 | 0.98 | 0.99 | 0.99 | 0.99 | 0.98 | 0.98 | 0.99 |
| $m'$ | 0.13 | 0.62 | 0.14 | 0.15 | 0.18 | 0.25 | 0.19 | 0.30 | 0.38 | 0.19 |

Table 5.2: Correlation coefficients ($r$, $r'$) and gradients of line of regression ($m$, $m'$) for the graphs of the average yield and standard deviation of the yield, respectively, as a function of the magnitude of the *temporal noise*.

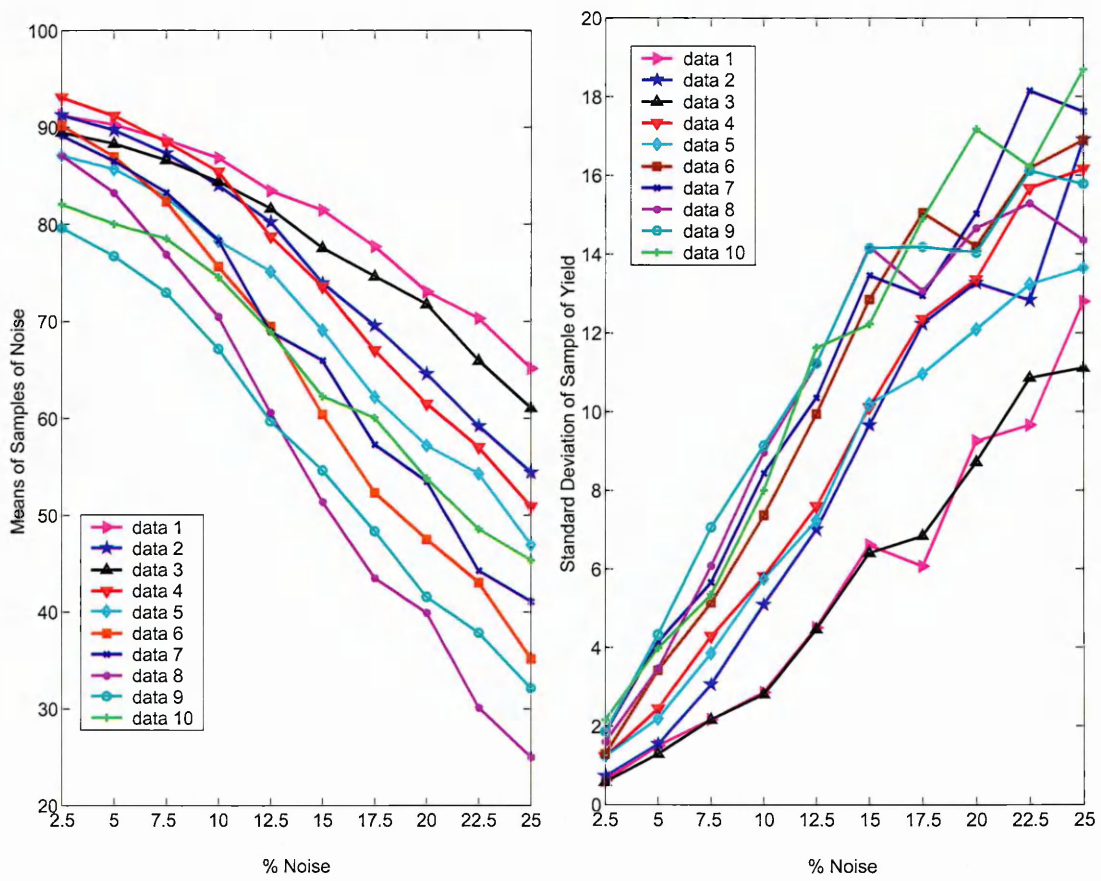


Figure 5.4: Average yield (left) and standard deviation of yield (right) versus magnitude of spectral noise for selected control fields.

| | 1 | 2 | 3 | 4 | 5 | 6 | 7 | 8 | 9 | 10 |
|---|---|---|---|---|---|---|---|---|---|---|
| $r$ | $-0.98$ | $-0.99$ | $-0.98$ | $-0.99$ | $-0.99$ | $-1.0$ | $-0.99$ | $-1.0$ | $-1.0$ | $-0.99$ |
| $m$ | $-1.2$ | $-1.7$ | $-1.3$ | $-2.0$ | $-1.9$ | $-2.6$ | $-2.3$ | $-2.9$ | $-2.2$ | $-1.8$ |
| $r'$ | 0.98 | 0.99 | 0.99 | 1.0 | 0.99 | 0.98 | 0.99 | 0.94 | 0.96 | 0.98 |
| $m'$ | 0.52 | 0.73 | 0.51 | 0.71 | 0.60 | 0.73 | 0.74 | 0.62 | 0.63 | 0.76 |

Table 5.3: Correlation coefficients ($r$, $r'$) and gradients of line of regression ($m$, $m'$) for the graphs of the average yield and standard deviation of the yield, respectively, as a function of the magnitude of the *spectral noise*.

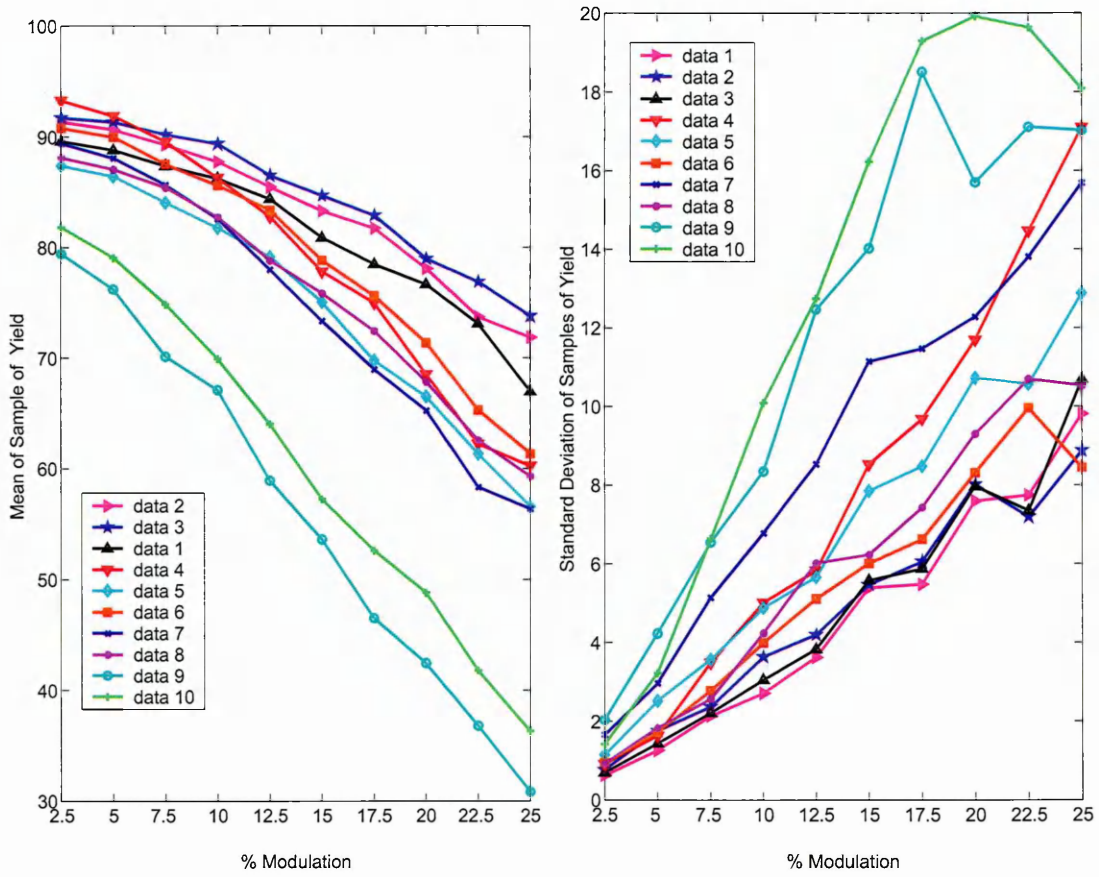


Figure 5.5: Average yield (left) and standard deviation of yield (right) versus uncertainty in the dipole moments for selected control fields.

| | 1 | 2 | 3 | 4 | 5 | 6 | 7 | 8 | 9 | 10 |
|---|---|---|---|---|---|---|---|---|---|---|
| $r$ | −0.98 | −0.98 | −0.97 | −0.99 | −0.98 | −0.98 | −0.99 | −0.99 | −1.0 | −1.0 |
| $m$ | −0.90 | −0.82 | −0.96 | −1.6 | −1.4 | −1.3 | −1.6 | −1.3 | −2.2 | −2.1 |
| $r'$ | 0.99 | 0.99 | 0.98 | 0.99 | 0.99 | 0.98 | 0.99 | 0.99 | 0.94 | 0.94 |
| $m'$ | 0.40 | 0.36 | 0.41 | 0.71 | 0.51 | 0.39 | 0.62 | 0.47 | 0.73 | 0.88 |

Table 5.4: Correlation coefficients ($r$, $r'$) and gradients of line of regression ($m$, $m'$) for the graphs of the average yield and standard deviation of the yield, respectively, as a function of the *uncertainty of the dipole moments.*

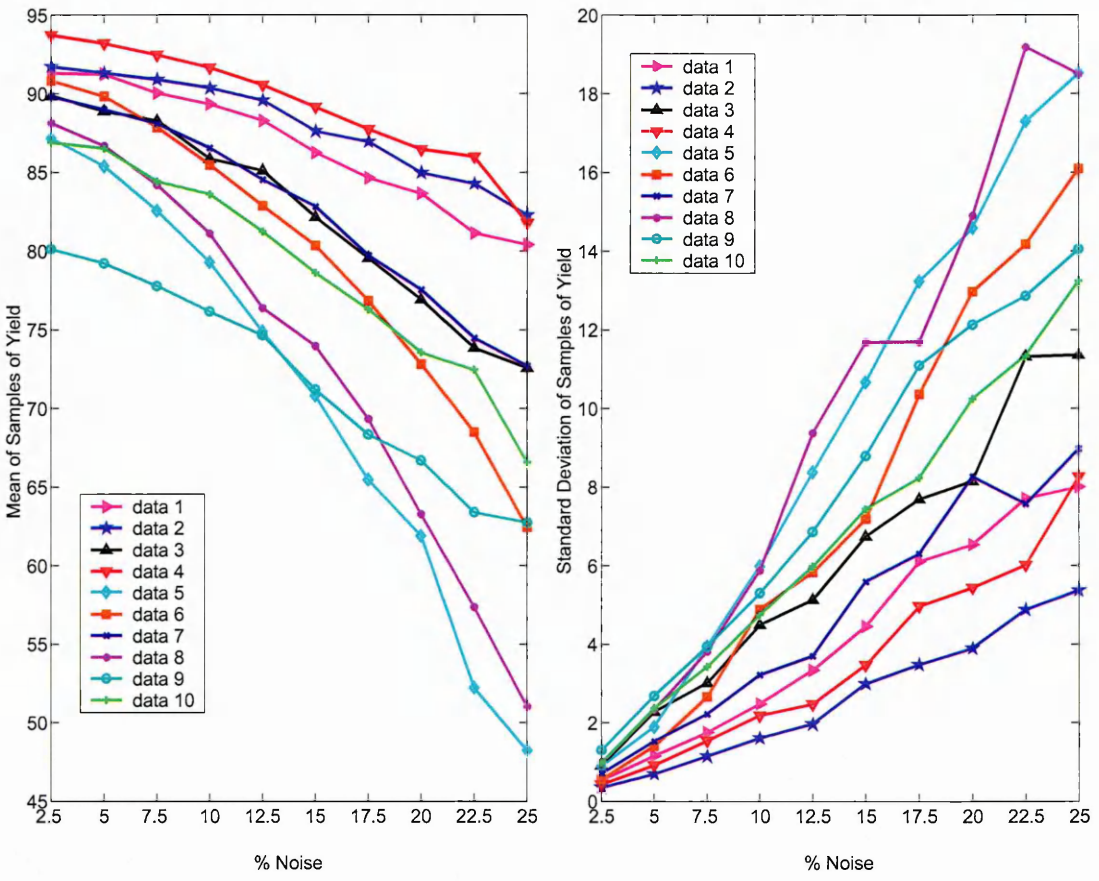


Figure 5.6: Average yield (left) and standard deviation of yield (right) against uncertainty in the energy levels for selected control fields.

| | 1 | 2 | 3 | 4 | 5 | 6 | 7 | 8 | 9 | 10 |
|---|---|---|---|---|---|---|---|---|---|---|
| $r$ | −0.99 | −0.98 | −0.99 | −0.97 | −0.99 | −0.98 | −0.99 | −0.98 | −0.99 | −0.98 |
| $m$ | −0.53 | −0.43 | −0.82 | −0.49 | −1.8 | −1.2 | −0.80 | −1.7 | −0.85 | −0.88 |
| $r'$ | 0.99 | 0.99 | 0.99 | 0.98 | 1.0 | 0.99 | 0.99 | 0.99 | 1.0 | 1.0 |
| $m'$ | 0.36 | 0.23 | 0.47 | 0.33 | 0.83 | 0.72 | 0.38 | 0.85 | 0.60 | 0.53 |

Table 5.5: Correlation coefficients ($r$, $r'$) and gradients of line of regression ($m$, $m'$) for the graphs of the average yield and standard deviation of the yield, respectively, as a function of the *uncertainty of the energy levels*.

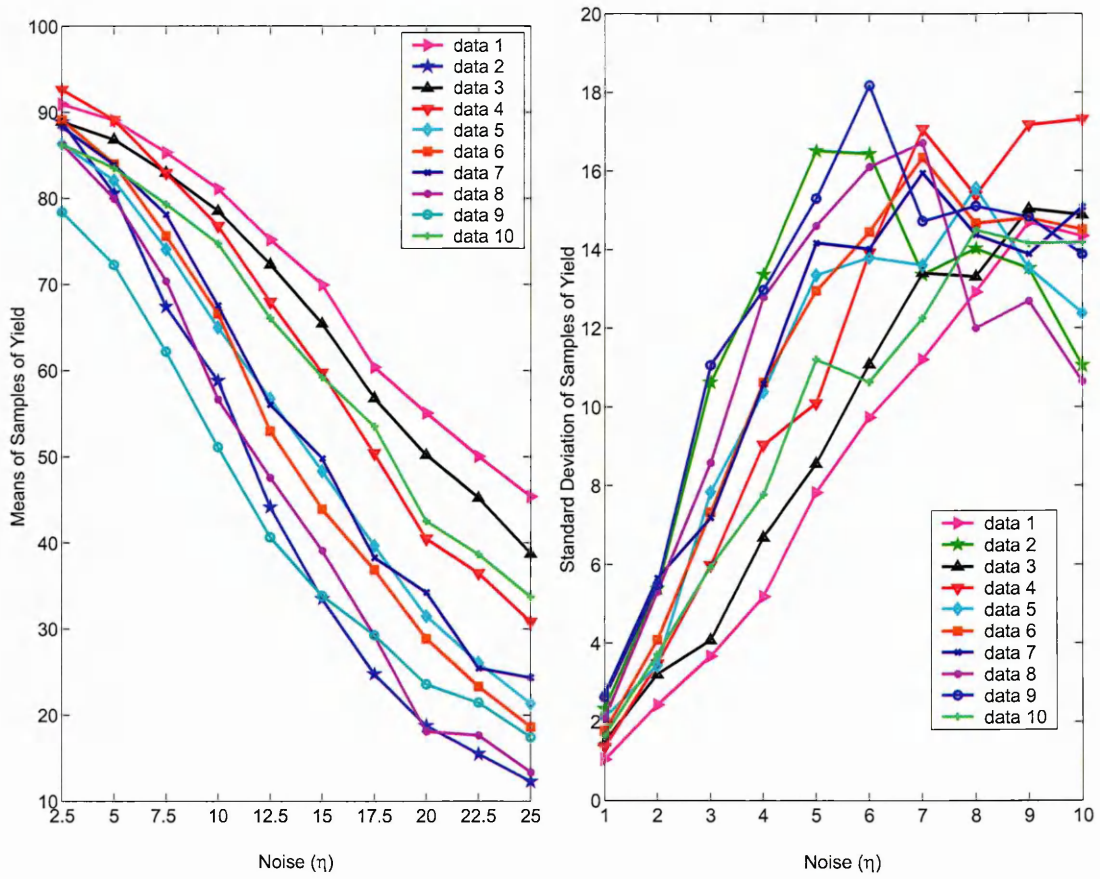


Figure 5.7: Average yield (left) and standard deviation of yield (right) versus total magnitude of errors and uncertainties for a combination of temporal and spectral noise and uncertainty in the system parameters for selected control fields.

| | 1 | 2 | 3 | 4 | 5 | 6 | 7 | 8 | 9 | 10 |
|---|---|---|---|---|---|---|---|---|---|---|
| $r$ | −0.99 | −0.98 | −0.99 | −1.0 | −1.0 | −0.99 | −0.99 | −0.99 | −0.98 | −0.99 |
| $m$ | −2.2 | −3.6 | −2.4 | −3.0 | −3.1 | −3.4 | −3.1 | −3.5 | −2.8 | −2.5 |
| $r'$ | 0.99 | 0.61 | 0.98 | 0.96 | 0.84 | 0.89 | 0.88 | 0.62 | 0.74 | 0.96 |
| $m'$ | 0.66 | 0.37 | 0.66 | 0.76 | 0.51 | 0.59 | 0.54 | 0.39 | 0.47 | 0.59 |

Table 5.6: Correlation coefficients ($r$, $r'$) and gradients of line of regression ($m$, $m'$) for the graphs of the average yield and standard deviation of the yield, respectively, as a function of the total magnitude of errors and uncertainties for a combination of temporal and spectral noise and uncertainty in the system parameters.

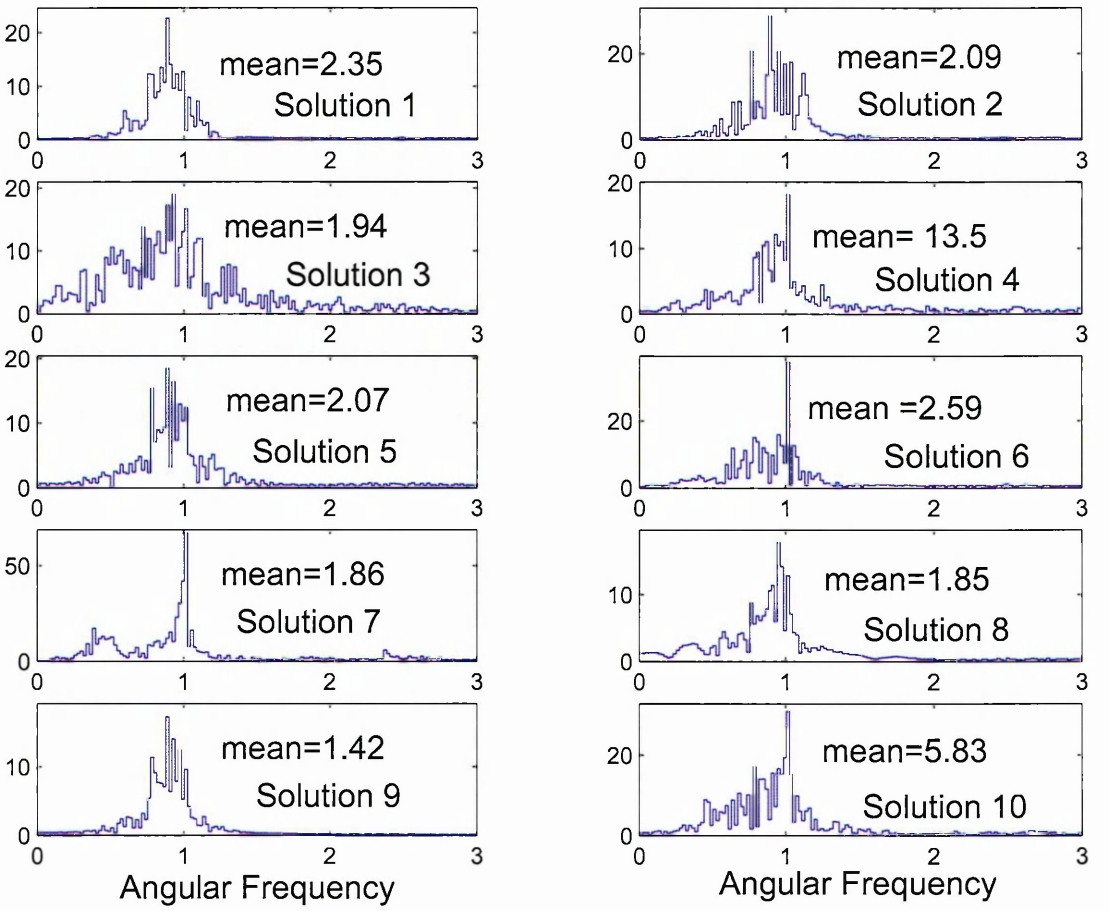


Figure 5.8: Fourier Transform of each Solution with value of the mean stated. The angular frequencies are measured in units of $\omega_0$ where $\omega_0 = 7.47 \times 10^{14}$ rad $s^{-1}$. The values on the other axes represent the moduli of the complex coefficients of the discretised Fourier Transforms.

| Solution No. | 1 | 2 | 3 | 4 | 5 | 6 | 7 | 8 | 9 | 10 |
|---|---|---|---|---|---|---|---|---|---|---|
| Before | 2.35 | 2.09 | 1.94 | 13.5 | 2.07 | 2.59 | 1.86 | 1.85 | 1.42 | 5.83 |
| After | 0.872 | 0.898 | 0.906 | 14.7 | 0.891 | 0.841 | 0.828 | 0.820 | 0.876 | 0.847 |

Table 5.7: Mean of the Fourier Transform of the Solution Before and After setting to zero values of the magnitude that were less than 5% of the maximum.

| Solution No. | 1 | 2 | 3 | 4 | 5 | 6 | 7 | 8 | 9 | 10 |
|---|---|---|---|---|---|---|---|---|---|---|
| $Y$ | 93.8 | 89.9 | 88.6 | 91.8 | 87.1 | 87.7 | 80.4 | 91.5 | 89.9 | 91.2 |
| $Y_L$ | 90.5 | 86.9 | 87.3 | 0.6 | 85.9 | 49.0 | 71.7 | 90.7 | 88.2 | 85.8 |

Table 5.8: $Y$ is original yield, $Y_L$ is the yield after limiting the field to the greatest 128 values of the discretised Fourier Transform

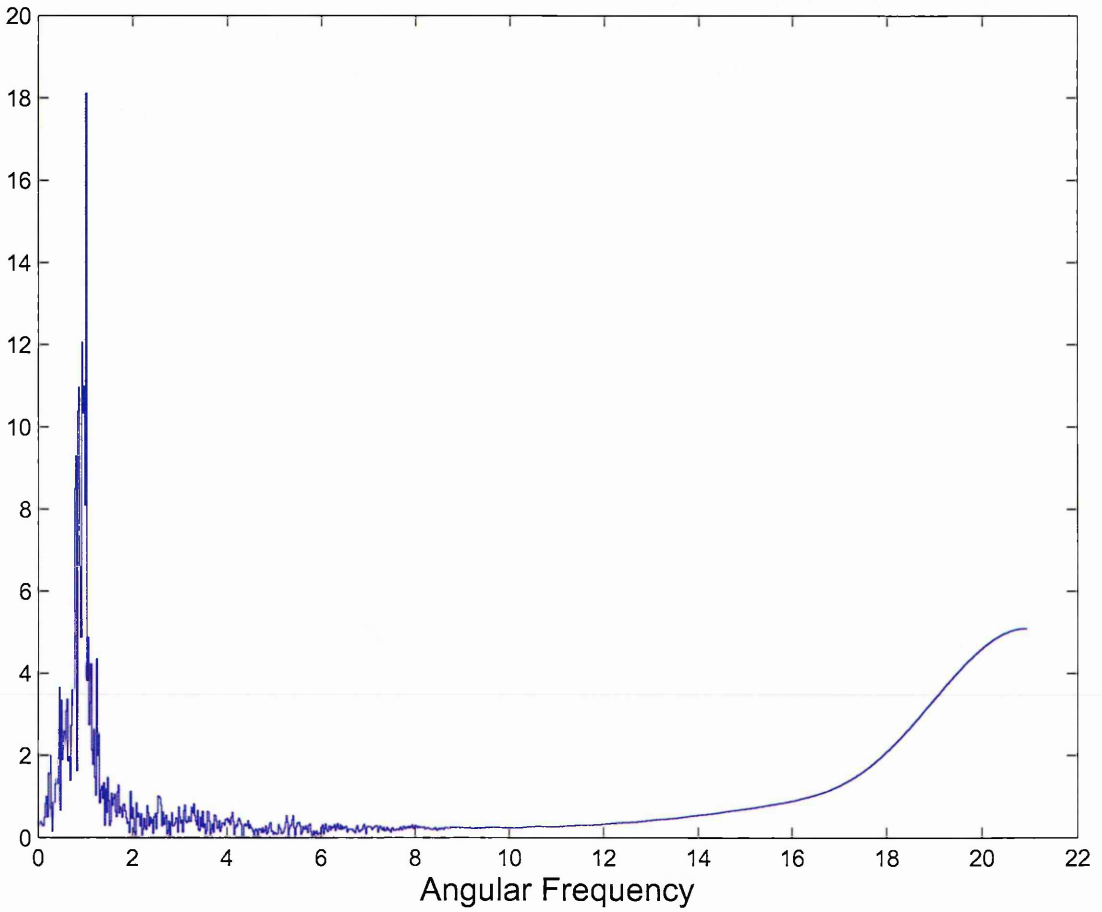


Figure 5.9: Fourier Transform of Solution 4. The angular frequencies are measured in units of $\omega_0$ where $\omega_0 = 7.47 \times 10^{14}$ rad $s^{-1}$. The values on the other axis represent the moduli of the complex coefficients of the discretised Fourier Transform. The relatively high frequencies are likely to be the result of numerical errors as some of the frequencies of the field were too high to be resolved by the time step used.

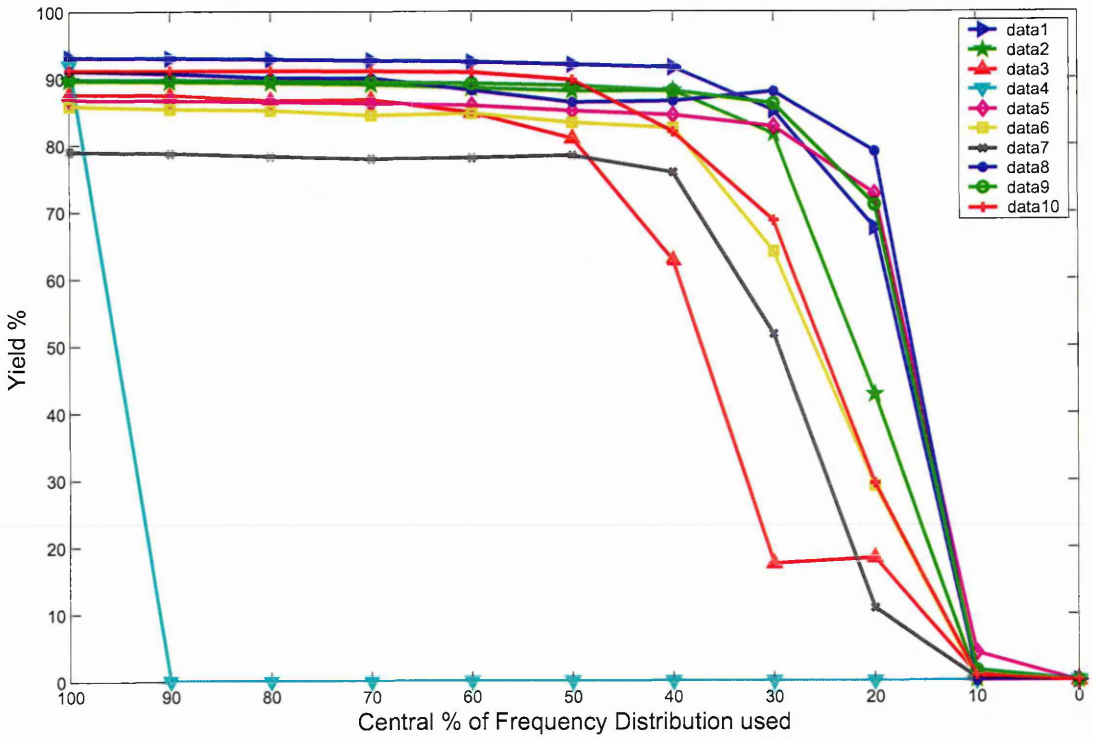


Figure 5.10: Yield against % Bandwidth limiting symmetrically each side of a central value.

# Chapter 6

# Concluding Remarks

We have considered various aspects of optimal quantum control and concentrated on their application to open-loop controllability of closed quantum systems subject to Hamiltonian dynamics.

Two results worthy of noting are among those obtained concerning the robustness of optimal solutions. Firstly, optimal solutions are much more sensitive to changes in the value of the energy levels used in the model than they are to variations in other model parameters or to noise. Secondly, optimal solutions give almost the same performance in terms of yield if only their middle frequencies are used.

The numerical implementation of the algorithm contains a number of parameters and chosen values describing the physical situation. It is difficult to appreciate the effect of changes to these. A further area of study is to examine in more detail how changes to, for instance, $\alpha$, $\beta$, $\lambda$, the length of the time interval, the number of subintervals it is divided into and the features of initial trial field, could be used to develop the efficiency of the algorithm and the quality of the solutions it produces.

The work on robustness was applied to the Hydrogen Fluoride model. Extension of this to quantum dots would help to confirm which aspects may have been specific to the Hydrogen Fluoride model, if any, and how many of the techniques could be applied more generally. This would lead to a situation where a number of optimal robust solutions may be suggested to experimenters for investigation. Any laboratory results obtained would be useful feedback in further development of the algorithm.

Progress may also be made by revisiting the assumptions that dissipation takes place

in a much longer time frame than interactions with the control field and that feedback from some form of measurement of the system may interact so strongly with the system that the effects would be difficult to anticipate. The algorithm does allow for dissipation and just requires a more complicated numerical procedure for the evolution of the density matrix. Further study would be needed to extend the algorithm to closed-loop control.

As is often the case the process of progress to an improved algorithm is likely to involve a number of different lines of enquiry including some of those discussed above.

# Appendix A

# Lie algebra Basics

## A.1 The Lie algebra $su(N)$

A standard basis representation [66] for the Lie algebra $su(N)$ in terms of trace-zero, skew-Hermtian $N \times N$ matrices is

$$\begin{aligned} x_{m,n} &\equiv |m\rangle\langle n| - |n\rangle\langle m| \\ y_{m,n} &\equiv i(|m\rangle\langle n| + |n\rangle\langle m|) \\ h_m &\equiv i(|m\rangle\langle m| - |m+1\rangle\langle m+1|) \end{aligned} \tag{A.1}$$

where $1 \leq m \leq N-1$, $m < n \leq N$ and $i = \sqrt{-1}$. There are $\ell = N-1$ generators $h_m$ and $\frac{1}{2}\ell(\ell+1)$ generators of type $x_{m,n}$ and $y_{m,n}$ each. Hence, the total number of generators is $N^2-1$ and thus the dimension of the Lie algebra $su(N)$ is $N^2-1$.

## A.2 The Lie algebra $so(2\ell+1)$

$so(N)$ usually refers to the real Lie algebra of trace-zero, anti-symmetric matrices [66]. However, since we are dealing with subalgebras of $su(N)$ generated by $N \times N$ skew-Hermitian matrices, we require a representation of $so(N)$ in terms of trace-zero, skew-Hermitian matrices. For $N = 2\ell+1$, the standard representation of the complex Lie algebra $B_\ell$ [67] leads to the following skew-Hermitian basis for the real Lie algebra $so(2\ell+1)$:

$$
\begin{aligned}
&h_m = i(|m+1\rangle\langle m+1| - |m+\ell+1\rangle\langle m+\ell+1|) \\
&x_{\epsilon_m} = x_{1,m+1} - x_{m+\ell+1,1} \qquad y_{\epsilon_m} = y_{1,m+1} - y_{m+\ell+1,1} \\
&x_{\epsilon_m+\epsilon_n} = x_{m+\ell+1,n+1} - x_{n+\ell+1,m+1} \qquad y_{\epsilon_m+\epsilon_n} = y_{m+\ell+1,n+1} - y_{n+\ell+1,m+1} \\
&x_{\epsilon_m-\epsilon_n} = x_{n+1,m+1} - x_{m+\ell+1,n+\ell+1} \qquad y_{\epsilon_m-\epsilon_n} = y_{n+1,m+1} - y_{m+\ell+1,n+\ell+1}
\end{aligned}
\tag{A.2}
$$

where $1 \leq m \leq \ell$ and $m < n \leq \ell$. Since there are $\ell$ elements $h_m$, $x_{\epsilon_m}$ and $y_{\epsilon_m}$ each, as well as $\frac{1}{2}\ell(\ell-1)$ elements $x_{\epsilon_m+\epsilon_n}$, $y_{\epsilon_m+\epsilon_n}$, $x_{\epsilon_m-\epsilon_n}$ and $y_{\epsilon_m-\epsilon_n}$ each, the total number of basis elements is $\ell(2\ell+1)$. Thus the dimension of $so(2\ell+1)$ is $\ell(2\ell+1)$. Using the general commutation relations

$$
\begin{aligned}
&[x_{\epsilon_m}, x_{\epsilon_m-\epsilon_n}] = x_{\epsilon_n} \qquad [x_{\epsilon_m}, y_{\epsilon_m-\epsilon_n}] = y_{\epsilon_n} \\
&[x_{\epsilon_m}, x_{\epsilon_n}] = x_{\epsilon_m-\epsilon_n} - x_{\epsilon_m+\epsilon_n} \qquad [x_{\epsilon_m}, y_{\epsilon_n}] = y_{\epsilon_m-\epsilon_n} + y_{\epsilon_m+\epsilon_n} \\
&[x_{\epsilon_m}, y_{\epsilon_m}] = -2h_m \qquad [x_{\epsilon_m\pm\epsilon_n}, y_{\epsilon_m\pm\epsilon_n}] = -2(h_m \pm h_n) \\
&[h_m, x_{\epsilon_m\pm\epsilon_n}] = -y_{\epsilon_m\pm\epsilon_n} \qquad [h_m, y_{\epsilon_m\pm\epsilon_n}] = x_{\epsilon_m\pm\epsilon_n}
\end{aligned}
\tag{A.3}
$$

for $m \neq n$, shows that the elements $x_m$ and $y_m$ with

$$
\begin{aligned}
&x_1 = x_{\epsilon_1} \qquad x_{m+1} = x_{\epsilon_m-\epsilon_{m+1}} \qquad 1 \leq m \leq \ell-1 \\
&y_1 = y_{\epsilon_1} \qquad y_{m+1} = y_{\epsilon_m-\epsilon_{m+1}} \qquad 1 \leq m \leq \ell-1
\end{aligned}
\tag{A.4}
$$

are not diagonal with respect to the Cartan elements $h_m$ of the Lie algebra and generate the full Lie algebra $so(2\ell+1)$.

## A.3 The Lie algebra $sp(\ell)$

A basis representation for the Lie algebra $sp(\ell)$ for $N = 2\ell$ in terms of trace-zero, skew-Hermitian $N \times N$ matrices can be derived from the standard basis for $C_\ell$ [67]:

$$
\begin{aligned}
&h_m = i(|m\rangle\langle m| - |m+\ell\rangle\langle m+\ell|) \\
&x_{2\epsilon_m} = x_{m+\ell,m} \qquad y_{2\epsilon_m} = y_{m+\ell,m} \\
&x_{\epsilon_m+\epsilon_n} = x_{m+\ell,n} + x_{n+\ell,m} \qquad y_{\epsilon_m+\epsilon_n} = y_{m+\ell,n} + y_{n+\ell,m} \\
&x_{\epsilon_m-\epsilon_n} = x_{n,m} - x_{m+\ell,n+\ell} \qquad y_{\epsilon_m-\epsilon_n} = y_{n,m} - y_{m+\ell,n+\ell}
\end{aligned}
\tag{A.5}
$$

where $1 \leq m \leq \ell$ and $m < n \leq \ell$. Since there are $\ell$ elements $h_m$, $x_{2\epsilon_m}$ and $y_{2\epsilon_m}$ each, as well as $\frac{1}{2}\ell(\ell-1)$ elements $x_{\epsilon_m+\epsilon_n}$, $y_{\epsilon_m+\epsilon_n}$, $x_{\epsilon_m-\epsilon_n}$ and $y_{\epsilon_m-\epsilon_n}$ each, the total number of basis elements is $\ell(2\ell+1)$. Thus the dimension of $sp(\ell)$ is thus $\ell(2\ell+1)$. Using the general commutation relations

$$
\begin{aligned}
&[x_{2\epsilon_m}, x_{\epsilon_m-\epsilon_n}] = x_{\epsilon_m+\epsilon_n} && [x_{2\epsilon_m}, y_{\epsilon_m-\epsilon_n}] = y_{\epsilon_m+\epsilon_n} \\
&[x_{\epsilon_m+\epsilon_n}, x_{\epsilon_n-\epsilon_n}] = 2(x_{2\epsilon_m} - x_{2\epsilon_n}) && [x_{\epsilon_m+\epsilon_n}, y_{\epsilon_n=-\epsilon_m}] = 2(y_{2\epsilon_m} + y_{2\epsilon_n}) \\
&[x_{2\epsilon_m}, y_{2\epsilon_m}] = -2h_m && [x_{\epsilon_m\pm\epsilon_n}, y_{\epsilon_m\pm\epsilon_n}] = -2(h_m \pm h_n) \\
&[h_m, x_{\epsilon_m\pm\epsilon_n}] = -y_{\epsilon_m\pm\epsilon_n} && [h_m, y_{\epsilon_m\pm\epsilon_n}] = x_{\epsilon_m\pm\epsilon_n}
\end{aligned}
\tag{A.6}
$$

for $m \neq n$, shows that the elements $x_m$ and $y_m$ with

$$
\begin{aligned}
&x_m = x_{\epsilon_m-\epsilon_{m+1}} && 1 \leq m \leq \ell-1 && x_\ell = x_{2\epsilon_\ell} \\
&y_m = y_{\epsilon_m-\epsilon_{m+1}} && 1 \leq m \leq \ell-1 && y_\ell = y_{2\epsilon_\ell}.
\end{aligned}
\tag{A.7}
$$

are not diagonal with respect to the Cartan elements $h_m$ of the Lie algebra and generate the full Lie algebra $sp(\ell)$.

## A.4 The Lie algebra $so(2\ell)$

Using the standard representation for the complex Lie algebra $D_\ell$ [67], we can derive the following skew-Hermitian basis for $so(2\ell)$:

$$
\begin{aligned}
&h_m = i(|m\rangle\langle m| - |m+\ell\rangle\langle m+\ell|) \\
&x_{\epsilon_m+\epsilon_n} = x_{m+\ell,n} - x_{n+\ell,m} && y_{\epsilon_m+\epsilon_n} = y_{m+\ell,n} - y_{n+\ell,m} \\
&x_{\epsilon_m-\epsilon_n} = x_{n,m} - x_{m+\ell,n+\ell} && y_{\epsilon_m-\epsilon_n} = y_{n,m} - y_{m+\ell,n+\ell}
\end{aligned}
\tag{A.8}
$$

where $1 \leq m \leq \ell$ and $m < n \leq \ell$. There are $\ell$ elements $h_m$, as well as $\frac{1}{2}\ell(\ell-1)$ elements $x_{\epsilon_m+\epsilon_n}$, $y_{\epsilon_m+\epsilon_n}$, $x_{\epsilon_m-\epsilon_n}$ and $y_{\epsilon_m-\epsilon_n}$ each, i.e., the total number of basis elements is $\ell(2\ell-1)$. Thus, the dimension of $so(2\ell)$ is $\ell(2\ell-1)$.

To see why there is no $(2\ell)$-level system with $\hat{H} = \hat{H}_0 + f(t)\hat{H}_1$, where $\hat{H}_0$ and $\hat{H}_1$ are defined in (2.5) and (2.9) respectively, such that $\tilde{\mathcal{L}} = so(2\ell)$, note that

$$
\begin{aligned}
&x_m = x_{\epsilon_m-\epsilon_{m+1}} && 1 \leq m \leq \ell-1 && x_\ell = x_{\epsilon_{\ell-1}+\epsilon_\ell} \\
&y_m = y_{\epsilon_m-\epsilon_{m+1}} && 1 \leq m \leq \ell-1 && y_\ell = y_{\epsilon_{\ell-1}+\epsilon_\ell}.
\end{aligned}
\tag{A.9}
$$

forms a minimal, complete set of generators for $so(2\ell)$ if $\ell \geq 2$. Each of the $\ell$ generators $y_m$ has four distinct, non-zero entries, which corresponds to a total of $4\ell$ non-zero entries. However, $i\hat{H}_1$ for a $(2\ell)$-level system with only nearest neighbour interactions can have at most $2(2\ell-1) = 4\ell-2$ non-zero entries on the first supre- and sub-diagonal. Hence, a $(2\ell)$-level system with dynamical Lie-algebra $so(2\ell)$ must have interactions between non-adjacent energy levels.

# Appendix B

# Proof of Contollability Theorems

## B.1 Results for Odd-dimensional Systems

### B.1.1 $\tilde{\mathcal{L}}$ is a subalgebra of $so(2\ell+1)$

We first show that the Lie algebra $\tilde{\mathcal{L}}$ generated by the system $\hat{H} = \hat{H}_0' + f(t)\hat{H}_1$ with $i\hat{H}_0$ and $i\hat{H}_1$ as in *(2.12)* is

contained in $so(2\ell+1)$, i.e., $\tilde{\mathcal{L}} \subseteq so(2\ell+1)$.

Let $y_{n,m} = i(|n\rangle\langle m| + |m\rangle\langle n|)$. Using $d_n = d_{2\ell+1-n}$ and $y_{m,n} = y_{n,m}$ we have

$$i\hat{H}_1 = \sum_{n=1}^{\ell} d_{\ell+1-n}\Big(y_{\ell+2-n,\ell+1-n} + y_{\ell+n,\ell+n+1}\Big).$$

To compute $\hat{H}_0'$, note that $E_n = E_1 + \sum_{s=1}^{n-1}\omega_s$. Thus, using $\omega_n = \omega_{2\ell+1-n}$ leads to

$$\mathrm{Tr}(\hat{H}_0) = (2\ell+1)E_1 + (2\ell+1)\sum_{s=1}^{\ell}\omega_s.$$

Hence, the energy levels $E_n'$ of $\hat{H}_0'$ are $E_{\ell+1}' = 0$ and

$$E_{\ell+1-n}' = -\sum_{s=\ell+1-n}^{\ell}\omega_s \qquad E_{\ell+1+n}' = \sum_{s=\ell+1}^{\ell+n}\omega_s = \sum_{s=\ell+1-n}^{\ell}\omega_s$$

for $1 \le n \le \ell$. Consequently, we have

$$i\hat{H}_0' = \sum_{n=1}^{\ell}\Big(-\sum_{s=\ell+1-n}^{\ell}\omega_s\Big)i(|\ell+1-n\rangle\langle\ell+1-n| - |\ell+1+n\rangle\langle\ell+1+n|).$$

Let $\sigma$ be an isomorphism of the Hilbert space of pure states defined by

$$\sigma(|n\rangle) = \begin{cases} |\ell+2-n\rangle & 1 \le n \le \ell+1 \\ (-1)^{n-\ell-1}|n\rangle & \ell+2 \le n \le 2\ell+1 \end{cases} \tag{B.1}$$

and set $|m\rangle = \sigma(|n\rangle)$ as well as $\tilde{E}_m = -\sum_{s=\ell+1-m}^{\ell} \omega_s$ and $d_m = d_{\ell+1-m}$. Then the representations of $i\hat{H}_0'$ and $i\hat{H}_1$ with respect to the new basis $|m\rangle$ are

$$\begin{aligned} i\hat{H}_0' &= \sum_{m=1}^{\ell}\Big(-\sum_{s=\ell+1-m}^{\ell}\omega_s\Big) i(|m+1\rangle\langle m+1| - |\ell+1+m\rangle\langle\ell+1+m|) = \sum_{m=1}^{\ell}\tilde{E}_m h_m \\ i\hat{H}_1 &= d_\ell(y_{1,2}+y_{1,\ell+2}) + \sum_{m=2}^{\ell} d_{\ell+1-m}(y_{m,m+1} - y_{m+\ell,m+\ell+1}) = \sum_{m=1}^{\ell}\tilde{d}_m y_m \end{aligned} \tag{B.2}$$

with $h_m$ and $y_m$ as defined in A.2 and A.4 respectively. Hence, $i\hat{H}_0'$ and $i\hat{H}_1$ are both in $so(2\ell+1)$ and thus the Lie algebra $\tilde{\mathcal{L}}$ they generate must be contained in $so(2\ell+1)$.

### B.1.2 Lemma

Before we prove the theorems establishing explicit criteria for the Lie algebra $\tilde{\mathcal{L}}$ generated by $i\tilde{H}_0'$ and $i\hat{H}_1$ in Eq. (2.12) to be equal to $\tilde{\mathcal{L}} = so(2\ell+1)$, we first show that it suffices to show that the Lie algebra contains one generator of the Lie algebra.

**Lemma 2** *Let $\tilde{\mathcal{L}}$ be the Lie algebra by $i\hat{H}_0'$ and $\hat{H}_1$ as defined in Eq. 2.12. If $y_1 \in \tilde{\mathcal{L}}$ the $x_m, y_m \in \tilde{\mathcal{L}}$ for $1 \le m \le \ell$ and hence $\tilde{\mathcal{L}} = so(2\ell+1)$.*

**Proof:** Using Eqs (A.3) shows that $y_1 \in \tilde{\mathcal{L}}$ implies $[i\hat{H}_0', y_1] = \epsilon_1 x_1$ and $[x_1, y_1] = 2h_1$; thus $x_1, h_1 \in \tilde{\mathcal{L}}$. Furthermore, we have

$$\begin{aligned} Z^{(1)} &= i\hat{H}_0' - \epsilon_1 h_1 = \sum_{m=2}^{\ell}\epsilon_m h_m, \\ Y^{(1)} &= i\hat{H}_1 - \delta_1 y_1 = \sum_{m=2}^{\ell}\delta_m y_m, \\ X^{(1)} &= -[i\hat{H}_0', i\hat{H}_1] + \epsilon_1\delta_1 x_1 = \sum_{m=2}^{\ell}(\epsilon_m - \epsilon_{m-1})\delta_m x_m \\ \left[Z^{(1)}, Y^{(1)}\right] &= -\epsilon_2\delta_2 x_2 - \sum_{m=3}^{\ell}(\epsilon_m - \epsilon_{m-1})\delta_m x_m \end{aligned}$$

which shows the $X^{(1)} + \left[Z^{(1)}, Y^{(1)}\right] = -\epsilon_1\delta_2 x_2$, i.e., $x_2 \in \tilde{\mathcal{L}}$, and $\left[Z^{(1)}, x_2\right] = \epsilon_2 y_2$, $[x_2, y_2] = 2(h_2 - h_1)$ implies $y_2, h_2 \in \tilde{\mathcal{L}}$. In general, defining recursively

$$Z^{(k)} = Z^{(k-1)} - \epsilon_k h_k, \quad Y^{(k)} = Y^{(k-1)} - \delta_k y_k, \quad X^{(k)} = X^{(k-1)} - (\epsilon_k\epsilon_{k-1})\delta_k x_k$$

shows that

$$\begin{aligned} X^{(k)} + \left[Z^{(k)}, Y^{(k)}\right] &= -\epsilon_k\delta_{k+1}x_{k+1}, \\ \left[Z^{(k)}, x_{(k+1)}\right] &= \epsilon^{(k+1)}y_{(k+1)}, \\ \left[x_{k+1}, y_{k+1}\right] &= 2(h_{k+1} - h_k). \end{aligned}$$

Thus, $x_{k+1}$, $y_{k+1}$ and $h^{k+1}$ are in $\tilde{\mathcal{L}}$ for $k = 2, 3, \ldots, \ell - 1$.

### B.1.3 Theorem 4

**Theorem 4.** Let $\omega_m = \epsilon_{m+1} - \epsilon_m$ for $1 \leq m < \ell$ and $\omega_0 = \epsilon_1$. The dynamical Lie algebra $\tilde{\mathcal{L}}$ generated by the system $\hat{H} = \hat{H}_0' + f(t)\hat{H}_1$ with $i\hat{H}_0$ and $i\hat{H}_1$ as in *(2.12)* is $so(2\ell + 1)$ if $\omega_m^2 \neq \omega_0^2$ for $1 \leq m \leq l$.

**Proof.** Using the properties of the generators $h_m$ and $y_m$ leads to

$$\begin{aligned} V^{(0)} &\equiv \left[\left[i\hat{H}_0', i\hat{H}_1\right], i\hat{H}_0'\right] \\ &= \sum_{m=1}^{\ell} \delta_m\omega_{m-1}^2 y_m \\ V^{(1)} &\equiv \left[\left[i\hat{H}_0', V^{(0)}\right], i\hat{H}_0'\right] - \omega_{\ell-1}^2 V^{(0)} \\ &= \sum_{m=1}^{\ell-1} \delta_m\omega_{m-1}^2(\omega_{m-1}^2 - \omega_{\ell-1}^2)y_m \\ V^{(2)} &\equiv \left[\left[i\hat{H}_0', V^{(1)}\right], i\hat{H}_0'\right] - \omega_{\ell-2}^2 V^{(1)} \\ &= \sum_{m=1}^{\ell-2} \delta_m\omega_{m-1}^2(\omega_{m-1}^2 - \omega_{\ell-1}^2)(\omega_{m-1}^2 - \omega_{\ell-2}^2)y_m \\ &\vdots \\ V^{(\ell-1)} &\equiv \left[\left[i\hat{H}_0', V^{(\ell-2)}\right], i\hat{H}_0'\right] - \omega_1^2 V^{(\ell-2)} \\ &= \delta_1\omega_0^2 \prod_{m=1}^{\ell-1}(\omega_0^2 - \omega_m^2)y_1. \end{aligned}$$

By hypothesis $\omega_m^2 \neq \omega_0^2$ for $m > 0$ and $\delta_1 \neq 0$, $\omega_0 = \epsilon_1 \neq 0$. Hence, all the factors in the last expression above are non-zero, i.e., we have $y_1 \in \tilde{\mathcal{L}}$ and thus $\tilde{\mathcal{L}} = so(2\ell+1)$ by lemma 2.

### B.1.4 Theorem 5

**Theorem 5.** *Let* $v_m \equiv 2\tilde{\delta}_m^2 - \tilde{\delta}_{m+1}^2 - \tilde{\delta}_{m-1}^2$ *for* $1 \leq m \leq l$, *where* $\tilde{\delta}_0 = \tilde{\delta}_1$, $\tilde{\delta}_{l+1} = 0$. *The dynamical Lie algebra* $\hat{\mathcal{L}}$ *generated by the system* $\hat{H} = \hat{H}_0' + f(t)\hat{H}_1$ *with* $i\hat{H}_0'$ *and* $i\hat{H}_1$ *as in* (2.12) *is* $so(2\ell+1)$ *if* $\omega_{m-1} = \omega_0$ *but* $v_m \neq v_1$ *for all* $m \in \mathcal{M} - \{1\}$.

**Proof.** Since $\omega_{m-1} = \omega_0$ for all $m \in \mathcal{M}$, we have

$$\begin{aligned} X^{(0)} &\equiv \omega_0^{-1}\left[i\hat{H}_0', Y^{(0)}\right] \\ Z &\equiv 2^{-1}\left[X^{(0)}, Y^{(0)}\right] = \sum_{m=1}^{\ell}(\tilde{\delta}_{m+1}^2 - \tilde{\delta}_m^2)h_m. \end{aligned}$$

Suppose $\mathcal{M} - \{1\}$ has $\ell'$ elements labelled $m_1$, $m_2$ up to $m_\ell'$. If $v_m \neq v_1$ for all $m \in \mathcal{M} - \{1\}$ then

$$\begin{aligned} Y^{(1)} &\equiv \left[Z, X^{(0)}\right] - v_{m_{\ell'}}Y^{(0)} \\ &= \tilde{\delta}_1(v_1 - v_{m_{\ell'}})y_1 - \sum_{k=1}^{\ell'-1}\tilde{\delta}_{m_k}(v_{m_k} - v_{m_{\ell'}})y_{m_k} \\ X^{(1)} &\equiv \left[Y^{(0)}, Z\right] - v_{m_{\ell'}}X^{(0)} \\ &= \tilde{\delta}_1(v_1 - v_{m_{\ell'}})x_1 - \sum_{k=1}^{\ell'-1}\tilde{\delta}_{m_k}(v_{m_k} - v_{m_{\ell'}})x_{m_k} \\ Y^{(2)} &\equiv \left[Z, X^{(1)}\right] - v_{m_{\ell'-1}}Y^{(1)} \\ &= \tilde{\delta}_1(v_1 - v_{m_{\ell'}})(v_1 - v_{m_{\ell'-1}})y_1 - \sum_{k=1}^{\ell'-2}\tilde{\delta}_{m_k}(v_{m_k} - v_{m_{\ell'}})(v_{m_k} - v_{m_{\ell'-1}})y_{m_k} \\ X^{(2)} &\equiv \left[Y^{(1)}, Z\right] - v_{m_{\ell'-1}}X^{(1)} \\ &= \tilde{\delta}_1(v_1 - v_{m_{\ell'}})(v_1 - v_{m_{\ell'-1}})x_1 - \sum_{k=1}^{\ell'-2}\tilde{\delta}_{m_k}(v_{m_k} - v_{m_{\ell'}})(v_{m_k} - v_{m_{\ell'-1}})x_{m_k} \\ &\vdots \\ Y^{(\ell')} &\equiv \tilde{\delta}_1\prod_{k=1}^{\ell'}(v_1 - v_{m_k})y_1 \end{aligned}$$

shows that $y_1 \in \tilde{\mathcal{L}}$ and hence $\tilde{\mathcal{L}} = so(2\ell+1)$ by lemma 2.

### B.1.5 Theorem 6

**Theorem 6.** *The dynamical Lie algebra $\hat{\mathcal{L}}$ generated by the system $H = \tilde{H}_0 + f(t)\hat{H}_1$ with $N = 2\ell + 1$ equally spaced energy levels $\omega_m = \omega_1$ and uniform dipole moments $d_m = d$ is $so(2\ell + 1)$.*

**Proof.** Note the conditions $\omega_m = \omega_1$ and $d_m = d$ are the same as $\omega_m = \epsilon_1$ and $\delta_m = \delta$ respectively. Let $Y^{(1)} = \delta_{-1} i\hat{H}_1$ and $X^{(1)} = \epsilon_1^{-1}\left[i\hat{H}_0', Y^{(1)}\right]$. Then $h_\ell = -2^{-1}\left[X^{(1)}, Y^{(1)}\right]$, $y_\ell = \left[h_\ell, X^{(1)}\right]$ and $x_\ell = [y_\ell, h_\ell]$. Thus, $x_\ell$, $y_\ell \in \tilde{\mathcal{L}}$. Next, set $Y^{(k+1)} = Y^{(k)} - y_{\ell+1-k}$ and $X^{(k+1)} = X^{(k)} - x_{\ell+1-k}$ for $1 \leq k < \ell$, and note that $h_{\ell-k} = 2^{-1}\left[Y^{(k+1)}, X^{(k+1)}\right]$, $y_{\ell-k} = \left[h_{\ell-k}, X^{(k+1)}\right]$ and $x_{\ell-k} = [y_{\ell-k}, h_{\ell-k}]$. This show that $\tilde{\mathcal{L}}$ contains all the generators $x_m$ and $y_m$ of $so(2\ell+1)$. Hence, $\tilde{\mathcal{L}} = so(2\ell+1)$.

## B.2 Results for Even-dimensional Systems

### B.2.1 $\tilde{\mathcal{L}}$ is a subalgebra of $sp(\ell)$

We first show that $\tilde{\mathcal{L}} \subseteq sp(\ell)$. Let $y_{n,m} = i(|n\rangle\langle m| + |m\rangle\langle n|)$. Using $d_n = d_{2\ell-n}$ we can write $i\hat{H}_1$ as,

$$i\hat{H}_1 = d_\ell y_{\ell,\ell+1} + \sum_{n=1}^{\ell-1} d_n (y_{n,n+1} + y_{2\ell-n,2\ell+1-n}).$$

To compute $\hat{H}_0'$, we note the $E_n = E_1 + \sum_{s=1}^{n-1} \omega_s$.
Thus, using $\omega_n = \omega_{2\ell-n}$ for $1 \leq n \leq \ell - 1$ leads to

$$\mathrm{Tr}(\hat{H}_0) = (2\ell)E_1 + (2\ell)\sum_{s=1}^{\ell-1} \omega_s + \ell\omega_\ell.$$

Hence, $\mathrm{Tr}(\hat{H}_0)/(2\ell) = E_1 + \sum_{s=1}^{\ell-1} \omega_s + \frac{1}{2}\omega_\ell$ and the energy levels $E_n'$ of $\hat{H}_0'$ are $E_\ell' = -\frac{1}{2}\omega_\ell$, $E_{\ell+1}' = \frac{1}{2}\omega_\ell$ and

$$E_{\ell-n}' = -\sum_{s=\ell-n}^{\ell-1} \omega_s - \frac{\omega_\ell}{2} \qquad E_{\ell+1+n}' = \sum_{s=\ell+1}^{\ell+n} \omega_s + \frac{\omega_\ell}{2} = \sum_{s=\ell-n}^{\ell} \omega_s + \frac{\omega_\ell}{2}$$

for $1 \leq n \leq \ell - 1$. Consequently, we have

$$i\hat{H}_0' = \sum_{n=1}^{\ell} -\left(\frac{\omega_\ell}{2} + \sum_{s=n}^{\ell-1} \omega_s\right) i(|n\rangle\langle n| - |2\ell + 1 - n\rangle\langle 2\ell + 1 - n|).$$

Let $\sigma$ be an isomorphism of the Hilbert space of pure states defined by

$$\sigma(|n\rangle) = \begin{cases} |n\rangle & 1 \le n \le \ell \\ (-1)^{n-\ell-1}|3\ell+1-n\rangle & \ell+1 \le n \le 2\ell \end{cases} \tag{B.3}$$

and set $|m\rangle = \sigma(|n\rangle)$ as well as $\tilde{E}_m = -\frac{1}{2}\omega_\ell - \sum_{s=m}^{\ell-1}\omega_s$ for $1 \le m \le \ell-1$, $\tilde{E}_\ell = -\frac{1}{2}\omega_\ell$ and $\tilde{d}_\ell = d_\ell$. Then the representation of $i\hat{H}_0'$ and $i\hat{H}_1$ with respect to the new basis $|m\rangle$ are

$$\begin{aligned} i\hat{H}_0' &= \sum_{m=1}^{\ell} - \left(\frac{\omega_\ell}{2} + \sum_{s=m}^{\ell-1}\omega_s\right) i(|m\rangle\langle m| - |\ell+m\rangle\langle \ell+m|) = \sum_{m=1}^{\ell}\tilde{E}_m h_m \\ i\hat{H}_1 &= d_\ell y_{\ell,2\ell} + \sum_{m=1}^{\ell-1} d_m(y_{m+1,m} - y_{m+\ell,m+\ell+1}) = \sum_{m=1}^{\ell}\tilde{d}_m y_m \end{aligned} \tag{B.4}$$

with $h_m$ and $y_m$ as defined in A.5 and A.7 respectively, and we note that $y_{m,m+1} = y_{m+1,m}$, $y_{m+\ell,m+\ell+1} = y_{m+\ell+1,m+\ell}$ Hence, the dynamical Lie algebra generated by $i\hat{H}_0'$ and $i\hat{H}_1$ must be a subalgebra of $sp(\ell)$.

### B.2.2 Lemma

Again, before we prove the theorems establishing explicit criteria for the Lie algebra $\tilde{\mathcal{L}}$ generated by $i\tilde{H}_0'$ and $i\hat{H}_1$ in Eq. (2.15) to be equal to $\tilde{\mathcal{L}} = sp(\ell)$, we first show that it suffices to show that the Lie algebra contains one generator of the Lie algebra.

**Lemma 3** *Let $\tilde{\mathcal{L}}$ be the Lie algebra by $i\hat{H}_0'$ and $\hat{H}_1$ as defined in If $y_\ell \in \tilde{\mathcal{L}}$ then $x_m, y_m \in \tilde{\mathcal{L}}$ for $1 \le m \le \ell$ and hence $\tilde{\mathcal{L}} = sp(\ell)$.*

**Proof.** Using A.6 shows that $y_\ell \in \tilde{\mathcal{L}}$ implies $[i\hat{H}_0', y_\ell] = 2\epsilon_\ell x_\ell$ and $[x_\ell, y_\ell] = 2h_\ell$; thus $x_\ell, h_\ell \in \tilde{\mathcal{L}}$.

Furthermore, we have

$$\begin{aligned} Z^{(1)} &= i\hat{H}_0' - \epsilon_\ell h_\ell = \sum_{m=1}^{\ell-1}\epsilon_m h_m \qquad Y^{(1)} = i\hat{H}_1 - \delta_\ell y_\ell = \sum_{m=1}^{\ell-1}\delta_m y_m \\ X^{(1)} &= -[i\hat{H}_0', i\hat{H}_1] + 2\epsilon_\ell\delta_\ell x_\ell = \sum_{m=1}^{\ell-1}(\epsilon_{m+1} - \epsilon_m)\delta_m x_m \\ \left[Z^{(1)}, Y^{(1)}\right] &= \epsilon_{\ell-1}\delta_{\ell-1}x_{\ell-1} - \sum_{m=1}^{\ell-2}(\epsilon_{m+1} - \epsilon_m)\delta_m x_m \end{aligned}$$

which shows the $X^{(1)} + \left[Z^{(1)}, Y^{(1)}\right] = \epsilon_\ell \delta_{\ell-1} x_{\ell-1}$, $\left[Z^{(1)}, x_{\ell-1}\right] = -\epsilon_{\ell-1} y_{\ell-1}$ and $[x_{\ell-1}, y_{\ell-1}] = 2(h_\ell - h_{\ell-1})$; thus $x_{\ell-1}, y_{\ell-1}, h_{\ell-1} \in \tilde{\mathcal{L}}$.

In general, defining recursively

$$Z^{(k+1)} = Z^{(k)} - \epsilon_{\ell-k} h_{\ell-k} \quad Y^{(k+1)} = Y^{(k)} - \delta_{\ell-k} y_{\ell-k}$$
$$X^{(k+1)} = X^{(k)} - (\epsilon_{\ell-k+1} - \epsilon_{\ell-k}) \delta_{\ell-k} x_{\ell-k}$$

shows that

$$\begin{aligned} X^{(k+1)} + \left[Z^{(k+1)}, Y^{(k+1)}\right] &= \epsilon_{\ell-k} \delta_{\ell-k-1} x_{\ell-k-1} \\ \left[Z^{(k+1)}, x_{(\ell-k-1)}\right] &= -\epsilon^{(\ell-k-1)} y_{(\ell-k-1)} \\ \left[x_{\ell-k-1}, y_{\ell-k-1}\right] &= 2(h_{\ell-k} - h_{\ell-k-1}). \end{aligned}$$

Thus, $x_{\ell-k-1}$, $y_{\ell-k-1}$ and $h_{\ell-k-1}$ are in $\tilde{\mathcal{L}}$ for $k = 1, 2, \ldots, \ell - 2$.

### B.2.3 Theorem 7

**Theorem 7** *Let $\omega_m = \epsilon_{m+1} - \epsilon_m$ for $1 \leq m < \ell$ and $\omega_\ell = 2\epsilon_\ell$. The dynamical Lie algebra $\hat{\mathcal{L}}$ generated by $i\hat{H}_0'$ and $i\hat{H}_1$ as in (2.15) and with the symmetrical relations given in (2.11) is $sp(\ell)$ if $\omega_m^2 \neq \omega_\ell^2$ for $m < \ell$.*

**Proof.** Using the properties of the generators $h_m$ and $y_m$ leads to

$$\begin{aligned} V^{(1)} &\equiv \left[\left[i\hat{H}_0', i\hat{H}_1\right], i\hat{H}_0'\right] - \omega_1^2 (i\hat{H}_1) \\ &= \sum_{m=2}^{\ell} \delta_m (\omega_m^2 - \omega_1^2) y_m \\ V^{(2)} &\equiv \left[\left[i\hat{H}_0', V^{(1)}\right], i\hat{H}_0'\right] - \omega_2^2 V^{(1)} \\ &= \sum_{m=3}^{\ell} \delta_m (\omega_m^2 - \omega_1^2)(\omega_m^2 - \omega_2^2) y_m \\ V^{(2)} &\equiv \left[\left[i\hat{H}_0', V^{(1)}\right], i\hat{H}_0\right] - \omega_{\ell-2}^2 V^{(1)} \\ &\vdots \\ V^{(\ell-1)} &\equiv \left[\left[i\hat{H}_0', V^{(\ell-2)}\right], i\hat{H}_0\right] - \omega_{\ell-1}^2 V^{(\ell-2)} \\ &= \delta_\ell \prod_{m=1}^{\ell-1} (\omega_\ell^2 - \omega_m^2) y_\ell. \end{aligned}$$

By hypothesis $\omega_m^2 \neq \omega_\ell^2$ for $m, \ell$ and $\delta_\ell \neq 0$. Hence, all the factors in the last expression above are non-zero, i.e., we have $y_\ell \in \tilde{\mathcal{L}}$ and thus $\tilde{\mathcal{L}} = sp(\ell)$ by lemma 3.

### B.2.4 Theorem 8

**Theorem 8.** *Let* $v_m = 2\tilde{\delta}_m^2 - \tilde{\delta}_{m+1}^2 - \tilde{\delta}_{m-1}^2$ *for* $1 \leq m \leq \ell$ *and* $\tilde{\delta}_{\ell+1} = \tilde{\delta}_{\ell-1}$, $\tilde{\delta}_0 = 0$. *The dynamical Lie algebra* $\hat{\mathcal{L}}$ *generated by the system* $H = \tilde{H}_0 + f(t)\hat{H}_1$ *with* $i\tilde{H}_0$ *and* $i\hat{H}_1$ *as in* (2.8) *and* (2.9) *and with the symmetrical relations given in* (2.11) *is* $sp(\ell)$ *if* $\omega_m = \omega_\ell$ *but* $v_m \neq v_l$ *for all* $m \in \mathcal{M} - \{\ell\}$.

**Proof.**

$$\begin{aligned} X^{(0)} &\equiv \omega_\ell^{-1}\left[i\hat{H}_0', Y^{(0)}\right] \\ Z &\equiv 2^{-1}\left[X^{(0)}, Y^{(0)}\right] = \sum_{m=1}^{\ell}(\tilde{\delta}_{m-1}^2 - \tilde{\delta}_m^2)h_m. \end{aligned}$$

Suppose $\mathcal{M} - \{\ell\}$ has $\ell'$ elements labelled $m_1$, $m_2$ up to $m_\ell'$ and let $m_{\ell'+1} = \ell$. Then

$$\begin{aligned} Y^{(1)} &\equiv \left[Z, X^{(0)}\right] - v_1 Y^{(0)} = \sum_{k=2}^{\ell'+1} \tilde{\delta}_{m_k}(v_{m_k} - v_{m_1})y_{m_k} \\ X^{(1)} &\equiv \left[Y^{(0)}, Z\right] - v_{m_1} X^{(0)} = \sum_{k=2}^{\ell'+1} \tilde{\delta}_{m_k}(v_{m_k} - v_{m_1})x_{m_k} \\ Y^{(2)} &\equiv \left[Z, X^{(1)}\right] - v_{m_2} Y^{(1)} = \sum_{k=3}^{\ell'+1} \tilde{\delta}_{m_k}(v_{m_k} - v_{m_1})(v_{m_k} - v_{m_2})y_{m_k} \\ X^{(2)} &\equiv \left[Y^{(1)}, Z\right] - v_{m_2} X^{(1)} = \sum_{k=3}^{\ell'+1} \tilde{\delta}_{m_k}(v_{m_k} - v_{m_1})(v_{m_k} - v_{m_2})x_{m_k} \\ &\vdots \\ Y^{(\ell')} &\equiv \prod_{k=1}^{\ell'} \tilde{\delta}_\ell(v_\ell - v_{m_k})y_\ell \end{aligned}$$

shows that $y_\ell \in \tilde{\mathcal{L}}$ and hence $\tilde{\mathcal{L}} = sp(\ell)$ by lemma 3.

### B.2.5 Theorem 9

**Theorem 9.** *The dynamical Lie algebra* $\hat{\mathcal{L}}$ *generated by a system* $H = \tilde{H}_0 + f(t)\hat{H}_1$ *with* $N = 2\ell$ *equally spaced energy levels and uniform dipole moments is* $sp(\ell)$.

**Proof.** We have $x_\ell = \omega^{-1}\left[i\hat{H}_0', i\hat{H}_1\right]$, $y_\ell = -2^{-1}\left[\hat{H}_0', x_\ell\right]$ and $h_\ell = -2^{-1}\left[x_\ell, y_\ell\right]$. Next, set $Y^{(k)} = Y^{(k-1)} - y_{\ell+1-k}$ and $Z^{(k)} = Z^{(k-1)} - h_{\ell+1-k}$ for $1 \leq k < \ell$, with $Y^{(0)} = \delta^{-1}i\hat{H}_1$ and $Z^{(0)} = i\hat{H}_0'$, and note that $x_{\ell-k} = \left[Z^{(k)}, Y^{(k)}\right]$, $y_{\ell-k} = -2^{-1}\left[Z^{(k)}, x_{\ell-k}\right]$ and

$h_{\ell-k} = -2^{-1}\Big[x_{\ell-k}, y_{\ell-k}\Big]$. This show that $\tilde{\mathcal{L}}$ contains all the generators $x_m$ and $y_m$ of $sp(\ell)$. Hence, $\tilde{\mathcal{L}} = sp(\ell)$.

## B.3 Theorem 10

**Theorem 10.** *A quantum system with Hamiltonian* (2.16) *and* (2.17) *is completely controllable if* $d_n \neq 0$ *for* $1 \leq n \leq N-1$, $\omega_r \neq 0$ *and* $d_{r+1}^2 \neq d_{r-1}^2$.

**Proof.** $i\hat{V}_0$ and $i\hat{V}_1$ can be expressed as follows

$$iV_0 \equiv \sum_{n=1}^{N} E_n i|n\rangle\langle n| + \sum_{n=1, n\neq r}^{N} d_n y_n, \qquad iV_1 \equiv d_r y_r \tag{B.5}$$

We aim to show that the Lie algebra $\mathcal{L}_V$ generated by $i\hat{V}_0$ and $i\hat{V}_1$ contains $x_n \equiv x_{n,n+1}$ and $y_n \equiv y_{n,n+1}$ for $1 \leq n \leq N-1$. As $d_r \neq 0$ by hypothesis, $i\hat{V}_1 = d_r y_r$ implies $y_r \in \mathcal{L}_V$ and

$$\begin{aligned}
X_0 &\equiv [y_r, iV_0] = d_{r-1}x_{r-1,r+1} - d_{r+1}x_{r,r+2} - \omega_r x_r \\
Y_0 &\equiv [X_0, y_r] = d_{r-1}y_{r-1} + d_{r+1}y_{r+1} - 2\omega_r h_r \\
X_0' &\equiv [Y_0, y_r] = -d_{r-1}x_{r-1,r+1} + d_{r+1}x_{r,r+2} + 4\omega_r x_r \\
Y_0' &\equiv [X_0', y_r] = -d_{r-1}y_{r-1} - d_{r+1}y_{r+1} + 8\omega_r h_r
\end{aligned}$$

yields $x_r = (3\omega)^{-1}(X_0 + X_0') \in \mathcal{L}_V$ since $\omega_r \neq 0$ by hypothesis, and $h_r = 2^{-1}[x_r, y_r] \in \mathcal{L}_V$. Furthermore, setting

$$\begin{aligned}
Y_1 &\equiv 3^{-1}(4Y_0 + Y_0') = d_{r-1}y_{r-1} + d_{r+1}y_{r+1} \\
X_1 &\equiv [[x_r, Y_1], y_r] = d_{r-1}x_{r-1} + d_{r+1}x_{r+1} \\
Z_1 &\equiv 2^{-1}[X_1, Y_1] = d_{r-1}^2 h_{r-1} + d_{r+1}^2 h_{r+1} \\
Y_1' &\equiv 2^{-1}[Z_1, X_1] = d_{r-1}^3 y_{r-1} + d_{r+1}^3 y_{r+1} \\
X_1' &\equiv 2^{-1}[Y_1, Z_1] = d_{r-1}^3 x_{r-1} + d_{r+1}^3 x_{r+1}
\end{aligned}$$

leads to

$$\begin{aligned}
Y_1' - d_{r+1}^2 Y_1 &= d_{r-1}^3\left(1 - \frac{d_{r+1}^2}{d_{r-1}^2}\right) y_{r-1} \\
Y_1' - d_{r-1}^2 Y_1 &= d_{r+1}^3\left(1 - \frac{d_{r-1}^2}{d_{r+1}^2}\right) y_{r+1}
\end{aligned}$$

$$X_1' - d_{r+1}^2 X_1 = d_{r-1}^3\left(1 - \frac{d_{r+1}^2}{d_{r-1}^2}\right)x_{r-1}$$
$$X_1' - d_{r-1}^2 X_1 = d_{r+1}^3\left(1 - \frac{d_{r-1}^2}{d_{r+1}^2}\right)x_{r+1}$$

Since $d_{r+1}^2 \neq d_{r-1}^2$ by hypothesis, we have $y_{r-1}$, $x_{r-1}$, $y_{r+1}$ and $x_{r+1}$ in $\mathcal{L}_V$. Next let

$$V_0^{(1)} \equiv iV_0 - Y_1 = \sum_{n=1}^{N} E_n i|n\rangle\langle n| + \sum_{n\in I^{(1)}} d_n y_n$$
$$Y_2' \equiv [[Z_1, V_0^{(1)}], Z_1] = d_{r-2}d_{r-1}^4 y^{r-2} + d_{r+1}^4 d_{r+2} y_{r+2}$$
$$V_0^{(2)} \equiv V_0^{(0)} - d_{r-1}^{-4} Y_2' = \sum_{n=1}^{N} E_n i|n\rangle\langle n| + \sum_{n\in I^{(2)}} d_n y_n + k_{r+2} y_{r+2},$$

where $I^{(1)}$ is the index set $\{1, 2, \ldots, N-1\}$ minus the subset $\{r-1, r, r+1\}$, $I^{(2)}$ is the index set $I^{(1)}$ minus the subset $\{r-2, r+2\}$ and $k_{r+2} = d_{r+2}\left(1 - \frac{d_{r+1}^4}{d_{r-1}^4}\right)$. Computing

$$X_2 \equiv [Z_1, V_0^{(2)}] = d_{r+1}^2 k_{r+2} x_{r+2}$$
$$Y_2 \equiv [X_2, Z_1] = d_{r+1}^4 k_{r+2} y_{r+2}.$$

shows that $x_{r+2}$, $y_{r+2}$ and $h_{r+2} = 2^{-1}[x^{r+2}, y_{r+2}] \in \mathcal{L}_V$. Setting

$$V_0^{(3)} = V_0^{(2)} - d_{r+2} y_{r+2}$$
$$x_{r+3} = d_{r+3}^{-1}[h_{r+2}, V_0^{(3)}]$$
$$y_{r+3} = [x_{r+3}, h_{r+2}]$$
$$h_{r+3} = 2^{-1}[x_{r+3}, y_{r+3}]$$

now shows that $x^{r+3}$, $y^{r+3}$ are in $\mathcal{L}_V$. By repeating this procedure we obtain

$$V_0^{(k+1)} = V_0^{(k)} - d_{r+k} y_{r+k}$$
$$x_{r+k+1} = d_{r+k+1}^{-1}[h_{r+k}, V_0^{(k+1)}]$$
$$y_{r+k+1} = [x_{r+k+1}, h_{r+k}]$$
$$h_{r+k+1} = 2^{-1}[x_{r+k+1}, y_{r+k+1}]$$

which shows that $x_{r+k+1}$ and $y_{r+k+1}$ are in $\mathcal{L}_V$ for $3 \leq k \leq N-r-2$. To show that the elements $x_{r-k}$, $y_{r-k}$ for $2 \leq k \leq r-1$ are in $\mathcal{L}_V$, we note that

$$y_{r-2} = d_{r-2}^{-1} d_{r-1}^{-4}(Y_2' - d_{r+1}^4 d_{r+2} y_{r+2})$$
$$x_{r-2} = [h_{r-1}, y_{r-2}]$$
$$h_{r-2} = 2^{-1}[x_{r-2}, y_{r-2}]$$

implies $y_{r-2}, x_{r-2} \in \mathcal{L}_V$. Setting $W_0^{(2)} = V_0^{(N-r-1)}$ and

$$\begin{aligned} x_{r-k-1} &= d_{r-k-1}^{-1}[h_{r-k}, W_0^{(k)}] \\ y_{r-k-1} &= [x_{r-k-1}, h_{r-k}] \\ h_{r-k-1} &= 2^{-1}[x_{r-k-1}, y_{r-k-1}] \\ W_0^{(k+1)} &= W_0^{(k)} - d_{r-k-1} y_{r-k-1} \end{aligned}$$

shows that $x_{r-k-1}$ and $y_{r-k-1}$ are in $\mathcal{L}_V$ for $2 \leq k \leq r-2$.

## B.4 Theorem 11

**Theorem 11.** *The independent components of a decomposable system with Hamiltonian (2.3) of the form (2.18) are* simultaneously mixed-state controllable *if and only if the dimension of the dynamical Lie algebra $\mathcal{L}$ is*

$$dim\, \mathcal{L} = r + \sum_{\ell=1}^{L} (N_\ell^2 - 1)$$

*where $r \leq min(M+1, L)$ is the rank of the matrix (2.19).*

**Proof.** Assume $\hat{H}[\mathrm{f}(t)]$ is of the form

$$\hat{H}[\mathrm{f}(t)] = \hat{H}_0 + \sum_{m=1}^{M} f_m(t) \hat{H}_m$$

and $\hat{\rho}(t)$ and $\hat{H}_m$ are of the form

$$\begin{aligned} \hat{\rho}(t) &= \mathrm{diag}(\hat{\rho}_1(t), \ldots, \hat{\rho}_L(t)) \\ \hat{H}_m &= \mathrm{diag}(\hat{H}_{m,1}, \ldots, \hat{H}_{m,L}) \qquad m = 0, 1, \ldots, M. \end{aligned}$$

For $m = 0, \ldots, M$ and $\ell = 1, \ldots, L$ define the diagonal generators

$$\tilde{D}_m = \mathrm{diag}(\alpha_{m,1} \hat{I}_{N_1}, \ldots, \alpha_{m,P} \hat{I}_{N_L})$$

where $\alpha_{m,\ell} = \mathrm{Tr}(\hat{H}_{m,\ell})$ and $\hat{I}_\ell$ is the identity matrix of dimension $\ell$, and the trace-zero generators

$$\tilde{H}_m = \mathrm{diag}(\tilde{H}_{m,1}, \ldots, \tilde{H}_{m,L}),$$

where the blocks on the diagonal are given by

$$\tilde{H}_{m,\ell} = \hat{H}_{m,\ell} - \frac{\alpha_{m,\ell}}{N_\ell} \hat{I}_\ell$$

The diagonal elements $\tilde{D}_m$ commute with $\hat{\rho}(t)$ for all $m = 0, \ldots, M$. Hence, the orbits of $\hat{\rho}(t)$ generated by $\hat{H}[\mathbf{f}(t)]$ and $\tilde{H}[\mathbf{f}(t)] = \tilde{H}_0 + \sum_{m=1}^{M} f_m(t)\tilde{H}_m$ are identical.

Let $\tilde{\mathcal{L}} = \mathcal{L}(\{\tilde{H}_m\})$ be the Lie algebra generated by the trace-zero skew-Hermitian matrices $i\tilde{H}_m$. Due to the structure of the generators, the Lie algebra $\tilde{\mathcal{L}}$ must be a subalgebra of $\oplus_{\ell=1}^{L} su(N_\ell)$, and it follows from classical results [15] that the orbits of a generic mixed state [68] will be maximal if and only if $\tilde{\mathcal{L}} = \oplus_{\ell=1}^{L} su(N_\ell)$.

Now let $\mathcal{L} = \mathcal{L}(\{\hat{H}_m\})$ be the Lie algebra generated by $i\hat{H}_m$, and $\mathcal{L}_D = \mathcal{L}(\{\tilde{D}_M\})$ be the Lie algebra generated by the $M+1$ diagonal (skew-Hermitian) matrices $i\tilde{D}_m$. Since the diagonal generators $i\tilde{D}_m$ commute with the trace-zero matrices $\tilde{H}_m$, i.e. $[\tilde{D}_m, \tilde{H}_{m'}] = 0$ for all $m, m' = 1, 2, \ldots, M$, we have

$$\mathcal{L} = \tilde{\mathcal{L}} \oplus \mathcal{L}_D$$

i.e., the Lie algebra $\mathcal{L}$ is the direct sum of the Lie algebras $\tilde{\mathcal{L}}$ and $\mathcal{L}_D$. Noting that the dimension of $su(N_\ell)$ is $N_\ell^2 - 1$ and the dimension of $\mathcal{L}_D$ is equal to the rank of the matrix (2.19), we obtain the Lie algebra dimension condition of Theorem 11 as a necessary and sufficient condition for simultaneous (mixed-state) controllability.

# Appendix C

# Convergence Results

## C.1 Euler-Lagrange Equations

The Euler-Lagrange Equations are

$$\lambda_m f_m(t) = -i\langle\langle \hat{A}_v(t)|\mathcal{L}_m|\hat{\rho}_v(t)\rangle\rangle \tag{C.1}$$

$$i\hbar\frac{\partial}{\partial t}|\hat{\rho}_v(t)\rangle\rangle = \Big[\mathcal{L}_0 + \sum_{m=1}^{M} f_m(t)\mathcal{L}_m\Big]|\hat{\rho}_v(t)\rangle\rangle \tag{C.2}$$

$$i\hbar\frac{\partial}{\partial t}|\hat{A}_v(t)\rangle\rangle = \Big[\mathcal{L}_0 + \sum_{m=1}^{M} f_m(t)\mathcal{L}_m\Big]|\hat{A}_v(t)\rangle\rangle \tag{C.3}$$

The function $J$ is given by

$$J = \langle\langle \hat{A}|\hat{\rho}_v(t_F)\rangle\rangle - \int_{t_0}^{t_F}\langle\langle \hat{A}_v(t)|\frac{\partial}{\partial t} + \frac{i}{\hbar}\mathcal{L}_{tot}(\mathbf{f})|\hat{\rho}_v(t)\rangle\rangle dt - \sum_{m=1}^{M}\frac{\lambda_m}{2\hbar}\int_{t_0}^{t_F}|f_m(t)|^2 dt \tag{C.4}$$

where

$$\mathcal{L}_{tot} = \mathcal{L}_0 + \sum_{m=1}^{M} f_m\mathcal{L}_m \quad \text{and} \quad \mathbf{f} = (f_1, f_2, \ldots, f_M)^T$$

For $J$ to have a stationary path the variation of $J$ under independent variations of $\hat{A}_v$, $\hat{\rho}_m$ and $\mathbf{f}$ will be zero. This leads to the Euler-Lagrange equation as shown below. Firstly, consider the variation of $J$ under the independent variation of $f_m$

$$\frac{\delta J}{\delta f_m} = \frac{\delta}{\delta f_m}\Big(-\int_{t_0}^{t_F}\langle\langle \hat{A}_v(t)|\frac{\delta}{\delta t} + \frac{i}{\hbar}\mathcal{L}_{tot}(\mathbf{f})|\hat{\rho}_v(t)\rangle\rangle dt - \sum_{m=1}^{M}\frac{\lambda_m}{2\hbar}\int_{t_0}^{t_F}|f_m(t)|^2 dt\Big)$$

$$= \frac{\delta}{\delta f_m}\Big( - \int_{t_0}^{t_F} \langle\langle \hat{A}_v(t)| \frac{i}{\hbar}\mathcal{L}_0|\hat{\rho}_v(t)\rangle\rangle dt - \int_{t_0}^{t_F} \langle\langle \hat{A}_v(t)| \frac{i}{\hbar}\sum_{m=1}^{M} f_m\mathcal{L}_m|\hat{\rho}_v(t)\rangle\rangle dt$$
$$- \sum_{m=1}^{M}\frac{\lambda_m}{2\hbar}\int_{t_0}^{t_F}|f_m(t)|^2 dt\Big)$$
$$= \frac{\delta}{\delta f_m}\Big( - \int_{t_0}^{t_F} \langle\langle \hat{A}_v(t)| \frac{i}{\hbar}\sum_{m=1}^{M} f_m\mathcal{L}_m|\hat{\rho}_v(t)\rangle\rangle dt - \sum_{m=1}^{M}\frac{\lambda_m}{2\hbar}\int_{t_0}^{t_F}|f_m(t)|^2 dt\Big)$$
$$= -\frac{i}{\hbar}\langle\langle \hat{A}_v(t)|\mathcal{L}_m|\hat{\rho}_v(t)\rangle\rangle - \frac{\lambda_m}{\hbar}f_m(t)$$

Now $\dfrac{\delta J}{\delta f_m} = 0$ leads to

$$-\frac{i}{\hbar}\langle\langle \hat{A}_v(t)|\mathcal{L}_m|\hat{\rho}_v(t)\rangle\rangle - \frac{\lambda_m}{\hbar}f_m(t) = 0$$
$$\lambda_m f_m(t) = -i\langle\langle \hat{A}_v(t)|\mathcal{L}_m|\hat{\rho}_v(t)\rangle\rangle$$

which is (C.1).

Secondly, consider the variation of $J$ under the independent variation of $\hat{A}_v$, i.e.

$$\frac{\delta J}{\delta \hat{A}_v} = \frac{\delta}{\delta \hat{A}_v}\Big( - \int_{t_0}^{t_F} \langle\langle \hat{A}_v(t)| \frac{\delta}{\delta t} + \frac{i}{\hbar}\mathcal{L}_{tot}(\mathbf{f})|\hat{\rho}_v(t)\rangle\rangle dt\Big)$$

Now if, in general, this is zero then

$$\Big(\frac{\partial}{\partial t} + \frac{i}{\hbar}\mathcal{L}_{tot}(\mathbf{f})\Big)|\hat{\rho}_v(t)\rangle\rangle = 0$$

this leads to

$$\frac{\partial}{\partial t}|\hat{\rho}_v(t)\rangle\rangle + \frac{i}{\hbar}\mathcal{L}_{tot}(\mathbf{f})\Big)|\hat{\rho}_v(t)\rangle\rangle = 0$$
$$i\hbar\frac{\partial}{\partial t}|\hat{\rho}_v(t)\rangle\rangle - \mathcal{L}_{tot}(\mathbf{f})\Big)|\hat{\rho}_v(t)\rangle\rangle = 0$$
$$i\hbar\frac{\partial}{\partial t}|\hat{\rho}_v(t)\rangle\rangle = \Big[\mathcal{L}_0 + \sum_{m=1}^{M} f_m\mathcal{L}_m\Big]|\hat{\rho}_v(t)\rangle\rangle$$

which is (C.2).

Thirdly, consider the variation of $J$ under the independent variation of $\hat{\rho}_v$, that is

$$\frac{\delta J}{\delta \hat{\rho}_v} = \frac{\delta}{\delta \hat{\rho}_v}\Big(\langle\langle \hat{A}|\hat{\rho}_v(t_F)\rangle\rangle - \int_{t_0}^{t_F} \langle\langle \hat{A}_v(t)| \frac{\partial}{\partial t} + \frac{i}{\hbar}\mathcal{L}_{tot}|\hat{\rho}_v(t)\rangle\rangle dt\Big)$$
$$= \frac{\delta}{\delta \hat{\rho}_v}\Big(\langle\langle \hat{A}|\hat{\rho}_v(t_F)\rangle\rangle - \int_{t_0}^{t_F} \langle\langle \hat{A}_v(t)| \frac{\partial}{\partial t}|\hat{\rho}_v(t)\rangle\rangle dt - \int_{t_0}^{t_F} \langle\langle \hat{A}_v(t)| \frac{i}{\hbar}\mathcal{L}_{tot}|\hat{\rho}_v(t)\rangle\rangle dt\Big)$$

Using integration by parts this becomes

$$\frac{\delta J}{\delta \hat{\rho}_v} = \frac{\delta}{\delta \hat{\rho}_v}\Big(\langle\langle \hat{A}|\hat{\rho}_v(t_F)\rangle\rangle - \Big[\langle\langle \hat{A}_v(t)|\hat{\rho}_v(t)\rangle\rangle\Big]_{t_0}^{t_F} + \int_{t_0}^{t_F} \langle\langle \frac{\partial}{\partial t}(\hat{A}_v(t))|\hat{\rho}_v(t)\rangle\rangle dt$$

$$- \int_{t_0}^{t_F} \langle\langle \hat{A}_v(t)| \frac{i}{\hbar}\mathcal{L}_{tot}|\hat{\rho}_v(t)\rangle\rangle dt\Big)$$

$$\frac{\delta J}{\delta \hat{\rho}_v} = \frac{\delta}{\delta \hat{\rho}_v}\Big(\langle\langle \hat{A}_v(t_0)|\hat{\rho}_v(t_0)\rangle\rangle + \int_{t_0}^{t_F} \langle\langle \hat{\rho}_v(t)|\frac{\partial}{\partial t} + \frac{i}{\hbar}\mathcal{L}_{tot}^{\dagger}|\hat{A}_v(t)\rangle\rangle^* dt\Big)$$

Now $\frac{\delta J}{\delta \hat{\rho}_v} = 0$ leads to

$$\int_{t_0}^{t_F} \langle\langle \hat{\rho}_v(t)|\frac{\partial}{\partial t} + \frac{i}{\hbar}\mathcal{L}_{tot}^{\dagger}|\hat{A}_v(t)\rangle\rangle^* dt = 0$$

which, in general, will be true if

$$\Big(\Big[\frac{\partial}{\partial t} + \frac{i}{\hbar}\mathcal{L}_{tot}^{\dagger}\Big]|\hat{A}_v(t)\rangle\rangle\Big)^* = 0$$

$$\frac{\partial}{\partial t}|\hat{A}_v(t)\rangle\rangle + \frac{i}{\hbar}\Big[\mathcal{L}_0 + \sum_{m=1}^{M} f_m\mathcal{L}_m\Big]^{\dagger}|\hat{A}_v(t)\rangle\rangle = 0$$

$$\frac{\partial}{\partial t}|\hat{A}_v(t)\rangle\rangle + \frac{i}{\hbar}\Big[\mathcal{L}_0^{\dagger} + \sum_{m=1}^{M} f_m\mathcal{L}_m^{\dagger}\Big]|\hat{A}_v(t)\rangle\rangle = 0$$

$$i\hbar\frac{\partial}{\partial t}|\hat{A}_v(t)\rangle\rangle = \Big[\mathcal{L}_0 + \sum_{m=1}^{M} f_m\mathcal{L}_m\Big]|\hat{A}_v(t)\rangle\rangle$$

which is (C.3).

## C.2 Proof of Lemma 1

**Lemma 1.** *Suppose $U(t,t_0)$ is such that $U(t,t_0)^{-1}$ exists for $t \in [t_0,t_F]$ and $U(t,t_0)$ satisfies*

$$i\hbar\frac{\partial}{\partial t}\Big(U(t,t_0)\Big) = \tilde{\mathcal{L}}U(t,t_0) \tag{C.5}$$

*then*

$$|\delta\rho_v^{(n)}(t)\rangle\rangle = -\frac{i}{\hbar}\tilde{U}^{(n)}(t,t_0)\int_{t_0}^{t}\tilde{U}^{(n)}(t',t_0)^{-1}|\Delta^{(n)}(t')\rangle\rangle dt' \tag{C.6}$$

*is a solution of*

$$i\hbar\frac{\partial}{\partial t}|\delta\rho_v^{(n)}(t)\rangle\rangle = \tilde{\mathcal{L}}|\delta\rho_v^{(n)}(t)\rangle\rangle + |\Delta^{(n)}(t)\rangle\rangle. \tag{C.7}$$

**Proof.** Partially differentiating (C.6) with respect to $t$ and multiplying by $i\hbar$ gives

$$i\hbar\frac{\partial}{\partial t}|\delta\rho_v^{(n)}(t)\rangle\rangle = \frac{\partial}{\partial t}\Big(\tilde{U}^{(n)}(t,t_0)\int_{t_0}^{t}\tilde{U}^{(n)}(t',t_0)^{-1}|\Delta^{(n)}(t')\rangle\rangle dt'\Big)$$

and using the product rule

$$
\begin{aligned}
&= \frac{\partial}{\partial t}\Big(\tilde{U}^{(n)}(t,t_0)\Big)\int_{t_0}^{t}\tilde{U}^{(n)}(t',t_0)^{-1}|\Delta^{(n)}(t')\rangle\rangle dt' \\
&+ \tilde{U}^{(n)}(t,t_0)\frac{\partial}{\partial t}\Big(\int_{t_0}^{t}\tilde{U}^{(n)}(t',t_0)^{-1}|\Delta^{(n)}(t')\rangle\rangle dt'\Big) \\
&= -\frac{i}{\hbar}\tilde{\mathcal{L}}\tilde{U}^{(n)}(t,t_0)\int_{t_0}^{t}\tilde{U}^{(n)}(t',t_0)^{-1}|\Delta^{(n)}(t')\rangle\rangle dt' \\
&+ \tilde{U}^{(n)}(t,t_0)\tilde{U}^{(n)}(t,t_0)^{-1}|\Delta^{(n)}(t)\rangle\rangle \\
&= \tilde{\mathcal{L}}|\delta\rho_v^{(n)}(t)\rangle\rangle + |\Delta^{(n)}(t)\rangle\rangle
\end{aligned}
$$

## C.3 Convergence of $J$ Functional

**Theorem 12.** *For any bounded initial field* $\mathbf{f}^{(0)}(t)$*, with individual components,* $f_m(t)$*, that have the properties that they are real-valued, continuous, have continuous first derivatives and for* $\alpha, \beta \in [0,2]$ *we have*

$$\delta J^{(n)} = J^{(n+1)} - J^{(n)} \geq 0, \tag{C.8}$$

*and* $J^{(n)}$ *is bounded above. Hence as the sequence* $J^{(n)}$ *is monotonically increasing and bounded above it is convergent.*
*Moreover,* $\delta J^{(n)} = 0$ *if* $(\alpha,\beta) \in \{(0,0),(0,2),(2,0),(2,2)\}$.

The proof consists of two parts. In the first part it is shown that $J^{(n)}$ is a monotonically increasing sequence and $\delta J^{(n)} = 0$ if $(\alpha,\beta) \in \{(0,0),(0,2),(2,0),(2,2)\}$. In the second part it is shown that the sequence $J^{(n)}$ is bounded.

### C.3.1 Proof that $J^{(n)}$ is monotonically increasing

To prove that $J^{(n)}$ is monotonically increasing we need to show that $J^{(n+1)} - J^{(n)} \geq 0$. The method used is to put $\delta J^{(n)} = J^{(n+1)} - J^{(n)}$ and to show that $\delta J^{(n)}$ is the sum of non-negative (real-valued functions squared) terms and hence is $\geq 0$. Now

$$
\begin{aligned}
&\delta J^{(n)} = J^{(n+1)} - J^{(n)} \\
&= \langle\langle A|\rho_v^{(n+1)}(t_F)\rangle\rangle - \sum_{m=1}^{M}\frac{\lambda_m}{2\hbar}\parallel f_m^{(n+1)}\parallel_2^2 - \langle\langle A|\rho_v^{(n)}(t_F)\rangle\rangle + \sum_{m=1}^{M}\frac{\lambda_m}{2\hbar}\parallel f_m^{(n)}\parallel_2^2 \\
&= \langle\langle A|\rho_v^{(n+1)}(t_F)\rangle\rangle - \sum_{m=1}^{M}\frac{\lambda_m}{2\hbar}\int_{t_0}^{t_F}[f_m^{(n+1)}(t)]^2dt - \langle\langle A|\rho_v^{(n)}(t_F)\rangle\rangle + \sum_{m=1}^{M}\frac{\lambda_m}{2\hbar}\int_{t_0}^{t_F}[f_m^{(n)}(t)]^2dt
\end{aligned}
$$

$$= \langle\langle A|\rho_v^{(n+1)}(t_F)\rangle\rangle - \langle\langle A|\rho_v^{(n)}(t_F)\rangle\rangle - \sum_{m=1}^{M}\frac{\lambda_m}{2\hbar}\int_{t_0}^{t_F}[f_m^{(n+1)}(t)]^2dt + \sum_{m=1}^{M}\frac{\lambda_m}{2\hbar}\int_{t_0}^{t_F}[f_m^{(n)}(t)]^2dt$$

$$= \langle\langle A|(\rho_v^{(n+1)}(t_F) - \rho_v^{(n)}(t_F))\rangle\rangle - \sum_{m=1}^{M}\frac{\lambda_m}{2\hbar}\int_{t_0}^{t_F}[f_m^{(n+1)}(t)]^2 - [f_m^{(n)}(t)]^2dt$$

$$= \langle\langle A|\delta\rho_v^{(n)}(t_F)\rangle\rangle - \delta\mathcal{C}^{(n)}$$

Hence

$$\delta J^{(n)} = \langle\langle A|\delta\rho_v^{(n)}(t_F)\rangle\rangle - \delta\mathcal{C}^{(n)} \tag{C.9}$$

where

$$|\delta\rho_v^{(n)}(t_F)\rangle\rangle = |\rho_v^{(n+1)}(t_F)\rangle\rangle - |\rho_v^{(n)}(t_F)\rangle\rangle$$

and

$$\delta\mathcal{C}^{(n)} = \sum_{m=1}^{M}\frac{\lambda_m}{2\hbar}\int_{t_0}^{t_F}[f_m^{(n+1)}(t)]^2 - [f_m^{(n)}(t)]^2dt$$

We wish to find an expression for $|\delta\rho_v^{(n)}(t)\rangle\rangle$. To do this we use the fact that $|\rho_v^{(n)}(t)\rangle\rangle$ satisfies the equation

$$i\hbar\frac{\partial}{\partial t}|\rho_v^{(n)}(t)\rangle\rangle = (\mathcal{L}_0 + \sum_{m=1}^{M} f_m^{(n)}\mathcal{L}_m)|\rho_v^{(n)}(t)\rangle\rangle$$

Hence we have

$$\begin{aligned}
i\hbar\frac{\partial}{\partial t}|\delta\rho_v^{(n)}(t)\rangle\rangle &= i\hbar\frac{\partial}{\partial t}|\rho_v^{(n+1)}(t)\rangle\rangle - i\hbar\frac{\partial}{\partial t}|\rho_v^{(n)}(t)\rangle\rangle \\
&= (\mathcal{L}_0 + \sum_{m=1}^{M} f_m^{(n+1)}\mathcal{L}_m)|\rho_v^{(n+1)}(t)\rangle\rangle - (\mathcal{L}_0 + \sum_{m=1}^{M} f_m^{(n)}\mathcal{L}_m)|\rho_v^{(n)}(t)\rangle\rangle \\
&= (\mathcal{L}_0 + \sum_{m=1}^{M}[\tilde{f}_m^{(n)} + f_m^{(n+1)} - \tilde{f}_m^{(n)}]\mathcal{L}_m)|\rho_v^{(n+1)}(t)\rangle\rangle \\
&\quad -(\mathcal{L}_0 + \sum_{m=1}^{M}[\tilde{f}_m^{(n)} + f_m^{(n)} - \tilde{f}_m^{(n)}]\mathcal{L}_m)|\rho_v^{(n)}(t)\rangle\rangle \\
&= (\mathcal{L}_0 + \sum_{m=1}^{M}\tilde{f}_m^{(n)}\mathcal{L}_m)|\rho_v^{(n+1)}(t)\rangle\rangle - (\mathcal{L}_0 + \sum_{m=1}^{M}\tilde{f}_m^{(n)}\mathcal{L}_m)|\rho_v^{(n)}(t)\rangle\rangle \\
&\quad + \sum_{m=1}^{M}[f_m^{(n+1)} - \tilde{f}_m^{(n)}]\mathcal{L}_m|\rho_v^{(n+1)}(t)\rangle\rangle + \sum_{m=1}^{M}[\tilde{f}_m^{(n)} - f_m^{(n)}]\mathcal{L}_m|\rho_v^{(n)}(t)\rangle\rangle \\
&= (\mathcal{L}_0 + \sum_{m=1}^{M}\tilde{f}_m^{(n)}\mathcal{L}_m)|\delta\rho_v^{(n)}(t)\rangle\rangle + \sum_{m=1}^{M}[f_m^{(n+1)} - \tilde{f}_m^{(n)}]\mathcal{L}_m|\rho_v^{(n+1)}(t)\rangle\rangle
\end{aligned}$$

$$
\begin{aligned}
&+\sum_{m=1}^{M}[\tilde{f}_m^{(n)} - f_m^{(n)}]\mathcal{L}_m|\rho_v^{(n)}(t)\rangle\rangle \\
= \;& \tilde{\mathcal{L}}^{(n)}|\delta\rho_v^{(n)}(t)\rangle\rangle + |\Delta^{(n)}(t)\rangle\rangle
\end{aligned}
$$

where

$$
\tilde{\mathcal{L}}^{(n)} \;=\; (\mathcal{L}_0 + \sum_{m=1}^{M}\tilde{f}_m^{(n)}\mathcal{L}_m)
$$

and

$$
|\Delta^{(n)}(t)\rangle\rangle = \sum_{m=1}^{M}[f_m^{(n+1)} - \tilde{f}_m^{(n)}]\mathcal{L}_m|\rho_v^{(n+1)}(t)\rangle\rangle + \sum_{m=1}^{M}[\tilde{f}_m^{(n)} - f_m^{(n)}]\mathcal{L}_m|\rho_v^{(n)}(t)\rangle\rangle \quad \text{(C.10)}
$$

This gives us the following partial differential equation involving $|\delta\rho_v^{(n)}(t)\rangle\rangle$

$$
i\hbar\frac{\partial}{\partial t}|\delta\rho_v^{(n)}(t)\rangle\rangle = \tilde{\mathcal{L}}^{(n)}|\delta\rho_v^{(n)}(t)\rangle\rangle + |\Delta^{(n)}(t)\rangle\rangle
$$

The solution of this is given by Lemma 1 as

$$
\begin{aligned}
|\delta\rho_v^{(n)}(t)\rangle\rangle &= -\frac{i}{\hbar}\tilde{U}^{(n)}(t,t_0)\int_{t_0}^{t}\tilde{U}^{(n)}(t',t_0)^{-1}|\Delta^{(n)}(t')\rangle\rangle dt' \\
|\delta\rho_v^{(n)}(t_F)\rangle\rangle &= -\frac{i}{\hbar}\tilde{U}^{(n)}(t_F,t_0)\int_{t_0}^{t_F}\tilde{U}^{(n)}(t',t_0)^{-1}|\Delta^{(n)}(t')\rangle\rangle dt' \\
\langle\langle A|\delta\rho_v^{(n)}(t_F)\rangle\rangle &= -\frac{i}{\hbar}\langle\langle A|\tilde{U}^{(n)}(t_F,t_0)\int_{t_0}^{t_F}\tilde{U}^{(n)}(t',t_0)^{-1}|\Delta^{(n)}(t')\rangle\rangle dt' \\
&= -\frac{i}{\hbar}\int_{t_0}^{t_F}\langle\langle A|\tilde{U}^{(n)}(t_F,t_0)\tilde{U}^{(n)}(t',t_0)^{-1}|\Delta^{(n)}(t')\rangle\rangle dt' \\
&= -\frac{i}{\hbar}\int_{t_0}^{t_F}\langle\langle A|\tilde{U}^{(n)}(t_F,t_0)\tilde{U}^{(n)}(t_0,t')|\Delta^{(n)}(t')\rangle\rangle dt' \\
&= -\frac{i}{\hbar}\int_{t_0}^{t_F}\langle\langle A|\tilde{U}^{(n)}(t_F,t_0)\tilde{U}^{(n)}(t_0,t')|\Delta^{(n)}(t')\rangle\rangle dt' \\
&= -\frac{i}{\hbar}\int_{t_0}^{t_F}\langle\langle A|\tilde{U}^{(n)}(t_F,t')|\Delta^{(n)}(t')\rangle\rangle dt' \\
&= -\frac{i}{\hbar}\int_{t_0}^{t_F}\langle\langle A_n^{(n)}(t)|\Delta^{(n)}(t)\rangle\rangle dt \quad \text{with } t' \text{ replaced by } t \quad \text{(C.11)}
\end{aligned}
$$

Hence, we have

$$
\langle\langle A|\delta\rho_v^{(n)}(t_F)\rangle\rangle = -\frac{i}{\hbar}\int_{t_0}^{t_F}\langle\langle A_v^{(n)}(t)|\Delta^{(n)}(t)\rangle\rangle dt
$$

We now consider $\tilde{f}_m^{(n)}(t)$ and $f_m^{(n+1)}(t)$ which are defined as follows

$$
\tilde{f}_m^{(n)}(t) = (1-\beta)f_m^{(n)} - \frac{i\beta}{\lambda_m}\langle\langle A_v^{(n)}(t)|\mathcal{L}_m|\rho_v^{(n)}(t)\rangle\rangle
$$

which when rearranged with $\beta \neq 0$ can be written

$$\langle\langle A_v^{(n)}(t)|\mathcal{L}_m|\rho_v^{(n)}(t)\rangle\rangle = -i\lambda_m\{(\frac{1}{\beta}-1)f_m^{(n)} - \frac{1}{\beta}\tilde{f}_m^{(n)}\}$$

and

$$f_m^{(n+1)}(t) = (1-\alpha)\tilde{f}_m^{(n)} - \frac{i\alpha}{\lambda_m}\langle\langle A_v^{(n)}(t)|\mathcal{L}_m|\rho_v^{(n+1)}(t)\rangle\rangle$$

which when rearranged with $\alpha \neq 0$ can be written

$$\langle\langle A_v^{(n)}(t)|\mathcal{L}_m|\rho_v^{(n+1)}(t)\rangle\rangle = -i\lambda_m\{(\frac{1}{\alpha}-1)\tilde{f}_m^{(n)} - \frac{1}{\alpha}f_m^{(n+1)}\}$$

Using these we have

$$\begin{aligned}
\langle\langle A|\delta\rho_v^{(n)}(t_F)\rangle\rangle &= -\frac{i}{\hbar}\int_{t_0}^{t_F}\langle\langle A_v^{(n)}(t)|\Delta^{(n)}(t)\rangle\rangle dt \\
&= -\frac{i}{\hbar}\int_{t_0}^{t_F}\langle\langle A_m^{(n)}(t)|(\sum_{m=1}^{M}[f_m^{(n+1)} - \tilde{f}_m^{(n)}]\mathcal{L}_m|\rho_v^{(n+1)}(t)\rangle\rangle \\
&\qquad + \sum_{m=1}^{M}[\tilde{f}_m^{(n)} - f_m^{(n)}]\mathcal{L}_m|\rho_v^{(n)}(t)\rangle\rangle)dt \\
&= -\frac{i}{\hbar}\int_{t_0}^{t_F}\langle\langle A_m^{(n)}(t)|\sum_{m=1}^{M}[f_m^{(n+1)} - \tilde{f}_m^{(n)}]\mathcal{L}_m|\rho_v^{(n+1)}(t)\rangle\rangle \\
&\qquad + \langle\langle A_m^{(n)}(t)|\sum_{m=1}^{M}[\tilde{f}_m^{(n)} - f_m^{(n)}]\mathcal{L}_m|\rho_v^{(n)}(t)\rangle\rangle dt \\
&= -\frac{i}{\hbar}\int_{t_0}^{t_F}\sum_{m=1}^{M}\Big\{[f_m^{(n+1)} - \tilde{f}_m^{(n)}]\langle\langle A_m^{(n)}(t)|\mathcal{L}_m|\rho_v^{(n+1)}(t)\rangle\rangle\Big\} \\
&\qquad + \sum_{m=1}^{M}\Big\{[\tilde{f}_m^{(n)} - f_m^{(n)}]\langle\langle A_m^{(n)}(t)|\mathcal{L}_m|\rho_v^{(n)}(t)\rangle\rangle\Big\}\,dt \\
&= -\sum_{m=1}^{M}\int_{t_0}^{t_F}\frac{i}{\hbar}\Big\{[f_m^{(n+1)} - \tilde{f}_m^{(n)}](-i\lambda_m)[(\frac{1}{\alpha}-1)\tilde{f}_m^{(n)} - \frac{1}{\alpha}f_m^{(n+1)}] \\
&\qquad + [\tilde{f}_m^{(n)} - f_m^{(n)}](-i\lambda_m)[(\frac{1}{\beta}-1)f_m^{(n)} - \frac{1}{\beta}\tilde{f}_m^{(n)}]\Big\}dt \\
&= -\sum_{m=1}^{M}\frac{\lambda_m}{\hbar}\int_{t_0}^{t_F}\Big\{\frac{1}{\alpha}(f_m^{(n+1)} - \tilde{f}_m^{(n)})(\tilde{f}_m^{(n)} - f_m^{(n+1)}) - \tilde{f}_m^{(n)}(f_m^{(n+1)} - \tilde{f}_m^{(n)}) \\
&\qquad + \frac{1}{\beta}(\tilde{f}_m^{(n)} - f_m^{(n)})(f_m^{(n)} - \tilde{f}_m^{(n)}) - f_m^{(n)}(\tilde{f}_m^{(n)} - f_m^{(n)})\Big\}dt \\
&= \sum_{m=1}^{M}\frac{\lambda_m}{2\hbar}\int_{t_0}^{t_F}\Big\{\frac{2}{\alpha}(f_m^{(n+1)} - \tilde{f}_m^{(n)})^2 + 2\tilde{f}_m^{(n)}(f_m^{(n+1)} - \tilde{f}_m^{(n)}) \\
&\qquad + \frac{2}{\beta}(\tilde{f}_m^{(n)} - f_m^{(n)})^2 + 2f_m^{(n)}(\tilde{f}_m^{(n)} - f_m^{(n)})\Big\}dt
\end{aligned}$$

Hence

$$\langle\langle A|\delta\rho_v^{(n)}(t_F)\rangle\rangle = \sum_{m=1}^{M}\frac{\lambda_m}{2\hbar}\int_{t_0}^{t_F}\Big\{\frac{2}{\alpha}(f_m^{(n+1)}-\tilde{f}_m^{(n)})^2+2\tilde{f}_m^{(n)}(f_m^{(n+1)}-\tilde{f}_m^{(n)}) + \frac{2}{\beta}(\tilde{f}_m^{(n)}-f_m^{(n)})^2+2f_m^{(n)}(\tilde{f}_m^{(n)}-f_m^{(n)})\Big\}dt \quad \text{(C.12)}$$

Now consider $\delta\mathcal{C}^{(n)}$. From above we have

$$\begin{aligned}
\delta\mathcal{C}^{(n)} &= \sum_{m=1}^{M}\frac{\lambda_m}{2\hbar}\int_{t_0}^{t_F}[f_m^{(n+1)}]^2-[f_m^{(n)}]^2dt \\
&= \sum_{m=1}^{M}\frac{\lambda_m}{2\hbar}\int_{t_0}^{t_F}\Big[[f_m^{(n+1)}]^2-[f_m^{(n)}]^2\Big]dt \\
&= \sum_{m=1}^{M}\frac{\lambda_m}{2\hbar}\int_{t_0}^{t_F}\Big[[f_m^{(n+1)}]^2-2f_m^{(n+1)}\tilde{f}_m^{(n)}+[\tilde{f}_m^{(n)}]^2+2\tilde{f}_m^{(n)}f_m^{(n+1)}-2[\tilde{f}_m^{(n)}]^2+[\tilde{f}_m^{(n)}]^2 \\
&\qquad -2\tilde{f}_m^{(n)}f_m^{(n)}+[f_m^{(n)}]^2+2f^{(n)}\tilde{f}_m^{(n)}-2[f_m^{(n)}]^2\Big]dt \\
&= \sum_{m=1}^{M}\frac{\lambda_m}{2\hbar}\int_{t_0}^{t_F}\Big[(f_m^{(n+1)}-\tilde{f}_m^{(n)})^2+2\tilde{f}_m^{(n)}(f_m^{(n+1)}-\tilde{f}_m^{(n)}) \\
&\qquad +(\tilde{f}_m^{(n)}-f_m^{(n)})^2+2f_m^{(n)}(\tilde{f}_m^{(n)}-f_m^{(n)})\Big]dt
\end{aligned}$$

Hence

$$\delta\mathcal{C}^{(n)} = \sum_{m=1}^{M}\frac{\lambda_m}{2\hbar}\int_{t_0}^{t_F}\Big[(f_m^{(n+1)}-\tilde{f}_m^{(n)})^2+2\tilde{f}_m^{(n)}(f_m^{(n+1)}-\tilde{f}_m^{(n)}) +(\tilde{f}_m^{(n)}-f_m^{(n)})^2+2f_m^{(n)}(\tilde{f}_m^{(n)}-f_m^{(n)})\Big]dt \quad \text{(C.13)}$$

From ( C.9) we have

$$\delta J^{(n)} = \langle\langle A|\delta\rho_v^{(n)}(t_F)\rangle\rangle - \delta\mathcal{C}^{(n)}$$

Combining this with (C.12) and (C.13) gives

$$\begin{aligned}
\delta J^{(n)} &= \langle\langle A|\delta\rho_v^{(n)}(t_F)\rangle\rangle - \delta\mathcal{C}^{(n)} \\
&= \sum_{m=1}^{M}\frac{\lambda_m}{2\hbar}\int_{t_0}^{t_F}\Big[\frac{2}{\alpha}(f_m^{(n+1)}-\tilde{f}_m^{(n)})^2+2\tilde{f}_m^{(n)}(f_m^{(n+1)}-\tilde{f}_m^{(n)}) \\
&\qquad +\frac{2}{\beta}(\tilde{f}_m^{(n)}-f_m^{(n)})^2+2f_m^{(n)}(\tilde{f}_m^{(n)}-f_m^{(n)})\Big]dt \\
&\quad - \sum_{m=1}^{M}\frac{\lambda_m}{2\hbar}\int_{t_0}^{t_F}\Big[(f_m^{(n+1)}-\tilde{f}_m^{(n)})^2+2\tilde{f}_m^{(n)}(f_m^{(n+1)}-\tilde{f}_m^{(n)}) \\
&\qquad +(\tilde{f}_m^{(n)}-f_m^{(n)})^2+2f_m^{(n)}(\tilde{f}_m^{(n)}-f_m^{(n)})\Big]dt \\
&= \sum_{m=1}^{M}\frac{\lambda_m}{2\hbar}\int_{t_0}^{t_F}\Big[(\frac{2}{\alpha}-1)(f_m^{(n+1)}-\tilde{f}_m^{(n)})^2+(\frac{2}{\beta}-1)(\tilde{f}_m^{(n)}-f_m^{(n)})^2\Big]dt
\end{aligned}$$

$$= \sum_{m=1}^{M} \frac{\lambda_m}{2\hbar}\left[(\frac{2}{\alpha}-1) \parallel f_m^{(n+1)} - \tilde{f}_m^{(n)} \parallel_2^2 + (\frac{2}{\beta}-1) \parallel \tilde{f}_m^{(n)} - f_m^{(n)} \parallel_2^2\right] \quad \text{(C.14)}$$

For $\alpha = 0$ and $0 < \beta \leq 2$ we note that $f_m^{(n+1)} = \tilde{f}_m^{(n)}$ and a slight modification of the argument yields:

$$\begin{aligned} \delta J^{(n)} &= \sum_{m=1}^{M} \frac{\lambda_m}{2\hbar} \int_{t_0}^{t_F} (\frac{2}{\beta}-1)(\tilde{f}_m^{(n)} - f_m^{(n)})^2 dt \\ &= \sum_{m=1}^{M} \frac{\lambda_m}{2\hbar} (\frac{2}{\beta}-1) \parallel \tilde{f}_m^{(n)} - f_m^{(n)} \parallel_2^2 \end{aligned} \quad \text{(C.15)}$$

Similarly, for $\beta = 0$ and $0 < \alpha \leq 2$ we have $\tilde{f}_m^{(n)} = f_m^{(n)}$ and

$$\begin{aligned} \delta J^{(n)} &= \sum_{m=1}^{M} \frac{\lambda_m}{2\hbar} \int_{t_0}^{t_F} (\frac{2}{\alpha}-1)(f_m^{(n+1)} - \tilde{f}_m^{(n)})^2 dt \\ &= \sum_{m=1}^{M} \frac{\lambda_m}{2\hbar} (\frac{2}{\alpha}-1) \parallel f_m^{(n+1)} - \tilde{f}_m^{(n)} \parallel_2^2 \end{aligned} \quad \text{(C.16)}$$

$f_m^{(n+1)}$, $\tilde{f}_m^{(n)}$ and $f_m^{(n)}$ are real valued functions. Hence, the expressions $\parallel f_m^{(n+1)} - \tilde{f}_m^{(n)} \parallel_2^2$ and $\parallel \tilde{f}_m^{(n)} - f_m^{(n)} \parallel_2^2$, will be non-negative. Also $\lambda_m > 0$ for all $m$ such that $0 \leq m \leq M$ and $\hbar \geq 0$.

For $\alpha$ and $\beta$ in the ranges $0 < \alpha \leq 2$ and $0 < \beta \leq 2$ so that $\frac{2}{\alpha} - 1 \geq 0$ and $\frac{2}{\beta} - 1 \geq 0$ the expression given by (C.14) is the integral of a non-negative function and hence will be non-negative. This gives us $\delta J^{(n)} \geq 0$ and in the case $\alpha = \beta = 2$ it gives $\delta J^{(n)} = 0$. From C.15 we get $\delta J^{(n)} \geq 0$ for $\alpha = 0$ and $0 < \beta \leq 2$ and also $\delta J^{(n)} = 0$ when $\alpha = 0$ and $\beta = 2$. Similarly from C.16 we get $\delta J^{(n)} \geq 0$ for $\beta = 0$ and $0 < \alpha \leq 2$ and also $\delta J^{(n)} = 0$ when $\alpha = 2$ and $\beta = 0$.

Finally consider the case when $\alpha = \beta = 0$. From C.10 we get $|\Delta^{(n)}(t)\rangle\rangle = 0$ which in turn from C.11 gives $\langle\langle A|\delta\rho_v^{(n)}(t_F)\rangle\rangle = 0$. From C.13 we get $\delta C^{(n)} = 0$. Combining these in C.9 gives $\delta J^{(n)} = 0$ when $\alpha = \beta = 0$.

Hence it has been shown that the sequence $J^{(n)}$ is monotonically increasing and $\delta J^{(n)} = 0$ if $(\alpha, \beta) \in \{(0,0), (0,2), (2,0), (2,2)\}$. This concludes the first part of the proof.

### C.3.2 Proof of Boundedness

In this part of the proof it is shown that

**(a)** the control fields $|f_m^{(n)}(t)|$ are bounded

**(b)** the sequence $J^{(n)}$ is bounded.

(a) Proof that the control fields $|f_m^{(n)}(t)|$ are bounded.

Note that

$$\left\|A_v^{(n)}(t)\right\|_2^2 = \langle\langle A_v^{(n)}(t)|A_v^{(n)}(t)\rangle\rangle = \langle\langle A|A\rangle\rangle = \left\|A\right\|_2^2$$

and

$$\left\|\rho_v^{(n)}(t)\right\|_2^2 = \langle\langle \rho_v^{(n)}(t)|\rho_v^{(n)}(t)\rangle\rangle = \langle\langle \rho_0|\rho_0\rangle\rangle = \left\|\rho_0\right\|_2^2$$

We also have $\tilde{f}_m^{(n-1)}(t)$ and $f_m^{(n)}(t)$ which are defined as follows

$$\tilde{f}_m^{(n-1)}(t) = (1-\beta)f_m^{(n-1)} - \frac{i\beta}{\lambda_m}\langle\langle A_v^{(n-1)}(t)|\mathcal{L}_m|\rho_v^{(n-1)}(t)\rangle\rangle$$

and

$$f_m^{(n)}(t) = (1-\alpha)\tilde{f}_m^{(n-1)} - \frac{i\alpha}{\lambda_m}\langle\langle A_v^{(n-1)}(t)|\mathcal{L}_m|\rho_v^{(n)}(t)\rangle\rangle$$

Also note we have the Cauchy-Schwarz's inequality

$$|\langle\langle A|\rho_v^{(n)}(t)\rangle\rangle|^2 \leq \|A\|_2^2.\left\|\rho_v^{(n)}(t)\right\|_2^2 \leq \|A\|_2^2$$

Consider

$$\begin{aligned}
f_m^{(n)}(t) &= (1-\alpha)\tilde{f}_m^{(n-1)} - \frac{i\alpha}{\lambda_m}\langle\langle A_v^{(n-1)}(t)|\mathcal{L}_m|\rho_v^{(n)}(t)\rangle\rangle \\
&= (1-\alpha)\{(1-\beta)f_m^{(n-1)} - \frac{i\beta}{\lambda_m}\langle\langle A_v^{(n-1)}(t)|\mathcal{L}_m|\rho_v^{(n-1)}(t)\rangle\rangle\} \\
&\qquad -\frac{i\alpha}{\lambda_m}\langle\langle A_v^{(n-1)}(t)|\mathcal{L}_m|\rho_v^{(n)}(t)\rangle\rangle \\
&= (1-\alpha)(1-\beta)f_m^{(n-1)} - (1-\alpha)\frac{i\beta}{\lambda_m}\langle\langle A_v^{(n-1)}(t)|\mathcal{L}_m|\rho_v^{(n-1)}(t)\rangle\rangle \\
&\qquad -\frac{i\alpha}{\lambda_m}\langle\langle A_v^{(n-1)}(t)|\mathcal{L}_m|\rho_v^{(n)}(t)\rangle\rangle
\end{aligned}$$

Hence, for any $(\alpha,\beta) \in [0,2]^2 - \{(0,0),(2,2)\}$

$$\begin{aligned}
|f_m^{(n)}(t)|^2 &\leq |(1-\alpha)(1-\beta)f_m^{(n-1)}(t)|^2 + |(1-\alpha)\frac{\beta}{\lambda_m}\langle\langle A_v^{(n-1)}(t)|\mathcal{L}_m|\rho_v^{(n-1)}(t)\rangle\rangle|^2 \\
&\qquad +|\frac{\alpha}{\lambda_m}\langle\langle A_v^{(n-1)}(t)|\mathcal{L}_m|\rho_v^{(n)}(t)\rangle\rangle|^2 \\
|f_m^{(n)}(t)|^2 &\leq (1-\alpha)^2(1-\beta)^2|f_m^{(n-1)}(t)|^2 + \frac{(1-\alpha)^2\beta^2}{\lambda_m^2}|\langle\langle A_v^{(n-1)}(t)|\mathcal{L}_m|\rho_v^{(n-1)}(t)\rangle\rangle|^2 \\
&\qquad +\frac{\alpha^2}{\lambda_m^2}|\langle\langle A_v^{(n-1)}(t)|\mathcal{L}_m|\rho_v^{(n)}(t)\rangle\rangle|^2
\end{aligned}$$

$$
\begin{aligned}
|f_m^{(n)}(t)|^2 &\leq (1-\alpha)^2(1-\beta)^2|f_m^{(n-1)}(t)|^2 + \frac{(1-\alpha)^2\beta^2}{\lambda_m^2}\left\|A_v^{(n-1)}(t)\right\|_2^2.\left\|\mathcal{L}_m\right\|^2.\left\|\rho_v^{(n-1)}\right\|_2^2 \\
&\quad + \frac{\alpha^2}{\lambda_m^2}\left\|A_v^{(n)}(t)\right\|_2^2.\left\|\mathcal{L}_m\right\|^2.\left\|\rho_v^{(n)}\right\|_2^2 \\
|f_m^{(n)}(t)|^2 &\leq (1-\alpha)^2(1-\beta)^2|f_m^{(n-1)}(t)|^2 + \frac{(1-\alpha)^2\beta^2}{\lambda_m^2}\left\|A_v^{(n-1)}(t)\right\|_2^2.\left\|\mathcal{L}_m\right\|^2 \\
&\quad + \frac{\alpha^2}{\lambda_m^2}\left\|A_v^{(n)}(t)\right\|_2^2.\left\|\mathcal{L}_m\right\|^2 \\
|f_m^{(n)}(t)|^2 &\leq (1-\alpha)^2(1-\beta)^2|f_m^{(n-1)}(t)|^2 + \frac{(1-\alpha)^2\beta^2+\alpha^2}{\lambda_m^2}\left\|A\right\|_2^2.\left\|\mathcal{L}_m\right\|^2 \\
|f_m^{(n)}(t)|^2 &\leq [(1-\alpha)^2(1-\beta)^2]^n|f_m^{(0)}(t)|^2 \\
&\quad + \frac{(1-\alpha)^2\beta^2+\alpha^2}{\lambda_m^2}\left\|A\right\|_2^2.\left\|\mathcal{L}_m\right\|^2\sum_{k=0}^{n-1}[(1-\alpha)^2(1-\beta)^2]^k \\
|f_m^{(n)}(t)|^2 &\leq [(1-\alpha)^2(1-\beta)^2]^n|f_m^{(0)}(t)|^2 \\
&\quad + \frac{(1-\alpha)^2\beta^2+\alpha^2}{\lambda_m^2}\left\|A\right\|_2^2.\left\|\mathcal{L}_m\right\|^2\frac{1-[(1-\alpha)^2(1-\beta)^2]^n}{1-(1-\alpha)^2(1-\beta)^2} \\
|f_m^{(n)}(t)|^2 &\leq [(1-\alpha)^2(1-\beta)^2]^n|f_m^{(0)}(t)|^2 + \frac{C_{\alpha\beta}^2}{\lambda_m^2}\left\|A\right\|_2^2.\left\|\mathcal{L}_m\right\|^2\Big(1-[(1-\alpha)^2(1-\beta)^2]^n\Big)
\end{aligned}
$$

where

$$
C_{\alpha\beta} = \sqrt{\frac{\alpha^2+(1-\alpha)^2\beta^2}{1-(1-\alpha)^2(1-\beta)^2}}
$$

then we have

$$
|f_m^{(n)}(t)|^2 \leq [(1-\alpha)^2(1-\beta)^2]^n C_m^2 + C_m^2\Big(1-[(1-\alpha)^2(1-\beta)^2]^n\Big) = C_m^2
$$

for all $n$ and where

$$
C_m = \max\left\{|f_m^{(n)}(t)|, \frac{C_{\alpha\beta}}{\lambda_m}\parallel A\parallel_2 \parallel \mathcal{L}_m\parallel\right\}.
$$

Hence, $|f_m^{(n)}(t)| \leq C_m$ for all $n$, i.e the control fields are bounded.

(b) Proof that the sequence $J^{(n)}$ is bounded.

Now

$$
\begin{aligned}
J^{(n)} &= \langle\langle A|\rho_v^{(n)}(t_F)\rangle\rangle - \sum_{m=1}^{M}\frac{\lambda_m}{2\hbar}\int_{t_0}^{t_F}[f_m^{(n)}(t)]^2dt \\
|J^{(n)}| &\leq |\langle\langle A|\rho_v^{(n)}(t_F)\rangle\rangle| + |\sum_{m=1}^{M}\frac{\lambda_m}{2\hbar}\int_{t_0}^{t_F}[f_m^{(n)}(t)]^2dt| \\
|J^{(n)}| &\leq \left\|A\right\|_2 + \sum_{m=1}^{M}\frac{\lambda_m}{2\hbar}\{t_F-t_0\}C_m^2
\end{aligned}
$$

as we know from (a) that the control fields are bounded. Hence the sequence $J^{(n)}$ is bounded. This concludes the boundedness part of the proof. From this and the proof in Section C.3.1 it has been shown that the sequence $J^{(n)}$ is monotonically increasing and bounded above, hence $J^{(n)}$ is convergent.

# Bibliography


[1] W. Warren, H. Rabitz, and M. Dahleh. Coherent control of quantum dynamics: The dream is alive. *Science*, 259:1581, 1993.

[2] H. Rabitz, R. de Vivie-Riedle, M. Motzkus, and K. Kompa. Whither the future of controlling quantum phenomena? *Science*, 288:824, 2000.

[3] A. P. Peirce, M. A. Dahleh, and H. Rabitz. Optimal control of quantum-mechanical systems: Existance, numerical approximation, and applications. *Phys. Rev. A*, 37:4950, 1988.

[4] G. M. Huang, T.J. Tarn, and J. W. Clark. On the controllability of quantum-mechanical systems. *J. Math. Phys.*, 24:2608, 1983.

[5] T. J. Tarn, J. W. Clark, and D. G. Lucarelli. Controllability of quantum-mechanical systems with continuous spectra. In *Proceedings of the 39th IEEE Conference on Decision and Control*, pages 2803–2809, New York, 2000. IEEE.

[6] W. Karwowski and R. Mendes. Quantum control in infinite dimensions. *Phy. Lett. A*, 322:282, 2004.

[7] V. Ramakrishna, M. V. Salapaka, M. Dahleh, H. Rabitz, and A. Peirce. Controllability of molecular systems. *Phys. Rev. A*, 51:960–966, 1995.

[8] D. D'Alessandro. On the controllability of systems on compact lie groups and quantum-mechanical systems. In *Proceedings of the 39th IEEE Conference on Decision and Control*, pages 1086–1091, New York, 2000. IEEE.

[9] H. Fu, S. G. Schirmer, and A. I. Solomon. Complete controllability of finite-level quantum systems. *J. Phys. A*, 34:1679, 2001.

[10] S Lloyd. Coherent quantum feedback. *Phys. Rev. A*, 62:022108, 2000.

[11] M. D. Girardeau, S. G. Schirmer, J. V. Leahy, and R. M. Koch. Kinematical bounds on optimization of observables for quantum systems. *Phys. Rev. A*, 58:2684, 1998.

[12] S. G. Schirmer, J. V. Leahy, and A. I. Solomon. Degrees of controllability for quantum systems and applications to atomic systems. *J. Phys. A*, 35:4125, 2002.

[13] F. Albertini and D. D'Alessandro. Notions of controllability for quantum-mechanical systems. *quant-ph/0106128*, 2001.

[14] Sonia G. Schirmer, Ivan C. H. Pullen, and Allan I. Solomon. Controllability of quantum systems. In Astolfi, Gordillo, and van der Schaft, editors, *Hamiltonian and Lagrangian Methods in Nonlinear Control*, pages 311–316. Elsevier Science Ltd, 2003. Proceedings of 2nd IFAC Workshop, Seville, Spain, April 3-5, 2003.

[15] V. Jurdjevic and H. J. Sussmann. Control systems on Lie groups. *J. Diff. Eqn.*, 12:313, 1972.

[16] S. G. Schirmer, H. Fu, and A. I. Solomon. Complete controllability of quantum systems. *Phys. Rev. A*, 63:063410, 2001.

[17] G. Turinici and H. Rabitz. Quantum wavefunction controllability. *Chem. Phys.*, 267:1–9, 2001.

[18] C. Altafini. Controllability of quantum mechanical systems by root space decompositions of su(n). *J. Math. Phys.*, 43(5):2051–2062, 2002.

[19] S. G. Schirmer, I. C. H. Pullen, and A. I. Solomon. Identification of dynamical Lie algebras for finite-level quantum control systems. *J. Phys. A*, 35:2327, 2002.

[20] D. Bimberg, M. Grundmann, and N. N. Ledentsov. *Quantum Dot Heterostructures.* Wiley & Sons, New York, 1999.

[21] B. Li, G. Turinici, V. Ramakrishna, and H. Rabitz. Optimal dynamics discrimination of similar molecules through quantum learning control. *J. Phys. Chem. B*, 106:8125, 2002.

[22] S. G. Schirmer, I. C. H. Pullen, and A. I. Solomon. Controllability of multi-partite quantum systems and selective excitations of quantum dots. *J. Optics B*, 7:S293, 2005.

[23] G. Turinici, V. Ramakrishna, B. Li, and H. Rabitz. Optimal discrimination of multiple quantum systems: controllability analysis. *J. Phys. A*, 37:273, 2004.

[24] A. G. Butkovskiy and Yu. I. Saimolenko. *Control of Quantum-Mechanical Processes and Systems.* Kluwer Academic, Dordrecht, 1990.

[25] B. W. Shore. *Theory of coherent atomic excitation.* John Wiley & Sons, New York, 1990.

[26] J. Broeckhove and L. Lathouwers. *Time-dependent quantum molecular dynamics.* Plenum Press, New York, 1993.

[27] S. Rice and M. Zhao. *Optimal control of molecular dynamics.* Wiley & Sons, New York, 2000.

[28] A. Abraham. *The Principles of Nuclear Magnetism.* Oxford University Press, London, 1961.

[29] Shenghua Shi and Herschel Rabitz. Quantum mechanical optimal control of physical observables. *J. Chem. Phys.*, 92:364, 1990.

[30] S. H. Tersigni, P. Gaspard, and S. A. Rice. On using shaped light pulses to control the selectivity of product formation in a chemical reaction: An application to a multiple level system. *J. Chem. Phys.*, 93:1670, 1990.

[31] D. J. Tannor and S. A. Rice. Control of selectivity of chemical reaction via control of wave packet evolution. *J. Chem. Phys.*, 83:5013, 1985.

[32] D. Tannor, R. Kosloff, and S. Rice. Coherent pulse sequence induced control of selectivity of reactions: Exact quantum mechanical calculations. *J. Chem. Phy.*, 85:5805, 1986.

[33] P. Brumer and M. Shapiro. *Acc. Chm. Res.*, 22:407, 1989.

[34] M. Shapiro and P. Brumer. Laser control of product quantum state populations in unimolecular reactions. *J. Chem. Phy.*, 84:4103, 1986.

[35] N. V. Vitanov, T. Halfmann, B. W. Shore, and K. Bergmann. Laser-induced population transfer by adiabatic passage techniques. *Ann. Rev. Phys. Chem.*, 52:763–809, 2001.

[36] M. Alonso and E. Finn. *Fundamental University Physics.* Addison-Wesley, Reading, Massachusetts, 1968.

[37] V. S. Malinovsky and D. J. Tannor. Simple and robust extension of the stimulated raman adiabatic passage technique to n-level systems. *Phys. Rev. A*, 56:4929–4937, 1997.

[38] V. Jurdjevic. *Geometric Control Theory.* Cambridge University Press, Cambridge, UK, 1996.

[39] V. Ramakrishna, R. Ober, X. Sun, O. Steuernagel, J. Botina, and H. Rabitz. Explicit generation of unitary transformations in a single atom or molecule. *Phys. Rev. A*, 61:032106, 2000.

[40] D. D'Alessandro. Algorithms for quantum control based on decompositions of Lie groups. In *Proceedings of the 39th IEEE Conference on Decision and Control*, pages 1074–1075, New York, 2000. IEEE.

[41] N. Khaneja and S. Glaser. Cartan decomposition of $su(2^n)$ and control of spin systems. *Chem. Phys.*, 267:11–23, 2001.

[42] V. Ramakrishna, Kathryn L. Flores, H. Rabitz, and R. Ober. Quantum control by decompositions of SU(2). *Phys. Rev. A*, 62:053409, 2000.

[43] S. G. Schirmer, A. D. Greentree, V. Ramakrishna, and H. Rabitz. Constructive control of quantum systems using factorization of unitary operators. *J. Phys. A*, 35:8315–8339, 2002.

[44] L. M. K. Vandersypen and I. L. Chuang. NMR techniques for quantum control and computation. *Rev. Mod. Phys.*, 76:1037, 2004.

[45] R. S. Judson and H. Rabitz. Teaching lasers to control molecules. *Phys. Rev. Lett.*, 68:1500, 1992.

[46] G. Turinici, C. Le Bris, and H. Rabitz. Efficient algorithms for the laboratory discovery of optimal quantum controls. *Phys. Rev. E*, 70:016704, 2004.

[47] T. Baumert, T. Brixner, V. Seyfried, M. Strehle, and G. Gerber. Femtosecond pulse shaping by an evolutionary algorithm with feedback. *Appl. Phys. B*, 65:779–782, 1997.

[48] B. J. Pearson, J. L. White, T. C. Weinacht, and P. H. Bucksbaum. Coherence control using adaptive learning algorithms. *Phys. Rev. A*, 63:063412, 2001.

[49] H. M. Wiseman. Quantum theory of continuous feedback. *Phys. Rev. A*, 49:2133, 1994.

[50] A. C. Doherty and K. Jacobs. Feedback control of quantum systems using continuous state estimation. *Phys. Rev. A*, 60:2700, 1999.

[51] A. C. Doherty, S. Habib, K. Jacobs, H. Mabuchi, and S. M. Tan. Quantum feedback control and classical control theory. *Phys. Rev. A*, 62:012105, 2000.

[52] S. Lloyd and J. J. E. Slotine. Quantum feedback with weak measurements. *Phys. Rev. A*, 62:012307, 2000.

[53] R. J. Nelson, Y. Weinstein, D. Cory, and S. Lloyd. Experimental demonstration of fully coherent quantum feedback. *Phys. Rev. Lett.*, 85:3045, 2000.

[54] Y. Ohtsuki, K Nakagami, Y. Fujimura, W. Zhu, and H. Rabitz. Quantum optimal control of multiple targets: Development of a monotonically convergent algorithm and application to intramolecular vibrational energy redistribution control. *J. Chem. Phys.*, 114:8867, 2001.

[55] N. Khaneja, R. Brockett, and S. J. Glaser. Time optimal control in spin systems. *Phys. Rev. A*, 63:032308, 2001.

[56] R. Balian and M. Vénéroni. Time-dependent variational principle for predicting the expectation value of an observable. *Phys. Rev. Lett.*, 47:1353, 1981.

[57] H. Jirari and W. Pötz. Optimal coherent control of dissipative $n$-level systems. *Phys. Rev. A*, 72:013409, 2005.

[58] Yvon Maday and Gabriel Turinici. New formulations of monotonically convergent quantum control algorithms. *J. Chem. Phys.*, 118(18):8191, 2003.

[59] Y. Ohtsuki, G. Turinici, and H. Rabitz. Generalized monotonically convergent algorithms for solving quantum optimal control problems. *J. Chem. Phys.*, 120:5509, 2004.

[60] Wusheng Zhu and Herschel Rabitz. A rapid monotonically convergent iteration algorithm for quantum optimal control over the expectation value of a positive definite operator. *J. Chem. Phys.*, 109:385, 1998.

[61] Y. Ohtsuki, W. Zhu, and H. Rabitz. Monotonically convergent algorithm for quantum optimal control with dissipation. *J. Chem. Phys.*, 110:9825, 1999.

[62] S. G. Schirmer, M. D. Girardeau, and J. V. Leahy. Efficient algorithm for optimal control of mixed-state quantum systems. *Phys. Rev. A*, 61:012101, 2000.

[63] A. Iserles, H. Z. Munthe-Kaas, S. P. Norsett, and A. Zanna. Lie group methods. *Acta Numerica*, pages 215–365, 2000.

[64] S. Chelkowski, A. Bandrauk, and P. B. Corkum. Efficient molecular dissociation by a chriped ultrashort infrared laser pulse. *Phys. Rev. Lett.*, 65:2355, 1990.

[65] H. Rabitz. Optimal control of quantum systems: origins of inherent robustness to control field fluctuations. *Phys. Rev. A*, 66:063405, 2002.

[66] J. F. Cornwell. *Group Theory in Physics.* Academic Press Inc., London, 1984.

[67] N. Jacobson. *Lie Algebras.* Dover, New York, 1962.

[68] S. G. Schirmer, T. Zhang, and J. V. Leahy. Orbits of quantum states and geometry of Bloch vectors for $n$-level quantum systems. *J. Phys. A*, 37(4):1389–1402, 2004.